SISSA  **ISAS**

SCUOLA INTERNAZIONALE SUPERIORE DI STUDI AVANZATI
INTERNATIONAL SCHOOL FOR ADVANCED STUDIES

DARK MATTER IN SPIRAL GALAXIES

Thesis submitted for the degree of
Doctor Philosophiæ

CANDIDATE
Irina A. Yegorova

SUPERVISOR
Prof. Paolo Salucci

October 2007

Table of Contents

Published papers

Citations to Published and Submitted Works

The work presented in this thesis has been partially published in scientific papers.

Papers on refereed journals:

- **Yegorova I.**, Salucci P., "The Radial Tully-Fisher relation for spiral galaxies I", 2007, MNRAS, 377, 507
- Salucci P., Lapi A., Tonini C., Gentile G., **Yegorova I.**, Klein U., "The Universal Rotation Curve of Spiral Galaxies. II The Dark Matter Distribution out to the Virial Radius", 2007, MNRAS, 378, 41
- Salucci P., **Yegorova I.A.**, Drory N. "The disk mass of spiral galaxies" submitted to MNRAS
- **Yegorova I.**, Pizzella A., Salucci P., "Probing dark matter halos of spiral galaxies at unexplored distances through satellites kinematics" in preparation

Proceedings:

- **Yegorova I.**, Salucci P., "The Tully Fisher relation of spiral galaxies", 2004, bdmh.confE, 84Y
- **Yegorova I.**, Salucci P., "The Tully Fisher relation of spiral galaxies", 2005, nfcd.conf, 267

Acknowledgments

First of all I would like to thank my supervisor Prof. Paolo Salucci for his great enthusiasm in the work, experience, knowledge, patience and time. For his new ideas. And for his support during all these 4 years.

I would like to thank warmly astrophysical faculty members that gave me an unique opportunity to study in SISSA, where I have been able to participate in the vivid scientific life.

I would like to thank Prof. Alessandro Pizzella for his support, experience and astronomical spirit that he has imparted to me. And for the great enthusiasm in the work.

My thanks to Prof. Uli Klein for his suggestions that helped me a lot to improve this thesis.

My thanks to tigers Melita, Simona, Chiara and to Stefania and Christiane for their great support, cheerfulness and kindness.

And my hearty thanks to my parents for their love.

Introduction

During the last few decades, it has been discovered that most of the material in the Universe is invisible. Since it interacts only gravitationally with the rest of the Universe components. From the latest measurements of WMAP satellite we know that the Universe consists of 4% Baryons, 22% Cold Dark Matter, 74% Dark Energy.

Now it is clear a wonderful time to study cosmology. Using the latest technological advances we have obtained detailed picture of the early Universe and maps of the distribution of matter on the largest scales in the Universe today. And we have a physical model for the origin and evolution of the Universe. However on the small scales there are still a lot of open issues. The mass distribution in spiral galaxies is an interesting question that is tightly band to the galaxy formation and evolution process.

My PhD project is divided in two main parts. In the first part I study the distribution of dark and luminous matter in spiral galaxies at the inner radius. The main data tool that I use for this studies is the rotation curves of spirals. Although its already 50 years that the rotation curves are used in order to derive the matter distribution in spirals, a different approaches can be always applied, to get a more relevant information. For this purpose (to find this new approaches) during my PhD studies I analyzed more than 400 rotation curves. In my analysis I had spiral galaxies of early and late Hubble types, different luminosity range, different range of masses. One of the interesting approaches was to use the principles of the Tully-Fisher relation. But to look at this relationship in a more detailed way. We found a new relationship that we called Radial Tully-Fisher (RAF) relation. It turns out that Radial Tully-Fisher relation is a very good tool to investigate the distribution of matter in the optical regions of spiral galaxies.

In the second part of my PhD project I am studying the dark matter halos in outer radius. I proposed to use a satellites galaxies of spirals in order to make a detailed investigation of the dark matter halos. The novelty of the approach is that in the previous studies a large number of primaries were used and for each primary on average 3 satellites. I proposed to investigate a smaller number of primaries, but with the help of the more powerful telescopes that are able to detect enough faint objects. In order to double or even triple the number of satellites. For this studies I carried out two observational programs and data reduction process.

Below is the outline of my thesis.

Thesis Outline

- In **Chapter 1** I give an overview on dark matter problem in spiral galaxies and also in other types of galaxies. Moreover I broach a subject of galaxy formation.

- In **Chapter 2** I described the properties of the rotation curves of spiral galaxies. Since the rotation curves are one of the main tools used to study the distribution of mass in spiral galaxies, in our analysis we were mostly using the rotation curves. I described the techniques used to obtain the rotation curves. I discuss the dependence between the rotation curve and different properties of spiral galaxies, such as luminosity, mass, Hubble type.

- In **Chapter 3** I present a Tully-Fisher relation in spiral galaxies. We found a new Tully-Fisher-like relation for spiral galaxies holding at different galactocentric radii. This Radial Tully-Fisher (RTF) relation allows us to investigate the distribution of matter in the optical regions of spiral galaxies. This relation, applied to three different samples of rotation curves of spiral galaxies.

- In **Chapter 4** we studied a sample of galaxies in order to derive their disk masses. Sample contains spiral galaxies of different luminosity and Hubble

Type. We use two methods such as mass modeling of their RC's and fitting their SED with spectro-photometric models. The estimates from these two different methods agree very well confirming their reliability and allowing us to derive very accurate stellar mass-to-light ratio vs color and stellar mass relations.

- In **Chapter 5** using a sample of high-luminosity (M < -22.5) spiral galaxies we study their of their rotation curves. We have analyzed separately $H\alpha$ and HI data. We derived the average rotational curve and found that it remaining constant or is decreasing with radius in the range $3R_D - 6R_D$.

- In **Chapter 6** we are using the satellites galaxies in order to probe the dark matter halo of primary galaxies. I describe the sample that we have used. Then I describe the steps of the work, starting with the proposal, following with the data reduction and analysis of the data. Then I present the preliminary results. However the project is still in progress.

- And I discuss the results that we obtained in our studies.

Chapter 1

What are the evidences for dark matter?

1.1 Matter content in the Universe

The main principle of the Standard Cosmological Model is that in the large-scale average the Universe is close to homogeneous and isotropic. From the WMAP3 results of microwave background observations we know that the Universe is flat. $\Omega = 1 = \Omega_M + \Omega_\Lambda$, where Ω_Λ gives the contribution of vacuum energy. Such a high value of Ω_Λ shows that the Universe is expanding with acceleration. The mean energy density in the universe is equal to the critical density (within a 2% margin of error).

From the latest astrophysical measurments we know that the Universe consists of **4% Baryons**, **22% Cold Dark Matter**, **74% Dark Energy**.

Thus 96% of the energy density in the universe is in a form that has never been directly detected in the laboratory. The actual density of atoms is equivalent to roughly 1 proton per 4 m^3. The age of the Universe is 13.5 Gyr. The Hubble constant that gives the rate of expansion is ~ 72 km $s^{-1}Mpc^{-1}$.

The value for Ω_M has slightly changed from the first year WMAP observations $\Omega_M = 0.29 \pm 0.07$ to the third year WMAP observations $\Omega_M = 0.234 \pm 0.035$. Even

if the value of Ω_M is slightly decreased, it is clear that the amount of dark matter in the Universe is really big. We still do not know from which particles dark matter consists of. But the latests theories shows that more likely dark matter should be a cold dark matter (CDM). I.e. should consists of slowly moving particles, so that the CDM energy density is mainly due to the particle's rest mass. There being a large series of candidates for CDM particles, but axions and neutralinos being the most attractive possibilities.

Galaxies are the most common objects in the Universe. They are born out of primordial fluctuations with an evolution probably driven by gravitation as the dominant effect. Basically they are large systems of stars, gas and mysterious dark matter. In 1929 Hubble classified the galaxies into several types according to their overall observed shapes. Basically he divided galaxies into spirals (S's) and ellipticals (E's). A third froup is formed by the irregulars (Irr's). There two kinds of spiral galaxies: normal and barred. In normal spirals the spiral arms originate from the nuclear bulge. In barred spirals the arms appear at the end of a bar crossing the nucleus itself. Within these two groups several types can be distinguished according to their overall shape: Sa, Sb, Sc for normal spirals ans SBa, SBb, SBc for barred spirals, though, intermediate types also exist. The S0 galaxies or lenticular galaxies are midway between elliticals and spirals. Like spirals they have a nuclea bulge surrounded by a flat disc, but no spiral arms. The classification of the elliptical galaxies corresponds to the degree of roundness or elongation from E0 to E7. Those galaxies that cannot fit well into spirals, lenticulars, or ellipticals, having an amorphous shape without any kind of symmetry, are known as irregulars. Galaxies have varying range of luminosities, from $3 \times 10^5 L_\odot$ for the dwarf galaxy to 10^{12} for the supergiant galaxy. Also they are varying in mass from $10^7 M_\odot$ to $10^{12} M_\odot$ correspondingly.

In my studies I am using only spiral galaxies. That is why below I will describe in details the properties of this type of galaxies and dark matter problem in spirals. However, later I will also mention a dark matter problem in other types of galaxies.

1.2 Evidence of dark matter in spiral galaxies

About 77% of the observed galaxies in the universe are spiral galaxies (Fig... A typical spiral galaxy NGC 2903). Our own galaxy, the Milky Way, is a typical spiral galaxy. Not surprisingly, spiral galaxies look like spirals, with long arms winding toward a bright bulge at the center. The arms of a spiral galaxy have lots of gas and dust, and they are often areas where new stars are constantly forming. All are characterised by relatively thin (more or less) flat discs, and most have a central bulge which in many ways like an elliptical galaxy. The bulge of a spiral galaxy is composed primarily of old, red stars. Very little star formation goes on in the bulge. Spirals come in a wide variety of forms.

Figure 1.1: Spiral galaxy NGC 2903

If we can clearly see the spiral shape, the galaxy is called a "face-on spiral." If instead we see the galaxy from the side, it is called an "edge-on spiral." When one can clearly see their bright central bulges its obviously edge-on spiral galaxies. Face-on and edge-on spiral galaxies aren't really any different, they only look different because of the angle from which we see them.

The luminous matter is spirals is distributed in two components: a concentrated,

spheroidal bulge, with projected density distribution approximately described by

$$I(R) = I_0 e^{-7.67(R/R_e)^{1/4}}, \tag{1.1}$$

where R_e is the half-light radius. And an extended thin disk with surface luminosity distribution (Freeman 1970):

$$I(R) = I_0 e^{-R/R_D}, \tag{1.2}$$

where R_D is the disk scale-length, I_0 is the central value.

But most of the mass in the Universe is invisible. So, to estimate the mass of the galaxy we use Newton's Gravity:

$$M(R) = \frac{V_{rot}^2 R}{G}, \tag{1.3}$$

where V_{rot} is the rotational speed and G is a gravitational constant. So the estimate the mass of the galaxy we need to use the rotational velocity. The total velocity velocity of the spiral galaxy is given by velocity of the gas, stars, bulge and halo:

$$V_{total} = [V^{2_{gas}} + V^{2_{disk}} + V^{2_{bulge}} + V^{2_{halo}}]^{1/2} \tag{1.4}$$

If the halo is spherically symmetric its circular velocity is simply $V_{halo}^2 = GM(R)/R$. The bulge, stellar disk and gas disk are insufficient to give the observed V_{total} and therefore either dark matter is needed or forces other than gravity are involved.

1.2.1 Disk structure

The most clear evidence of the existance of dark matter in spiral galaxies comes from their rotational veocities. The rotation curves (RCs) of spiral galaxies do not show any Keplerian fall-of. This imlies, as the most natural explanation, the presence of an additional and invisible mass component.

Persic, Salucci & Stel (1996) and Salucci & Persic (1997) have analyzed a large number of rotation curves mainly catalogued by Persic & Salucci (1995), using $H\alpha$ data published by Mathewson, Ford & Buchhorn (1992) and also adopting some radio rotation curves. They found the existance of the universal rotation curve (URC). It means that for any luminosity of spiral galaxies exists its own profile of the rotation curve (see Fig...).

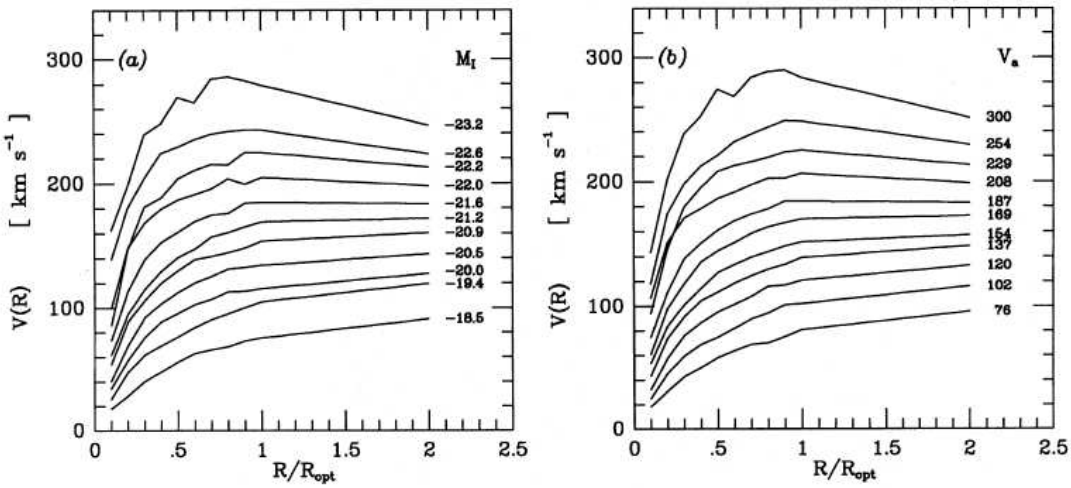

Figure 1.2: The universal rotation curve of spiral galaxies. Radii are in units of R_{opt}

The total velocity in the rotation curve can be represented as:

$$V = (V_{halo}^2 + V_{disk}^2)^{1/2} \tag{1.5}$$

where the velosity of the thin disk is:

$$V_{disk}^2 = V^2(R_{opt})\beta \frac{1.97x^{1.22}}{(x^2 + 0.78^2)^{1.43}} \tag{1.6}$$

and spherical halo is represented by:

$$V_{halo}^2 = V^2(R_{opt})(1-\beta)(1+\alpha^2)\frac{x^2}{x^2+\alpha} \tag{1.7}$$

where x is a radial variable taking R_{opt} as unit

$$x = \frac{R}{R_{opt}} \tag{1.8}$$

The disk + halo fits of the URC are extremely good (fitting errors are within 1% on average) at all luminosities when α and β defined as:

$$\beta = 0.72 + 0.44 \log\left(\frac{L}{L_*}\right) \tag{1.9}$$

$$\alpha = 1.5\left(\frac{L}{L_*}\right)^{1/5} \tag{1.10}$$

where $L_* = 10^{10.4} L\odot$. For a galaxy with luminosity L_*, α corresponds to a value of x of the order of R_{opt}, exactly $1.5R_{opt}$. Then for a spherically symmetric halo we will have:

$$M_{halo} = G^{-1}V^2(1)R_{opt}(1-\beta)(1+\alpha^2)\frac{x^2}{x^2+\alpha} \tag{1.11}$$

$$\rho = \frac{1}{4\pi R^2}\frac{dM}{dR} \propto \frac{x^2+3a^2}{(x^2+a^2)^2} \tag{1.12}$$

The total halo mass can be evaluated by extrapolating the halo out to the radius, R_{200}, encompassing a mean overdensity of 200. The Salucci & Persic (1997) found:

$$R_{200} = 250\left(\frac{L}{L_*}\right)^{0.2} kpc \tag{1.13}$$

$$M_{200} \sim 2 \times 10^{12}\left(\frac{L}{L_*}\right)^{0.5} M_\odot \tag{1.14}$$

The brighter galaxies have a halo that is more massive, but only slightly larger. The mass-luminosity ratio is then

$$\frac{M_{200}}{L_B} \simeq 75\left(\frac{L}{L_*}\right)^{-0.5} \tag{1.15}$$

Brighter galaxies have smaller mass-to-light ratios, hence the dark matter has more dominant e ects in small or low-surface brightness galaxies. We can also calculate the luminous to dark matter ratio

$$\frac{M_{lum}}{M_{200}} = 0.05 \left(\frac{L}{L_*}\right)^{0.8} \tag{1.16}$$

Bright galaxies have relatively smaller dark matter halos, while the very bright galaxies nearly reach the maximum M_{lum}/M_{dark} ratio (~ 1) established from primordial nucleosynthesis models for the baryonic Ω_B.

On scales (0.2 - 1)R_{200}, the halos have mostly the same structure with a density profile very similar at all masses and an amplitude that scales only very weakly with mass, like $V_{200} \propto M_{200}^{0.15}$. At very inner radii, the self-similarity of the profile breaks down, the core radius becoming smaller for decreasing M_{200} according to:

$$\frac{R_{core}}{R_{200}} = 0.075 \left(\frac{M_{200}}{10^{12} M_\odot}\right)^{0.6} \tag{1.17}$$

The central density scales with the mass as:

$$\rho_{halo}(0) = 6.3 \times 10^4 \rho_c \left(\frac{M_{200}}{10^{12} M_\odot}\right)^{-1.3} \tag{1.18}$$

where ρ_{halo} is the critical density of the Universe.

Therefore brighter galaxies have relatively large core radii and small values for the central halo density. Therefore, even the central region of low-brightness galaxies is dominated by dark matter, while bright galaxies have their internal regions dominated by visible matter.

1.2.2 Halo structure

CDM models predict a halo structure which is responsible for the rotation curve of the spiral galaxies. Halo structures and rotation curves are therefore closely connected problems. Let us assume that halos are spherical.

$$\rho(R) = \frac{\rho_0}{1 + \left(\frac{R}{R_c}\right)^2} \tag{1.19}$$

where ρ_0 the central density and R_c the core radius. In this case the circular velocity is defined as

$$V^2(R) = \frac{GM(R)}{R}, \tag{1.20}$$

where $M(R)$ is the mass in a sphere of radius R. The circular velocity can be defined also as:

$$V^2(R) = 4\pi G\rho_0 R_c^2 \left[1 - \frac{R}{R_c} \arctan \frac{R}{R_c}\right] \tag{1.21}$$

which is an increasing function of R, asymptotically reaching $V_{max} = V(R = \infty)$, where

$$V_{max} = \sqrt{4\pi G\rho_0 R_c^2} \tag{1.22}$$

Navarro, Frenk and White (1996, 1997) deduced from their CDM models that halos should be described by the so called "universal" or NFW profiles:

$$\frac{\rho(R)}{\rho_{crit}} = \frac{\delta_c}{\frac{R}{R_s}\left(1 + \frac{R}{R_s}\right)^2} \tag{1.23}$$

where R_s is a scale radius, δ_c is a characteristic (dimensionless) density, and ρ_{crit} is the density of the critical Einstein-de Sitter Universe $\rho_{crit} = 3H^2/8\pi G$.

The NFW profile was called "universal" because the authors found it in a large variety of halo masses, spanning 4 orders of magnitude, from individual galaxies to cluster halos, as well as for a large variety of cosmological scenarios.

The circular velocity of this NFW halo can be calculated by

$$\left(\frac{V_c(R)}{V_{200}}\right)^2 = \frac{1}{x}\frac{ln(1+cx) - \frac{cx}{1+cx}}{ln(1+cx) - \frac{c}{1+cx}} \tag{1.24}$$

where V_{200} is the circular velocity at R_{200} that is called virial radius. This is the radius for which $< \rho >= 200\rho_{crit}$, where $< \rho >$ is the mean density in a sphere of radius R_{200}. This radius approximately separates the virialized and infall regions. The parameter c, called the concentration, is defined as $c = R_{200}/R_s$ and is dimensionless. And $x = R/R_{200}$. Measuring V_{200} in kms^{-1} and R_{200} in kpc, then:

$$M_{200} = (200\rho_{crit})\frac{4}{3}\pi R_{200}^3 = 100\frac{H^2}{G}R_{200}^3 \tag{1.25}$$

And so

$$M_{200} \propto R_{200}^3 \propto V_{200}^2 \tag{1.26}$$

The NFW circular velocity reaches a maximum at $R \approx 2R_s = 2R_{200}/c$ and declines beyond that radius. NFW density profiles are two-parametric and it is possible to choose V_{200} and c to characterize the halos, or the equivalent set of characteristic density and halo mass. A very interesting result of these models is that the two free parameters show a clear correlation. The reason is that the halo density reflects, and is proportional to, the true density when the halo was formed, with the initial small halos being denser because they formed earlier, when the density of the expanding Universe was higher. But due to the hierarchical halo formation, more massive halos were born later. Then, the existence of decreasing functions $\rho_c(t)$ and $M_{200}(t)$ implies a correlation between them. Thus the rotation curves are intrinsically one-parametric.

Burkert (1995) for dwarf spiral galaxies found that their darkmatter halosrepresent a one-parameter family with self-similar density profiles. The observed universal mass profiles can be fitted as

$$\rho_{DM}(R) = \frac{\rho_0 R_0^3}{(R+R_0)(R^2+R_0^2)} \tag{1.27}$$

where ρ_0 and R_0 are free parameters which represent the central density and a scale radius, respectively. Density law resembles an isothermal profile in the inner regions ($R \ll R_0$) and predicts a finite central density ρ_0. For large radii, the mass distribution of the isothermal profile would diverge proportional to R Burketr prifile leads to mass profiles which diverge logarithmically with increasing R in agreement with the NFW profile.

There are many works that do agree with the NWF profile. Like Cole & Lacey (1996) Power et al. (2003). But there are some works that shows that the halos have profile different form that of NFW profile. Works supporting steeper profiles. Moore et al.(1999) found that the density profile of our high-resolution halo are well fitted by a density model

$$\rho(R) = \frac{\rho_0}{[(R/R_s)^{1.5}(1 + (R/R_s)^{1.5})]} \tag{1.28}$$

where R_s is a scale radius. This profile has a steeper asymptotic slope $\rho(R) \propto R^{-1.5}$.

Fukushige & Makino (2001) simulated 12 halos with masses of $6.6 \times 10^{11} - 8 \times 10^{14} M_{\odot}$. The found the density profile that is in good agreement with the profile proposed by Moore et al.(1999) with a central slope proportional to $R^{-1.5}$.

Hayashi et al. (2004) using high-resolution cosmological N-body simulations found that the density profiles of simulated haloes become progressively shallower from the virial radius inwards, and show no sign of approaching a well-defined power law near the centre. At R_{conv}, the density profile is steeper than expected from the NFW profile, which has a $\rho \sim R^{-1}$ cusp, but significantly shallower than the steeply divergent $\rho \sim R^{-1.5}$ cusp proposed by Moore et al. (1999).

However a comparison of the theoretically predicted halos and the observations is necessary to answer these questions and to test the models. Navarro (1998) adopted about 100 disk galaxies from published observations and tried to deduce the NFW

free parameter in each case. This analysis was also made under the isothermal halo assumption. The M/L ratio in the bulge and in the disk assumed as a free parameter. And also assumed that the halo responds adiabatically to the growth of the disk. This means a variation of the NFW profile within the disk region. the formation of the disk must somewhat modify the halo density profile, probably in a way that is very di cult to model. This assumption was introduced in order to avoid disagreements with observations of the rotation of dwarf galaxies and therefore, as a correction of an initial theoretical failure. Indeed, the rotation curve of dwarf galaxies indicates that the halo circular velocity rises almost linearly, which would mean a constant density (i.e. a halo core) in clear contradiction with the NFW profiles. As mentioned above, this hypothesis of the adiabatic response of the halo to the formation of the disk also alleviates the problem of the halo-disk conspiracy.

The results indicate that theoretical models must introduce a higher degree of sophistication, because even isothermal profiles give similar or better results.

1.3 Formation history

Galaxies are born out of primordial fluctuations with an evolution probably driven by gravitation as the dominant effect. The models of galaxy formation have in common the hypothesis that the dark matter is cold (CDM) and that, at a given time, CDM halos arose through a hierarchy of different sized halos formed from mergers of smaller halos. At least four steps characterize the evolution of a galaxy:

- Small density fluctuations, probably originated by quantum fluctuations before the epoch of Inflation or at cosmological phase transitions, grow during the radiation dominated Universe and provide a fluctuation spectrum after the epoch of Recombination.

- CDM overdensities accrete matter and merge. The hierarchical formation of

greater and greater halos produces the present galactic and cluster structures.

- Baryons cool and concentrate at the centre of halos and constitute the visible component of galaxies. The explanation of the Hubble sequence and the origin of rotation of galaxies would be goals of the study of this phase.

- Once the basic structure of a galaxy with its different components has been established, it is necessary to follow its evolution due to star formation, gas ejected from stars, progressive metal enrichment, matter flows connecting the intra and extra media, small internal motions.

Dalcanton et al. 1997. proposed the following model of the disk formation:

- The tidal torquing spins up both dark matter and the baryonic matter in some region of space. Assuming that gas and dark matter are uniformly mixed.

- As the time passes, both the dark and baryonic matter begin to collapse in the overdence region. Initially, when the densities are low, the baryons cannot cool, and the pressureless collapse proceeds identically for both components.

- Because the dark matter cannot dissipate energy, its collapse halts when the system virializes.

- The authors appriximate the halo with Hernquist density profile, whese asymtotic radial profile scales as R^{-4}

$$M_{halo}(R) = (1 - F)M_{\infty}\left(\frac{R/R_0}{1 + R/R_0}\right) \tag{1.29}$$

where $M_{halo}(R)$ is the halo mass within radius R, R_0 a core radius, and F is the fraction of baryonic mass of the protogalaxy within some radius a.

The potential energy within a radius R is

$$\phi\left(x \equiv 1 + \frac{R}{R_0}\right) = -\frac{(1-F)GM_\infty^2}{6R_0}\left(1 - \frac{6x^2 - 8x + 3}{x^4}\right) \tag{1.30}$$

The size of the core radius depends only on the mass of the halo and the mean density density of the Universe.

- During the joint collapse of dark matter and baryons, at some point the density over some region becomes high enough that the baryons begin to cool and decouple from the dark matter. As they cool, their collapse accelerates, and the baryons begin to concentrate within the dark matter. This condensation increases the baryonic fraction within the inner parts of the halo. Since the baryons have nonzero angular momentum, they cannot collapse all the way to the center and instead settle into a rapidly rotating disk. The final mass distribution in the disk is determined both by the initial distribution of specific angular momentum and by the final rotation curve of the collapsed disk plus halo system.

- After the onset of cooling, the collapsing baryons further condense the dark matter halo by increasing the mass density in the inner parts of the halo, where the baryonic mass fraction has increased the most. This modifies the Hernquist potential which the halo had at the time when the cooling began. The condensation of the halo is assumed to proceed roughly adiabatically.

1.4 Dark matter in other galaxies

1.4.1 Elliptical galaxies

Elliptical galaxies as their name implies appear round on the sky. They vary from spherical to elliptical in shape. Their light is smoothly distributed, and they lack the bright clumps of young blue stars and patches of dust which are obvious features

of spiral galaxies. Ellipticals are mostly made up of old stars, and they almost do not have cool gas, except at the very center. These galaxies are more likely than the disc galaxies to be found in dence clusters, rather than in smaller units like our Local Group. The dense environment can mislead studies. In such an environment, the dark matter halos can be stripped away by gravitational tidal force and added to other galaxies or the group as a whole. Therefore, it is difficult to determine how much dark matter the original galaxies had, and how much they have lost to the group as a whole through interactions with their environment.

Their masses cover a range: from about 10^7 up to 10^{13} $M_\odot$. The corresponding range of diameters is about 1/10 kpc up to about 100 kpc. And the absolute blue magnitude varies over a correspondingly large range from $M_B \sim$ -8 to -23.

There are several methods for specifically estimating the mass of an elliptical galaxy:

- From the stellar velocity dispersion.
- From the neutral gas velocities found in the outermost region, in some galaxies.
- From the X-ray corona surrounding ellipticals.
- From the globular clusters velocity dispersion and PNe.
- Using gravitational lensing method.

There also exist complementary methods, using observations of ionized gas in the central parts, theoretical considerations about the bar instability and the chemical evolution.

The surface brightness of an elliptical galaxy can be fitted by de Vaucouleur's law

$$I(R) = I_e e^{-7.67((R/R_e)^{1/4}-1)} \tag{1.31}$$

(de Vaucouleurs, 1948), where R_e is the radius enclosing half of the light.

The observations of stellar velocity dispersion, interpreted in terms of Jeans equation or of the Virial theorem, can provide the total mass for $R < R_e$, or even at larger distances. The Virial theorem for a spherical, steady-state, static isothermal elliptical galaxy reduces to the simple expression

$$2R = \frac{GM}{\sigma^2}, \tag{1.32}$$

where R is a radius and σ^2 a velocity dispertion. The larger the mass, the larger the stellar velocities must be. This formula gives a first approximate mass. In practice much more sophisticated models than this one are used to interpret the velocity dispersions.

Bertin, Saglia and Stiavelli (1992) considered two-component spherically symmetric collisionless self-consistent models, which were used to interpret real data from 10 bright galaxies and found some evidence for dark matter to be of the order of the visible mass. De Paolis, Ingrosso and Strafella (1995) found that dark matter inside R_e is negligible with respect to the visible mass. Carollo et al. (1995) observed flat or gently declining velocity dispersion profiles in four elliptical galaxies, concluding that massive dark halos must be present in three of the four galaxies. It is difficult to draw some conclusions of the present of dark matter in ellipticals on the base steller velocity dispersion.

A small fraction of elliptical galaxies are surrounded by a ring of neutral hydrogen, in these cases, the determination of a dark matter halo is very similar to its determination in spiral galaxies, from the rotation curve. Schweizer, van Gorkom & Seitzer (1989) found evidence for a DM halo in IC 2006 with twice the mass of the luminous matter within $6.5R_e$, under the assumption that the HI ring is flat and circular. Bertola et al. (1993) analyzed five elliptical galaxies, combining the M/L ratios obtained with the inner ionized hydrogen component and the outer neutral hydrogen ring. M/L is constant out to about $R_e \sim 3.5 \pm 0.9$ but becomes very large in the ring region.

The most promising method to study dark matter in ellipticals is based on the existence of X-ray halos. A hot X-ray emitting gas typically extends out to 50 kpc (Forman, Jones & Tucker, 1985). The probable origin of the gas is mass loss from stars. Typical masses of this hot gas are $10^{10} M_{\odot}$.

Hydrostatic equilibrium is usually assumed for the gas. Thus for a spherical DM halo

$$M(R) = -\frac{kTR}{Gm}\left[\frac{d\ln\rho}{d\ln R} + \frac{d\ln T}{d\ln R}\right] \tag{1.33}$$

where ρ is the density of the gas. When $M(R)$ is known, we can obtain the dark matter halo profile.

In this formula, the temperature profile $T(R)$ is not provided by the observations with enough precision. The strengths of some X-ray lines or the shape of the X-ray continuum should provide this T-profile but, in practice, this is still rather problematic.

O'Sullivan & Ponman (2004) analysed a Chandra observation of the elliptical galaxy NGC 4555. They found that NGC 4555 has a large gaseous halo, extending to ~ 60 kpc. The gas temperature is 0.95 keV and the Iron abundance to be $\sim 0.5\ Z_{\odot}$. Authors model the surface brightness, temperature and abundance distribution of the halo and used these results to estimate parameters such as the entropy and cooling time of the gas, and the total gravitational mass of the galaxy. The results show that NGC 4555 has a massive dark halo and large mass-to-light ratio (56.8 $M_{\odot}/L_{B\odot}$ at 50 kpc, 42.7 at $5r_e$, 1 σ errors).

The image splitting of an individual gravitational lens system consisting of an elliptical is only slightly sensitive to the existence of a DM halo, and so, one cannot definitely discriminate between galaxies with and without halos, with some exceptions (Breimer & Sanders 1993, Kochanek 1995). In three cases where the lens is clearly a single galaxy, there is no need to consider any dark matter halo.

Globular clusters have been considered to deduce the existence of dark matter

halos in ellipticals, mainly in M87. Mould et al. (1990) support the conclusions obtained by other methods: models without dark halos do not fit the data in M87.

Romanowsky et al. (2003) studied three intermediate-luminosity elliptical galaxies using the planetary nebula (PN) kinematics. The result was that the galaxies velocity dispersion profiles are found to decline with radius. Dynamical modeling of the data indicates the presence of little if any dark matter in these galaxies halos.

Elliptical galaxies could have dark matter halos similar in mass and extent to those in spiral galaxies, but the evidence is not so clear.

1.4.2 Dwarf spheroidal galaxies

This type of galaxy is probably the most common in the Universe. It's a low luminosity galaxies. But they may contain large amounts of dark matter. Hence contribute greatly to the mass of the Universe. Dwarf spheroidal (dSph) do not have gas in the periphery and the determination of dark matter is more problematic. There are two methods for detecting DM in dwarf spheroidals:

First one is to use the dispersion of stars. This method based on the assumption that its distribution and that of the stars are similar. Mateo et al. (1992) found a M/L ratio ~ 100. Salucci & Persic (1997) found that the relation between luminosity and mass of this galaxies is $\mathrm{M} \sim L^{1/4}$.

If luminous and dark matter have the same spatial distribution, one can trace the central density and the central mass-to-luminosity ratio. From the Virial theorem:

$$\rho_0 = \frac{9\sigma_0^2}{4\pi G R_c^2} \tag{1.34}$$

where ρ_0 is the central density, σ_0 the central velocity dispersion and R_c a core radius. Within this radius the mass is $\rho_0 \frac{4}{3}\pi R_c^3$ and the luminosity is $\sum_0 \pi R_c^2$, where $\sum_0$ is the observable central surface brightness. The M/L ratio would be

$$\frac{M}{L} = \frac{3\sigma_0^2}{\pi G \sum_0 R_c} \tag{1.35}$$

Among the observational difficulties one is that velocity dispersions are low ~ 10 kms^{-1} and thus, a high spectral resolution is required.

The second method is to use the tidal radii. The dwarf spheroidal galaxy considered as the satellite of a primary galaxy (like Milky Way), could become tidally disrupted if it does not have enough dark matter. And thus increasing selfgravitation and preventing it. The radius of the satellite necessary for selfgravitation to match tidal disruption determined by the formula:

$$r = R\left(\frac{m}{M}\right)^{1/3}, \tag{1.36}$$

where r is the radius of dwarf galaxy and m its mass, R is the distance between two galaxies, M is a mass of primary galaxy. At a galactocentric radius equal to the critical value, r, stars would escape and would be trapped in the gravitational field of the primary galaxy. Thus at a tidal radius, r, the density should drop to zero. From the observational standpoint, the "tidal radius" not so easy to define. It is typically measured from the photometric profiles and fits to King-like models. However, tides are likely to elongate systems and cause the velocity distribution to become more radial near the tidal limits of the system (Piatek & Pryor 1995).

Dwarf spheroidals could contain large amounts of dark matter, but the observational difficulties prevent their precise determination.

1.4.3 Dwarf galaxies irregular galaxies

Dwarf irregulars (dIrr's) have a large gaseous companent. Using HI and optical observations of these galaxies can be measured the rotational velocities of these galaxies (like for normal spirals). The stellar component of these galaxies is distributed according to an exponential thin disk as in the spirals. At high luminosities dIrr's barely

join the low-L tail of the spirals, at low luminosities they reach down to $\sim 10^{-3}L_*$. Usually dIrr's have a well defined rotation curves. The maximum rotational velocity is of the order ~ 60 km s^{-1}. The rotation curve rise slowly to the last measured point. Because of the large gaseous companent this type of galaxies gives a possibility to measure the velocity to larger radious, with respect to spirals. Also the absance of the bulge make analyses simpler. The rising rotation curves implies an existance of essential dark matter halo.

Swaters (1999) obtained for 60 rotation curves form the 2.5m INT at La Palma and from Westerbrok Synthesis Radio Telescope. He found that the rotation curves may be steeper and that dark matter may be important in the outer parts only and that the inner parts do not require great amounts of dark matter.

Salucci and Persic (1997) showed that it exist the universal rotation curve (URC) also for the dwarf irregulars. In this case the coefficients α and β will take a form:

$$\alpha = 0.93 \times \left(\frac{V_{opt}}{63 kms^{-1}}\right)^{-0.5}, \tag{1.37}$$

and

$$\beta = 0.08 \times \left(\frac{V_{opt}}{63 kms^{-1}}\right)^{1.2}, \tag{1.38}$$

The halo structural parameters as a function of galaxy luminosity:

$$\beta = 63 \times \left(\frac{L}{0.04 L_*}\right)^{0.16} kms^{-1}, \tag{1.39}$$

The core radious of dIrr's is nearly large as optical radious and the contribution of the visible matter at the optical radius is nearly negligible. Therefore, dwarf irregulars are very dark galaxies, have very dense halos and large masses, with $\sim 8 \times 10^{10}(L/L_{max})$ with $L_{max} = 0.04 L_8$ being the maximum observed luminosity in dwarf irregulars.

1.5 Lensing

Gravitational lensing is a deflection of light rays from distant sources by the gravitational force arising from massive bodies present along the line of sight. Since gravitational light deflection is independent of the nature and state of the matter, it can be used to probe the structure of the dark matter distribution in the Universe, from small to large scales.

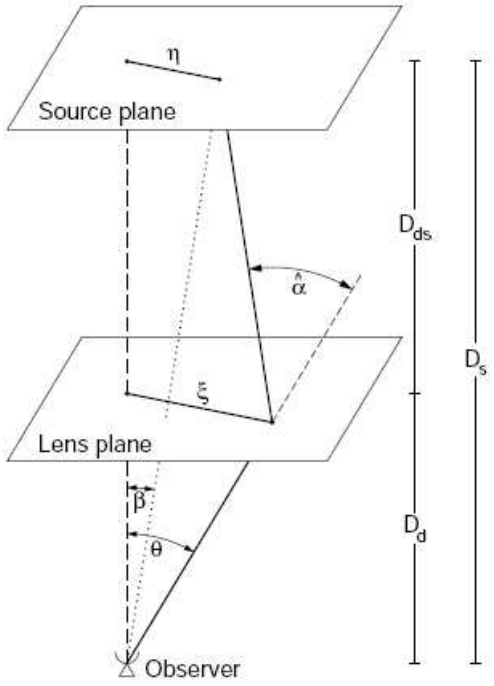

Figure 1.3: Sketch of a typical gravitational lens system

The lens equation relates the true position of the source to its observed position. We define the lens and source plane as planes perpendicular to the line-of-sight to the deflector, at the distance D_d and D_s of the lens and the source, respectively (see Fig. ....). θ is the angle of a light ray relative to the optical axis and β and the angular position of the unlensed source, then:

$$\beta = \theta - \frac{D_{ds}}{D_s}\hat{\alpha}(D_d\theta) \equiv \theta - \alpha(\theta), \tag{1.40}$$

where $\alpha(\theta)$ is the scaled deflection angle, which in terms of the dimensionless surface mass density (Schneider 2003).

Gravitational lensing phenomena fall into two cases: **strong lensing** (see Fig...), where multiple images of a source and arcs in clusters are seen. And **weak lensing** (fig...), where thousands of different sources have their shapes slightly warped in a coherent way.

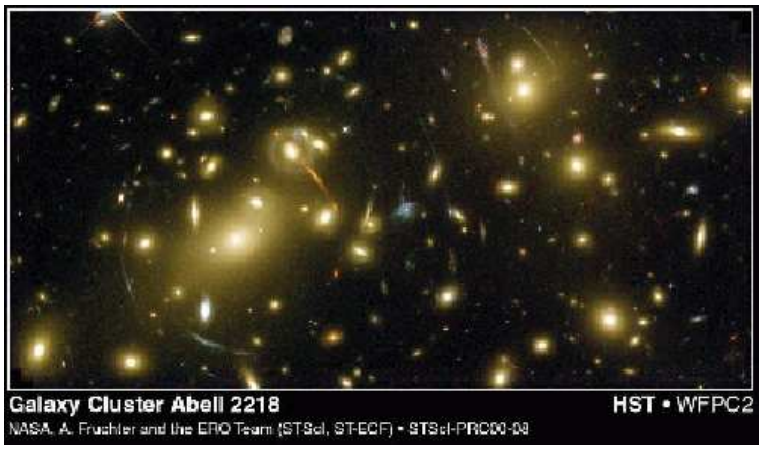

Figure 1.4: The galaxy cluster Abell 2218 ($z = 0.18$) displays an enormously rich structure of arcs, highly stretched images of background galaxies which curve around the main cluster center.

The first **strong lensing** phenomena detected were multiple images of distant $QSOs$ caused by the lensing e ect of a foreground galaxy. Gravitational lens models can be used to constrain the mass distribution in these lensing galaxies. To obtain accurate mass estimates, one needs detailed models, obtained by fitting images and galaxy positions. But a simple mass estimate is possible:

$$M(\theta_E) = \pi(D_d\theta_E)^2 \sum \tag{1.41}$$

The main results for the clusters of galaxies obtained with strong lensing methods

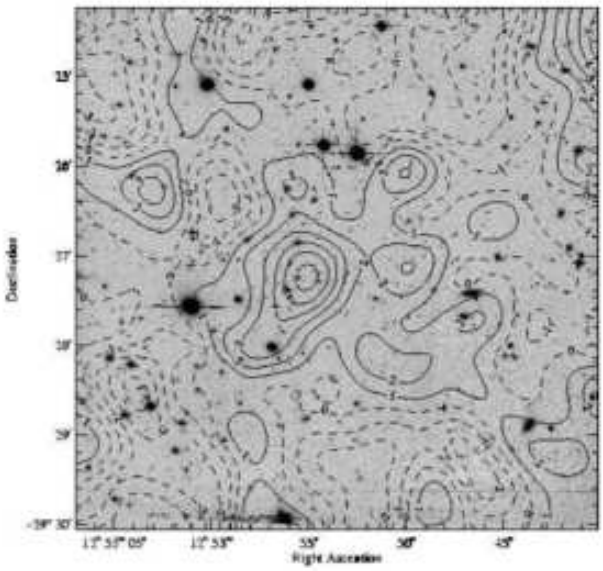

Figure 1.5: Mass reconstruction of the inner part of the galaxy cluster RDCS 1252.9-2927 at $z = 1.24$

are: the mass in cluster centers is much more concentrated than predicted by models based on X-ray observations. The mass distribution in the inner part of clusters often shows strong substructure, or multiple mass peaks. These are also seen in the galaxy distribution of clusters, but with the arcs can be verified to also correspond to mass peaks.

Weak lensing cannot be identified in individual sources, but only in a clusters of galaxies. A massive foreground cluster lens changes the shapes (shear effect) and number density (magnification effect) of the faint background galaxy population. The shear, magnification and combined information can be used to constrain cluster mass profiles.

The main results for the clusters of galaxies obtained with weak lensing methods shows that in many clusters the weak lensing mass estimates are in good agreement with those from dynamical estimates and X-ray determinations. However for the cluster MS1224+20 the mass-to-light ration obtained with lensing is much bigger than the value obtained the dispersion Fischer (1999).

One of the predictions of CDM models for structure formation is that clusters of galaxies are located at the intersection points of filaments. In particular, this implies that a physical pair of clusters should be connected by a bridge or filament of dark matter, and weak lensing mass reconstructions can in principle be used to search for them. Kaiser et al. (1998) for the supercluster MS0302 ($z = 0.42$) found an indication of a possible filament connecting two of the three clusters. Gray et al. (2002) saw a filament connecting the two clusters A901A/901B in their mass recosntruction of the A901/902 supercluster field. The weak lensing technique is a new promissing method (developed during the last 10 years), in the future can give a lot of interesting results about the structure and formation of the galaxies.

1.6 MOND

Here I want to describe briefly an alternative theory to dark matter one. Modified Newtonian dynamics (MOND) is an empirically motivated modification of Newtonian gravity or inertia suggested by Milgrom (Milgrom 1983a,b,c) as an alternative to cosmic dark matter. The basic idea is that at accelerations below $a \approx 10^{-8} cm/s^2 \approx cH_0/6$ the effective gravitational attraction approaches $\sqrt{g_n a_0}$, where g_n is the usual Newtonian acceleration.

The phenomenological basis of MOND consists of two observational facts about spiral galaxies: (1) The rotation curves of spiral galaxies are asymptotically flat and (2) there is a well-defined relationship between the rotation velocity in spiral galaxies and the luminositythe Tully-Fisher law. This latter implies a mass-velocity relationship of the form $M \propto V^{\alpha}$, where α is in the neighborhood of 4.

To modify gravity in order to explain flat rotation curves, an obvious first choice would be to propose that gravitational attraction becomes more like 1/r beyond some length scale that is comparable to the scale of galaxies. So the modified law of attraction about a point mass M would read

$$F = \frac{GM}{R^2} f(R/R_0) \tag{1.42}$$

where R_0 is a new constant of length on the order of a few kpc, and $f(x)$ is a function with the asymptotic behavior: $f(x) = 1$, where $x \ll 1$ and $f(x) = x$, where $x \gg 1$.

All of these modifications attached to a length scale have one thing in common: Equating the centripetal to the gravitational acceleration in the limit $R > R_0$ would lead to a mass-asymptotic rotation velocity relation of form the $V^2 = GM/R_0$.

MOND as initially formulated could be viewed as a modification of inertia or of gravity. In the first case the acceleration of a particle with mass m under the influence of an external force would be given by

$$\mathbf{F} = m\mathbf{a}\mu(a/a_0) \tag{1.43}$$

where a_0 is a new physical parameter with units of acceleration and $\mu(x)$ is a function that is unspecified but must have the asymptotic form $\mu(x) = x$ when $x \ll 1$ and $\mu(x) = 1$ when $x \gg 1$. Viewed as a modification of gravity, the true gravitational acceleration $\mathbf{g}$ is related to the Newtonian gravitational acceleration as $\mathbf{g}_n$ as

$$\mathbf{g}_n = \mathbf{g}\mu(|g|/a_0) \tag{1.44}$$

Although there are clear differences in principle and practice between these two formulations, the consequence for test particle motion in a gravitational field in the low acceleration regime is the same: The effective gravitational force becomes $g = \sqrt{g_n a_0}$. For a point mass M, if one sets g equal to the centripetal acceleration V^2/R, this gives

$$V^2 = GMa_0 \tag{1.45}$$

in the low acceleration regime. Thus MOND tries to explain why all rotation curves of isolated masses are asymptotically flat, and there is a mass-luminosity relation of the form $M \propto V^4$.

1.7 Latests observational evidences for the dark matter existance

1.7.1 X-ray Chandra observations leads to a new discovery

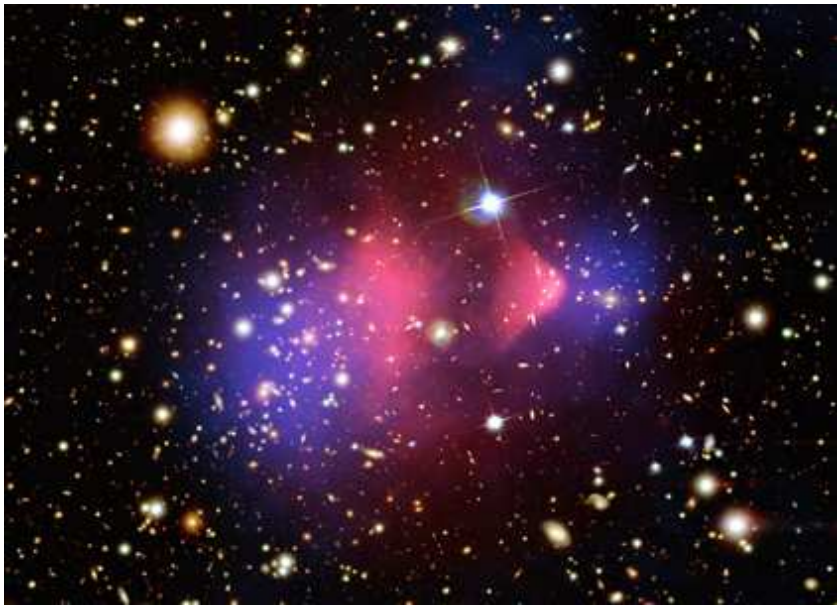

Figure 1.6: X-ray/Optical Composite of 1E 0657-56. Hot gas detected by Chandra in X-rays is seen as two pink clumps. The blue areas show where the most of the mass of the cluster is distributed.

Weak-lensing and X-ray Chandra observations of galaxy cluster 1E 0657-558 shows a strong evidence of dark matter (Clowe et al. 2006). Cluster 1E 0657-558 ($z = 0.296$) is the result of collision of two clusters. The dissipationless stellar component of the cluster and the fluid-like X-ray emitting plasma are spatially segregated. Using both wide-field ground-based images and HST/ACS images of the cluster cores, authors

created gravitational lensing maps showing that the gravitational potential does not trace the plasma distribution, the dominant baryonic mass component, but rather approximately traces the distribution of galaxies. An 8 σ significance spatial offset of the center of the total mass from the center of the baryonic mass peaks cannot be explained with an alteration of the gravitational force law and thus proves the evidence that the majority of the matter in the system is invisible.

1.7.2 A Ringlike Dark Matter Structure in cluster

Recently Jee at al. (2007) have done a mass reconstruction of the galaxy cluster Cl 0024+17 combining both strong- and weak-lensing data. Fig... shows a Hubble Space Telescope (HST) image. The blue streaks near the center of the image are the smeared images of distant galaxies. These individual galaxies are highly distorted by the clusters gravity. Cluster Cl 0024+17 is the result of collision between two massive clusters (Czoske et al., 2002) happened 1-2 Gyr ago. The resulting mass reconstruction reveals the $r \sim 0.4$ Mpc ringlike dark matter structure surrounding the dense core ($r \leq 50$ "). This peculiar substructure is not traced by the ICM nor by the cluster galaxies.

With a high-resolution collisionless N-body simulation, Jee at al. (2007) demonstrated that the ringlike structure can arise by radially expanding, decelerating dark matter shells that once comprised the precollision cores. The shells (and thus the projected ringlike structure) are observed to last even a few Gyr after the core pass-through. On fig. 1.8 shows a superposition of HST image and simulations.

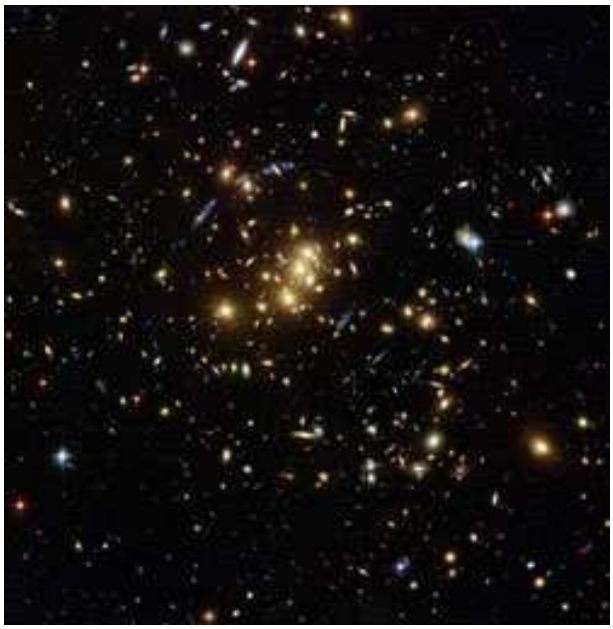

Figure 1.7: HST image of galaxy cluster Cl 0024+17

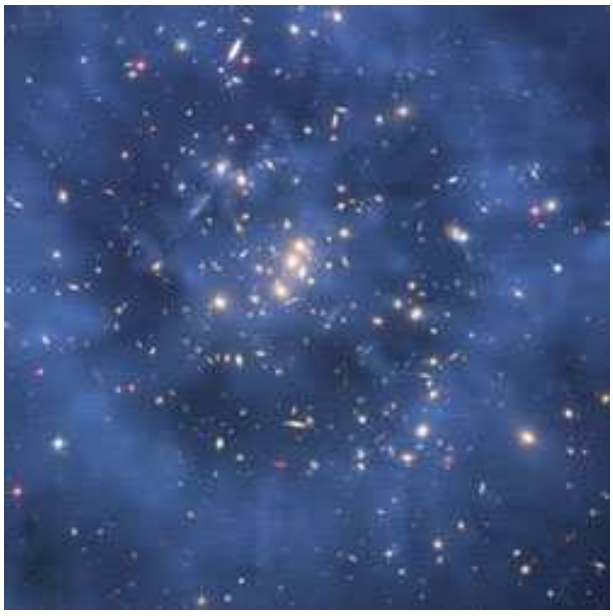

Figure 1.8: Cluster Cl 0024+17. Superposition of HST image and simulations

Chapter 2

Rotation curves of spiral galaxies

In this chapter I will describe the main characteristics of observed rotation curves. Rotation curves of spiral galaxies are one of the main tools used to study the distribution of mass in spiral galaxies. They constitute the best observational proof for the existence of dark matter in spiral galaxies. Rotation curves (RC's) provide important information for understanding the dynamics, evolution, and formation of spiral galaxies.

2.1 Introduction to the problem

The rotation of spiral galaxies was discovered in 1914, by Slipher (1914) when detected inclined absorption lines in the nuclear spectra of M31 galaxy and the Sombrero galaxy. And then by Wolf (1914) when detected inclined lines in the nuclear spectrum of M81 galaxy. It is obvious that the first spiral galaxy to investigate was M31, at that time known as "great nebula in Andromeda". Pease (1918) used the Mt. Wilson 60-in to investigate the rotation of M31 by obtaining a minor axis long slit spectrum with an exposure of 84 h, and a major axis spectrum taken over 79h. The absorption lines extended only 1.5 arcmin in radius along the major axis, that is less than 2% of the optical radius, but were sufficient to show the steep nuclear

velocity rise. Later Babcock (1939) and Mayall (1951) continued studies of M31 and extended major axis rotation velocities to almost 2° from the nucleus.

In the Babcock's mass model for M31 mass-to-light (M/L) ratio is increasing from 18 at r=18' to 62 at r=80'. This caused him to suggest that absorption plays a very important role in the outer parts of the spiral. Or perhaps, that new dynamical considerations are required, which will permit a smaller relative mass in the outer parts. He made a conclusion that the nearly constant angular velocity of the outer parts of M31 galaxy is the opposite of the planetary type of rotation believed to obtain in the outer parts of the Galaxy. Oort (1940) studying NGC 3115 noted that the distribution of mass appears to bear almost no relation to that of the light. Babcock and Oort share credit for uncovering the dark matter problem in individual spiral galaxies.

The modern era of optical observations of spiral galaxies rotation velocities becomes from Page (1952). And later Burbidge & Burbidge (1960), which exploited the new red sensitivity of photographic plates to observe the Hα and [NII] emission lines arising from HII regions within spiral disks.

Early radio observations of neutral hydrogen in external galaxies by van de Hulst et al. (1957) showed a slowly falling rotation curve for M31. And Volders (1959) showed a flat rotation curve for M33. The first published velocity field (spider diagram) was of M31 Argyle (1965). For M33, the flatness could be attributed to the side lobes of the beam and was consequently ignored.

Rotation curves are tools for several purposes: for studying the kinematics of galaxies; for inferring the evolutionary histories and the role that interactions have played; for relating departures from the expected rotation curve form to the amount and distribution of dark matter; for observing evolution by comparing rotation curves in distant galaxies with galaxies nearby. Rotation curves derived from emission lines such as Hα, HI, and CO lines, are particularly useful to derive the mass distribution in disk galaxies, because they manifest the motion of interstellar gas of population I,

which has much smaller velocity dispersion, of the order of 5-10 km s^{-1}, compared with the rotation velocities.

2.2 Data and measurements

2.2.1 Data

Optical measurements. Optical observations have several observing techniques for determining rotation curves and velocity fields for both ionized gas and stars (see Fig 2.1, 2.2, 2.3). The basic principle is to measure the Doppler shift of the spectral lines at different positions along the slit, hence on both sides of the center of the galaxy. Usually long slit spectra is used for obtaining the rotation curve of a galaxy from emission lines (Rubin et al. 1980, 1985, Mathewson et al. 1992, Mathewson & Ford 1996). The emission lines are: hydrogen Hα line (6562.8 $\mathring{A}$), nitrogen NII lines (6548.03 $\mathring{A}$, 6583.41 $\mathring{A}$) and sulfur SII lines (6716.47 $\mathring{A}$, 6730.84 $\mathring{A}$). There are also methods that return the entire velocity field, such as Fabry-Perot spectrographs or integral (fiber-optic) field instruments , they offer more velocity information, however, at the price of more complex and time-consuming reductions.

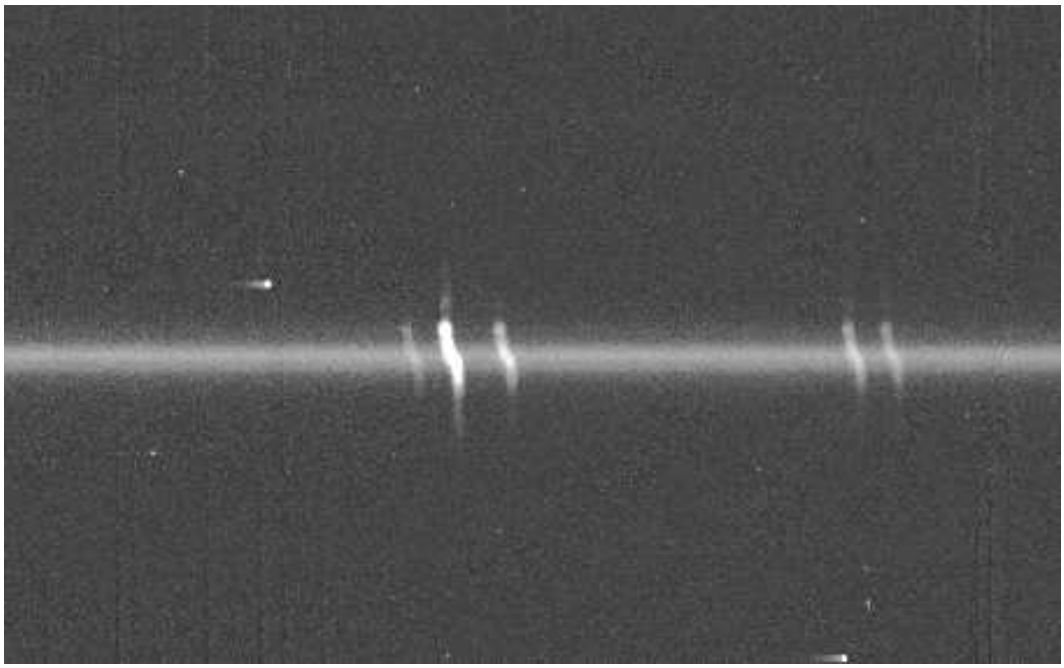

Figure 2.1: Spectrum of IC1210 galaxy with Hα, NII and SII lines

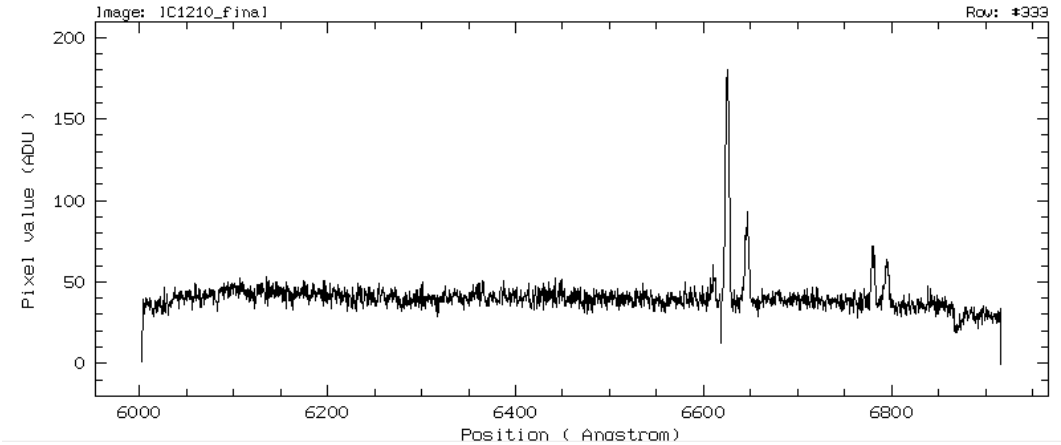

Figure 2.2: The central profile of the spectrum of IC1210 galaxy

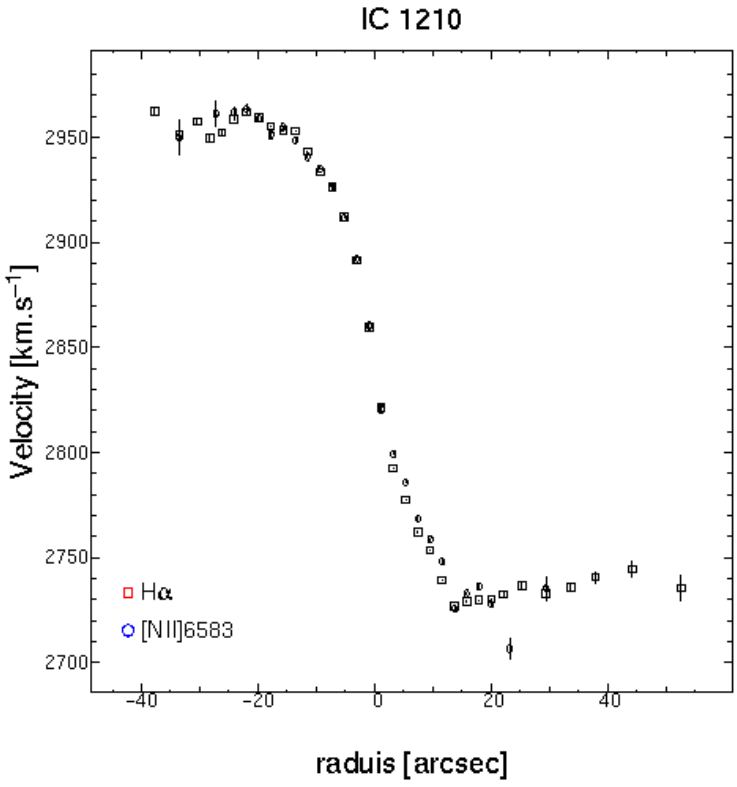

Figure 2.3: Rotation curve of IC1210 galaxy

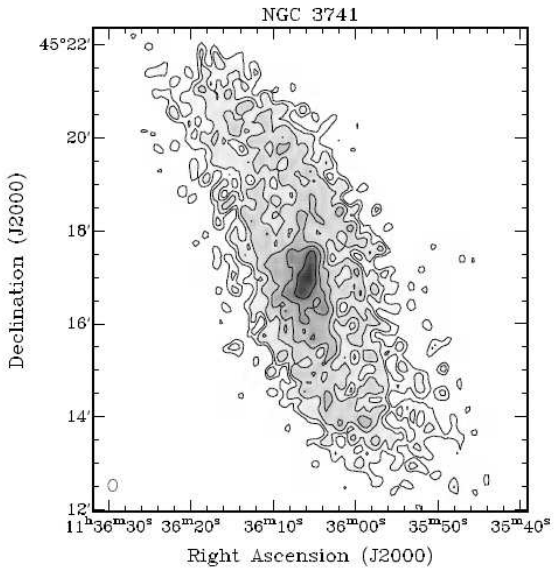

Figure 2.4: Spiral galaxy NGC 3741. HI total intensity map the high-resolution cube.

Radio measurements. The HI line produced by neutral hydrogen is a powerful tool to obtain kinematics of spiral galaxies. Sometimes its radial extent can be greater 3 or 4 times, than that of visible disk. Instrumental improvements in the past 20 years have increased the spatial resolution of the beam. In Fig. 2.4 I show the example of HI observations for the spiral galaxy NGC 3741 made with the WSRT telescope (from Gentile et. al 2007).

CO line. The rotational transition lines of carbon monoxide (CO) in the millimeter wave range are used in studying rotation kinematics of the inner disk and central regions of spiral galaxies (see Fig.2.6). The wavelength range is 115.27 GHz for ^{12}CO (J= 1-0) line and 230.5 GHz for J = 2-1 line. At CO wavelengths the central dusty disks are negligible for extinction. Edge-on and high-inclination galaxies are particularly useful for rotation curve analysis. In order to minimize the uncertainty arising from inclination corrections, for which extinction-free measurements are crucial, especially for central rotation curves.

Since the central few kiloparsecs of the disk are dominated by molecular gas

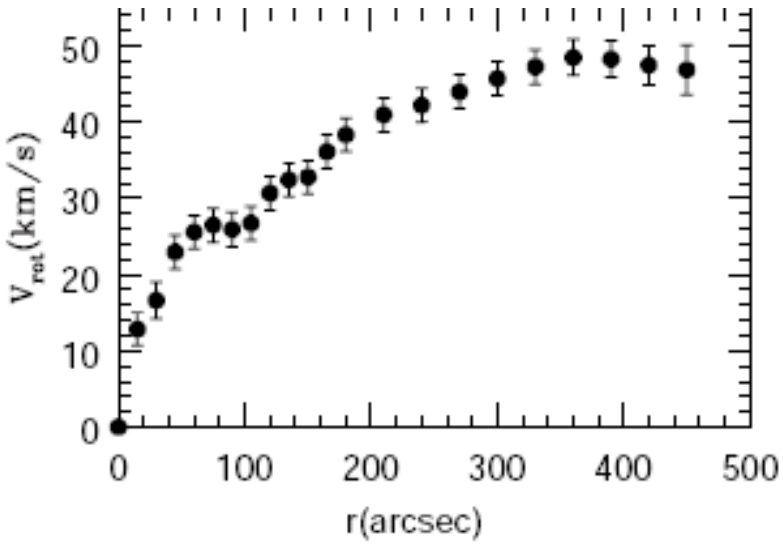

Figure 2.5: Rotation curve for NGC 3741. From Gentile et al. 2007

(Nishiyama & Nakai 1998), the molecular fraction, the ratio of the molecular-gas mass density to that of total molecular and HI masses, usually exceeds 90% (Sofue et al. 1995). CO lines are emitted from molecular clouds associated with star formation regions emitting the Hα line. The Hα, HI and CO rotation curves agree well with each other in the intermediate region disks of spiral galaxies (Sofue 1996, Sofue et al. 1999a,b).

Maser lines. Radial velocity observations of maser lines, such as SiO, OH, and H_2O lines, from circumstellar shells and gas clouds also allow us to measure the kinematics of stellar components in the disk and bulge of our Galaxy.

2.2.2 Measurements

Intensity-velocity method. A rotation curve of a galaxy is defined as the trace of velocities on a position velocity diagram along the major axis, corrected for the angle between the line of sight and the galaxy disk. A widely used method is to trace intensity weighted velocities (Warner et al. 1973). These are defined by

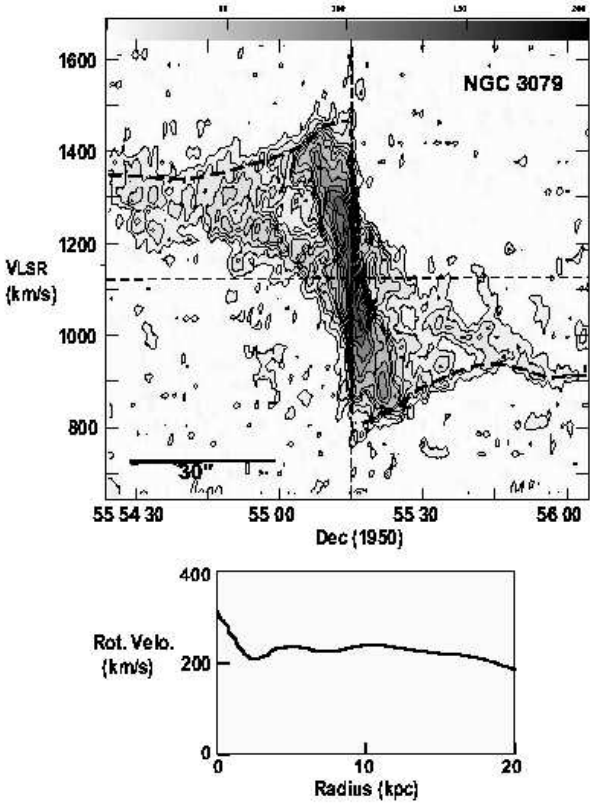

Figure 2.6: Position-velocity diagram along the major axis of the edge-on galaxy NGC 3079 in the CO (J = 1 - 0) line emission at a resolution of 1."5 observed with the 7-element interferometer consisting of the six-element millimeter-wave array and the 45-m telescope at Nobeyama (Sofue et al. 1999b). The lower panel shows a composite rotation curve produced by combining the CO result and HI data (Irwin & Seaquist 1991) for the outer regions.

$$V_{int} = \frac{\int I(v) v \, dv}{\int I(v) \, dv} \tag{2.1}$$

where $I(v)$ is the intensity profile at a given radius as a function of the radial velocity. Rotation velocity is then given by

$$V_{rot} = \frac{V_{int} - V_{sys}}{sini} \tag{2.2}$$

where i is the inclination angle and V_{sys} is the systemic velocity of the galaxy.

Centroid-velocity and peak-intensity-velocity methods. In outer galactic disks, the line profiles can be assumed to be symmetric around the peak-intensity value. Thus the intensity-weighted velocity can be approximated by a centroid velocity of half-maximum values of a line profile (Rubin et al. 1980, 1982a, 1985). Or it can be approximated by a velocity at which the intensity attains its maximum, peak-intensity velocity (Mathewson et al. 1992, Mathewson & Ford 1996). Both methods are used to derive rotation curves from the emission lines. But in the inner regions where the line profiles are superpositions of outer and inner-disk components, these two methods often underestimate the true rotation velocity.

Envelope-Tracing Method. The envelope-tracing method is using the terminal velocity V_t in a position-velocity diagram along the major axis. The terminal velocity is defined by a velocity at which the intensity becomes equal to

$$I_t = [((\eta I_{max})^2 + I_{lc}^2)]^{1/2}, \tag{2.3}$$

where I_{max} and I_{lc} are the maximum intensity and intensity corresponding to the lowest contour level, η is usually taken in the interval 0.2-0.5.

The rotation velocity is derived by using the terminal velocity V_t:

$$V_{rot} = \frac{V_{int} - V_{sys}}{sini} - (\sigma_{obs}^2 + \sigma_{ISM}^2)^{1/2}, \tag{2.4}$$

where σ_{obs} is the velocity resolution of observations, and σ_{ISM} is the velocity dispersion of the interstellar gas.

This method is not very strong in the innermost part of the position-velocity diagram. The two sides of the nucleus have a discontinuity at the nucleus due to the instrumental resolution.

Integration method. This method includes the following procedure. An initial rotation curve, RC_{in}, is adopted from a position-velocity diagram, PV_{in} (with the help of one of the method as above). Using this rotation curve and an observed radial distribution of intensity of the line, a $PV1$ diagram, is constructed. The difference between this calculated PV1 diagram and the original RC_{in}, e.g., is used to correct the initial rotation curve to obtain a corrected rotation curve, RC1. This RC is used to calculate another diagram, $PV2$, using the observed intensity distribution. And to obtain the next iterated rotation curve, $RC2$, (by correcting for the difference between $PV2$ and PV_{in}). This iteration is repeated until PVi and PV_{in} becomes identical, such that the summation of root mean square of the differences between PVi and PV_{in} becomes minimum and stable.

Absorption line velocities. The Fourier quotient technique (Simkin 1974, Sargent et al. 1977) and the correlation technique (Bender 1990) are methods to determine the rotation velocities in early type galaxies. Both methods assume that the stellar absorption can be fit by a Gaussian profile. However, recent instrumental improvements confirm that even disk galaxies consist of multicomponent kinematic structures, so more sophisticated methods of analysis are required to reveal velocity details of the separate stellar components. Various methods have been proposed to account for the non-Gaussian form of the line-of-sight velocity distribution.

Disk galaxies are a complex combination of various structural components. Observations from emission lines and absorption lines in the optical, millimeter, and radio regions may not sample identical regions along the same line of sight. Therefore the choice of the method depends on the task (i.e. in which region one is more interested).

2.3 Shapes of rotation curves

The overall similarity of shapes of rotation curves for spiral galaxies has led to a variety of attempts to categorize their forms, and to establish their statistical properties. Rubin et al. (1985) formed synthetic rotation curves as a function of luminosity for families of Sa, Sb, and Sc galaxies. Casertano & van Gorkom (1991), using velocities from HI data, studied rotation curves as a function of luminosity. Mathewson et al. (1992) and Mathewson & Ford (1996) used their massive set of Hα rotation curves together with optical luminosity profiles for 2447 southern galaxies to examine the Tully-Fisher (TF) (Tully & Fisher 1977) relation.

Persic & Salucci (1995) and Persic, Salucci & Fulvio (1996) using 1100 optical and radio rotation curves found the exitance of a universal rotation curve (URC). It means that the ***shape*** and ***amplitude*** of the observed rotation curves of spiral galaxies highly depends on their ***luminosity***. URC demonstrate that *high luminosity galaxies* show a *slightly declining* rotation curve in the outer part, following a broad maximum in the disk. *Intermediate galaxies* have *nearly flat* rotation across the disk. *Low luminosity* galaxies have monotonically *increasing* rotation velocities across the optical disk. It implies that for the low luminosity galaxies the dark matter contribution is bigger than for the high luminosity galaxies.

Catinella et al. (2006) studied a sample of $\sim$ 2200 low-redshift disk galaxies and reconstructed the template rotation curves. For the less luminous galaxies they found the same result of the URC. But for the more luminous galaxies there is a disagreement (I will discuss it more in the Chapter 5).

I have to note that in clusters of galaxies a variety of physical mechanisms can alter the internal kinematics of spirals. Gas stripping, star stripping, galaxy-galaxy encounters, and interaction with the general tidal field are all likely to occur. Early studies of optical rotation curves for galaxies in clusters detected a correlation between outer rotation velocity gradients and distances of galaxies from the cluster center

(Rubin et al. 1988, Whitmore et al. 1988, 1989). however later studies do not confirm this result. A study of spiral galaxies in Virgo (Rubin et al. 1999) shows that about half of the galaxies have disturbed rotation curves. Abnormalities include asymmetrical rotation velocities on the two sides of the major axis, falling outer-rotation curves, inner-velocity peculiarities.

Last years using the HST and VLT telescopes have been obtained the rotation curves for distant galaxies. We directly observe galaxy evolution by studying galaxies closer to their era of formation.

Rotation velocity is a fundamental parameter of galaxy dynamics and evolution. The TF relation (Tully & Fisher 1977) which is the correlation between the velocity and luminosity of the galaxy represents an oblique projection of the fundamental plane of spiral galaxies. This plane defines a three-dimensional relationship between the radius, rotation velocity, and luminosity (absolute magnitude). The TF relation emphasizes the essential role that rotation curves play in determining the principal galactic structures, and in our understanding of the formation of disk galaxies. I will discuss more the TF relation in the Chapter 3.

2.4 Galaxy types and rotation characteristics

In the previous section we have seen that the shape of the ***rotation curve*** depends on the luminosity of the galaxies. But it also depends on the ***total mass*** and ***morphological type***.

Massive galaxies of the Sa and Sb types show steeper rises and higher central velocities within a few hundred parsecs of the nucleus compared with less-massive Sc galaxies and dwarfs. Dwarf galaxies generally show gentle central rises.

For the galaxies with the same luminosity the maximum rotation velocity is higher for Sa galaxies than for Sb and Sc. Median values of V_{max} decrease from 300 to 220 to 175 kms^{-1} for the Sa, Sb, and Sc types, respectively (Rubin et al. 1985, Sandage

2000).

Sb galaxies have steep central rise at 100-200 pc that is associated with a velocity peak at radii $r \sim$ 100-300 pc. The rotation velocity then declines to a minimum at $r \sim 1$ kpc and is followed by a gradual rise to a broad maximum, arising from the disk potential. The disk rotation curve has superposed amplitude fluctuations of $\sim$ 10 kms^{-1} per caused mainly by spiral arms.

Sc galaxies show steep nuclear rises similar to those of *Sb* galaxies.

Large-scale rotation properties of *SBb* and *SBc* galaxies are generally similar to those of nonbarred galaxies of *Sb* and *Sc* types. However, the study of their kinematics is more complicated because their gas tracers are less uniformly distributed. Barred galaxies show velocity jumps from 30 kms^{-1} to 100 kms^{-1} on the leading edges of the bar, R $\sim$ 2-5kpc (for nonbarred spirals the variation is about $\sim$ 10-20 kms^{-1}, caused mainly by spiral arms). Barred galaxies require a more complete velocity field to understand their kinematics.

Chapter 3

The Radial Tully-Fisher relation for spiral galaxies

In this Chapter we have studied three different samples of rotation curves of spiral galaxies. We have found a new Tully-Fisher-like relation for spiral galaxies holding at different galactocentric radii. We call this relation as Radial Tully-Fisher (RTF) relation. We found that it allows to investigate the distribution of matter in the optical regions of spiral galaxies. This relation, proves that: 1) the rotation velocity of spirals is a good measure of their gravitational potential and both the RC's amplitudes and profiles are well predicted by galaxy luminosity 2) the existence of a dark component, less concentrated than the luminous one, and 3) a scaling law, according to which, inside the disk optical size: $M_{dark}/M_{lum} = 0.5(L_B/10^{11}L_{B\odot})^{-0.7}$.

3.1 The Tully-Fisher relation and new approaches

In 1977 Tully and Fisher discovered that the maximal rotational velocity V_{max} of a spiral galaxy, measured by the FWHM of the neutral hydrogen 21-cm line profile, correlates with the galaxy luminosity by means of a power law of exponent $a \sim 4$.

This equivalently reads as:

$$M = a \log V_{max} + b \tag{3.1}$$

with M the absolute magnitude in some specified band and b a constant. It was immediately realized that this relation, hereafter TF, could serve as a powerful tool to determine the distances of galaxies Pierce & Tully (1988) and to study their dynamics Persic & Salucci (1988). The rotational velocity reflects the equilibrium configuration of the underlying galaxy gravitational potential, especially when V_{max} is directly derived from extended rotation curves. Before proceeding further, let us point out that spiral galaxies have a characteristic size scale, R_{opt}, that sets also a characteristic reference velocity $V(R_{opt})$. R_D, the exponential thin disk length scale, is a natural choice for such reference radius; in this paper, however, we adopt for the latter a minimal variant, i.e. a multiple of this quantity: $R_{opt} \equiv 3.2R_D$ (see Persic, Salucci & Stel 1996, hereafter PSS). (No result here depends on the value of the multiplicity constant). This choice is motivated by the fact that $3.2R_D$, by enclosing 83% of the total light, is a good measure of the "physical size" of the stellar disk, and that, for many purposes, $V_{opt} \equiv V(R_{opt}) = V_{max}$. [1]

Some known kinematical quantities are not suitable reference velocities. For example, the value of V_{max} for a spirals depends on the extension and on the spatial resolution of the available RC and, in addition, it does not have a clear physical interpretation, sometimes coinciding with the outermost available velocity measure, in other cases with the innermost one. Also V_{last}, the velocity at the outermost measured point obviously does not have a proper physical meaning, in addition some spirals never reach the, so called, asymptotic flat regime (PSS and Salucci & Gentile 2006).

Coming back to the TF relation, its physical explanation, still not fully understood, very likely involves the argument that in self-gravitating rotating disks both the rotation velocity and the total luminosity are a measure of the same gravitational mass (e.g. Strauss & Willick 1995). Notice that, if this argument is correct, both

[1] For the PS95 sample: $\log V_{opt} = (0.08 \pm 0.01) + (0.97 \pm 0.006) \log V_{max}$.

V_{max} and V_{last} are just empirical quantities of different and not immediate physical meaning.

The existence of the TF can be understood as it follows. The stars in spiral galaxies are essentially settled in thin disks with an exponential surface mass distribution (Freeman 1970)

$$\Sigma(R) = \Sigma_0 e^{-R/R_D} , \quad \Sigma_0 = k_1 L^s , \tag{3.2}$$

where k_1 and s are constants, $\Sigma_0 = (M_d/L)I_0$ is the central surface mass density with I_0 the central surface brightness, that in first approximation, can be set constant among spirals. L and M_D are the total luminosity in a specific band and the disk mass. Since from eq (2): $M_D \propto \Sigma_0 R_D^2$, the above approximation implies: $R_D \propto L^{0.5}$. Let us now consider the condition of self-gravity equilibrium for the stellar disk, i.e. the ratio $E = GM_D/(V_{opt}^2 R_{opt})$. By writing:

$$E = k_2 L^t , \tag{3.3}$$

where k_2 and t are constants, we have that Freeman disks are completely self-gravitating for $k_2 \simeq 1.1$ and $t = 0$. By setting $s = 0$, i.e. by assuming that the disk mass-to-light ratios are constant among spirals, we arrive at the well known relation: luminosity $\propto$ (velocity)^4. Random departures from the above conditions induce a larger scatter in the TF relation, while systematic departures, e.g. variations of the stellar population with galaxy luminosity or violation of the condition of self-gravity, modify slope, zero-point and scatter, possibly in a band-dependent way. More generally we can write: $L \propto V_{opt}^{2/(s+0.5-t)}$ (here s and t can be band-dependent) while we can also envisage a more complex and perhaps non-linear relationship, if the above scaling laws are not just power laws and I_0 varies among galaxies. From an observational point of view, by studying several large samples of galaxies, it has been found that the TF has different slope and scatter in different bands: $a_I \simeq 10$, $s_I \sim 0.4$mag, while $a_B \simeq 7.7$, $s_B \sim 0.5$mag (e.g. Pierce & Tully 1992, Salucci et al. 1993). Furthermore, a non linearity in the TF is often found at low rotation velocities (Aaronson et al

1982).

We know that spiral galaxies are disks of stars embedded in (almost) spherical halos of dark matter and this is crucial for understanding the physical origin of the TF relation (Persic & Salucci 1988, Strauss & Willick 1995, Rhee 1996). It is well known that the dark halos paradigm is supported by the (complex) mass modelling of galactic rotation curves (e.g. PSS and references therein) and it implies that disks are not fully self-gravitating. At any radius, both the dark and luminous components contribute to the (observed) rotational velocity $V(R)$, with a relative weight that varies both radially and from galaxy to galaxy. The resulting model circular velocity can be written as a function of the useful radial coordinate $x \equiv R/R_{opt}$ as [2] :

$$V_{model}(x) = (GM_D/R_D)^{1/2}\,[f_d(x)/f_d(1) + \Gamma f_h(x,\alpha)]^{1/2}, \tag{3.4}$$

where $f_d(x)$ is the Freeman velocity disk profile

$$f_d(x) = \frac{1}{2}(3.2x)^2(I_0(1.6x)K_0(1.6x) - I_1(1.6x)K_1(1.6x))\,, \tag{3.5}$$

and

$$f_h(x,\alpha) = (\frac{x^2}{x^2+\alpha^2})(1+\alpha^2), \tag{3.6}$$

M_D is the disk mass, Γ is the ratio of the squared velocities of the dark-to-visible matter at R_{opt} and α is the halo velocity core radius in units of R_{opt}. The adopted halo function $f_h(x,\alpha)$ (see PSS) is the simplest way to describe, inside the optical radius, the contribution of dark matter halo; in fact, for an appropriate value of the parameter α, in $V_{model}(x)$, it describes both the "empirical" universal rotation curve halo velocity profile in PSS and, (by setting $\alpha = 1/3$) the N-Body' ΛCDM $V_{NFW}(x)$ Navarro-Frenk-White halo velocity profile.

Let us point out that, given the existence of the TF relation ($L \propto V_{opt}^k$, $k = const$), with the circular velocity described by eq (3.4), any dependence on luminosity of the mass distribution parameters Γ and α triggers, at radii jR_{opt} ($j = 0.2 - 1.4$), a whole

[2]For simplicity here we neglect the bulge, we will consider it in section 4.

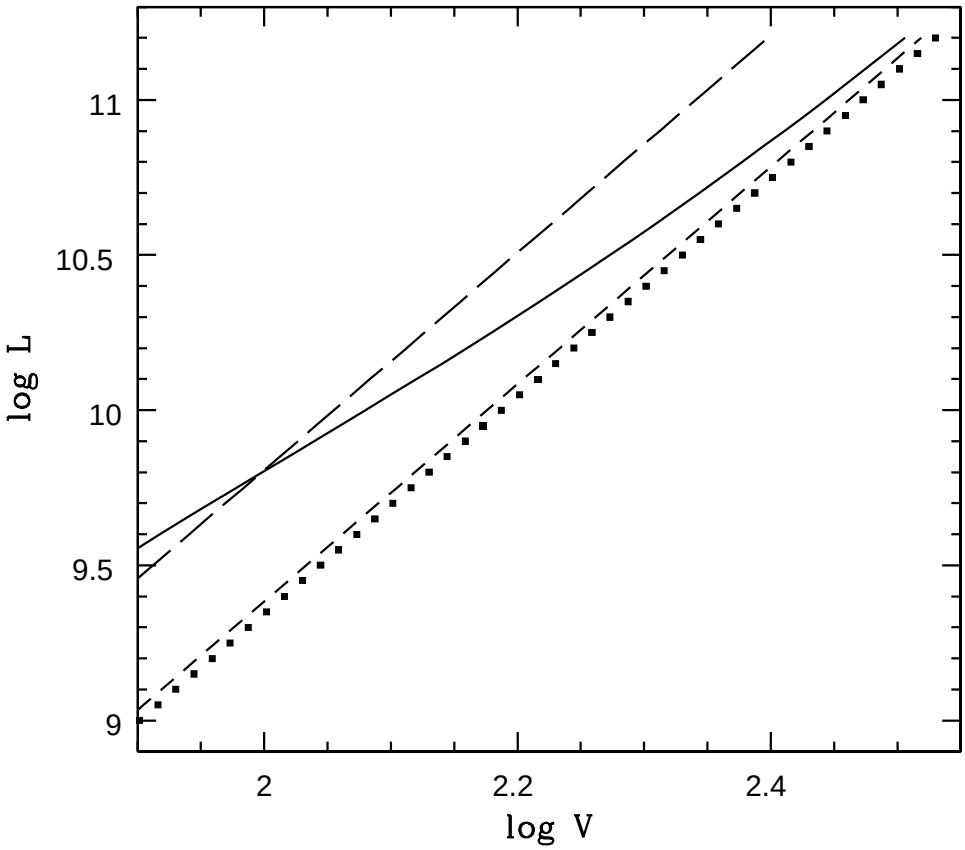

Figure 3.1: The TF relation at R_{opt} (*squares*) and the predicted relation at $0.6R_{opt}$ in the cases of: no-DM (*short dashed line*), $\Gamma = 1$ NFW halo (*long dashed line*), the URC mass model (see text, *solid line*).

family of relationships, similar to the TF one, but with slopes, scatters and zero points all different and all depending on the detailed characteristics of the mass distribution.

We show this in figure 3.1 where, from the *empirical* (TF) relation

$$L_B = \left(\frac{V_{opt}}{200km/s}\right)^{3.5} 10^{11}\ L_{B\odot}, \tag{3.7}$$

holding at R_{opt} we predict the new relation that holds at an inner radius according to specific mass models. Among those, it is worth to discuss in detail for the model that underlies the URC: i.e. $\Gamma = 0.5(L_B/(2.5 \cdot 10^{10} L_{\odot}^{0.2}))^{-0.9}$; $\alpha = 1.5(L_B/(5 \cdot 10^{10} L_{\odot}))^{0.2}$. In this case the predicted slope decreases from 3.5 at R_{opt} to 2.75 at 0.6 R_{opt} and to 2.5 at 0.4 R_{opt}. If above is considered just as a toy model obviously the predicted slopes do not carry any uncertainties, if, instead, it is considered as URC mass model, they carry a 15% uncertainty due propagation errors from Γ and α.

Therefore the Universal Rotation Curve paradigm implies, in addition to a Universal Velocity Profile at any chosen luminosity, also a "TF like" relationship at any chosen radius JR_{opt}, whose actual characteristics, however, are not investigated in PSS, and are not easy to recover from the underlying mass model.

This will be instead easily done in this chapter, meant to be complementary to PSS: we will come back to the rotation curves (RCs henceforth) to directly investigate them extracting from actual data the Radial Tully-Fisher relation (RTF), i.e. a family of TF-like relations holding at any properly chosen radial distance. To ensure a better statistical coverage this will be repeated for three samples of spirals with different selection criteria and reference Luminosity Bands. These samples mostly contain Sb-Sc spiral galaxies with the number of early type spirals and dwarfs being very small. Moreover, in general, the bulge affects only the first reference radius. Different investigation will be necessary to assess the present results in bulge dominated spirals and HI dominated dwarfs.

Finally, we will use the properties of such relationships to investigate the mass distribution in late type Spirals.

3.2 Data and analysis

Sample 1 consists of 794 original RCs of PS95 (note that for most of them the limited number of independent measurements and sometimes some non-circular motion make it difficult to derive a proper mass model, but instead this can be done with the method in section 2,3).

In each RC the data are radially binned on a $0.2R_{opt}$ scale so that we have 4-7 independent and reliable estimates of the circular velocity, according to its extension.

Sample 2 from Courteau (1997) consists of 86 RC's (selected from 304 galaxies) and Sample 3 of Vogt (2004) 81 RC's (selected from 329 galaxies). These samples have been built by selecting from the original samples only objects with high quality and high resolution kinematics yielding reliable determinations of both *amplitudes* and *profiles* of the RCs. To ensure this, we have set the following selection criteria. The RC's must: *(a)* extend out to $\simeq R_{opt}$; *(b)* have at least 30 velocity measurements distributed homogeneously with radius; and *(c)* show no global asymmetries or significant non-circular motions: the profiles of the approaching and receding arms must not disagree systematically by more than 15% over $1R_d$ length-scale. The velocity errors are between $1\% - 3\%$.

In each galaxy we measure the distance from its center R in units of R_{opt} ($R_{opt} \equiv 3.2R_D$) and we consider a number of radial bins centered at $R_n = (n/5)R_{opt}$ for the PS95 sample and at $R_n = (n/20)R_{opt}$ for the other two samples; we take the bin size $\delta = 0.2R_{opt}$ for the PS95 sample and $\delta = 0.06R_{opt}$ for the other two samples. Then we co-add and average the velocity values that fall in the bins, i.e. in the radial ranges $R_n - \delta/2 \leq R_n \leq R_n + \delta/2$ and we get the average circular velocity V_n at the chosen reference radii R_n. (For the PS95 sample this was made in the original paper).

A "large" radial bin size has been chosen for the (much bigger) PS95 sample because, by selection, most of its RCs have a relatively smaller number of measurements. For the other two samples, that, exclusively include extended high quality RC and

large number of measurements we decrease the bin size by a factor 3.2.

In short, we will use two different kind of samples: sample 1 includes 794 Sb-Sd galaxies with I magnitudes whose RCs are estimated inside large radial bins that smooth out non circular motions and observational errors; samples 2 and 3 include 167 galaxies with R magnitudes, whose RCs of higher quality are estimated inside smaller radial bins providing so a larger number of independent data per object.

We look for a series of correlations, at the radii R_n between the absolute magnitude M (in bands indicated below) and $\log\ V_n \equiv \log\ V(R_n)$. Data in the I Mathewson et al (1992) and r Courteau (1996), Vogt et al (2004) bands will allow us to check the dependence of our results on the type of stellar populations in spiral galaxies. Finally let us stress that the uncertainties of photometry are about 10% and therefore negligible.

3.3 The Radial TF relationship

Given a sample of galaxies of magnitude M_{band} and reliable rotational curves, the Radial Tully-Fisher (RTF further on) relation is defined, as the ensemble of the fitting relationships:

$$M_{band} = a_n \log V_n + b_n\,, \tag{3.8}$$

with a_n, b_n, the parameters of the fits and R_n the radial coordinates at which the relationship is searched. The latter is defined for all object as a fixed multiple of the disk length-scale (or equivalently of R_{opt}). Parameters a_n, b_n are estimated by the least squares method (without considering the velocity/magnitude uncertainties).

The existence of the Radial TF relation is clearly seen in Fig. 3.2 and Fig. 3.3, where all the TF-like relations for the PS95 sample are plotted together and identified with a different color. It is immediate to realize that they mark an ensemble of linear relations in log-log representation whose slopes and zero-points vary continuously with the reference radius R_n.

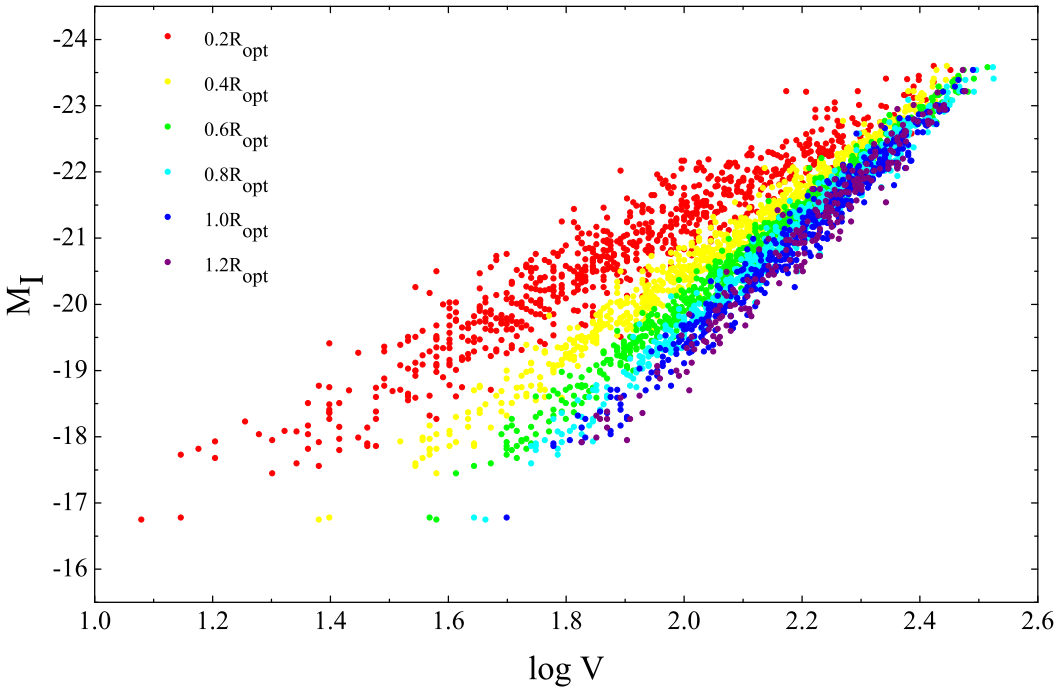

Figure 3.2: The Radial Tully-Fisher relations for the PS95 sample. Each one of the 6 relations is indicated with different color.

Independent Tully-Fisher like relationships exist in spirals at any "normalized" radius R_n. We confirm this in a very detailed and quantitative way in the Figures 3.11, 3.12 and in the Tables 3.1, 3.2, 3.3, where very similar results are found for the other two samples. It is noticeable that the various investigations lead to the same consistent picture.

The slope a_n increases monotonically with R_n; the scatter s_n has a minimum at about two disk length-scales, $0.6R_{opt}$. In the I-band the values of the slopes are about 15% larger than those in the r-band. This difference, well known also for the standard TF, can be interpreted as due to the decrease, from the r to the I band, of the parameter s (see Eq. 2), as effect of a different importance in the luminosity of the population of recently formed stars (Strauss&Willick 1995).

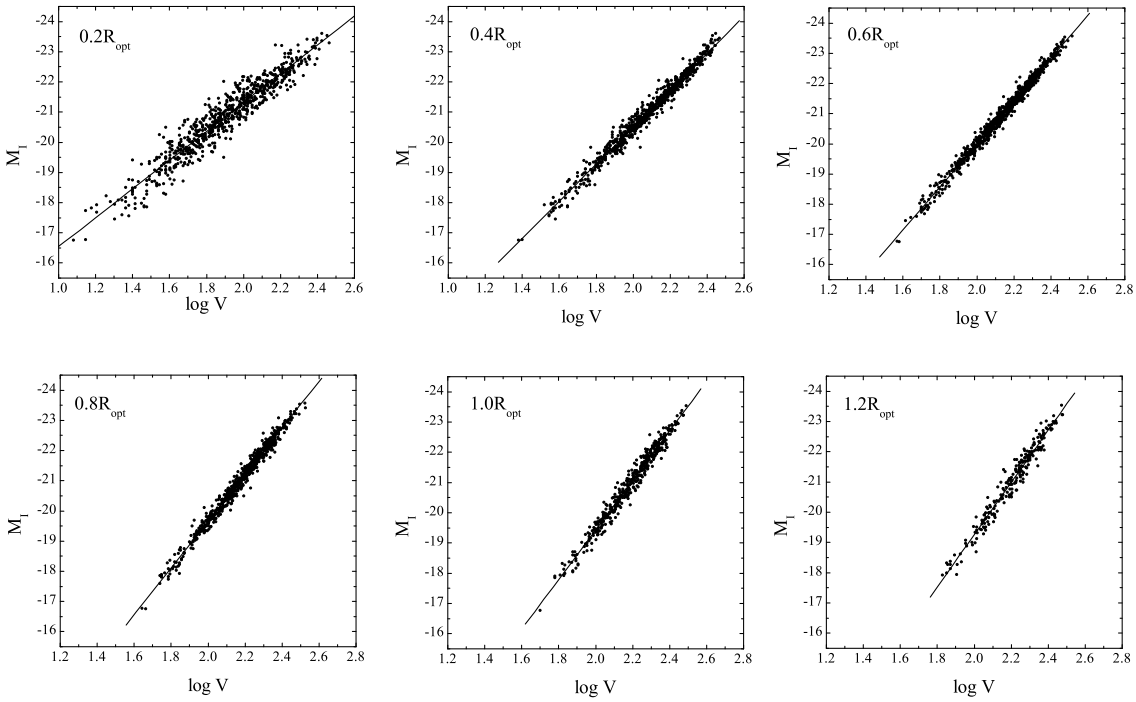

Figure 3.3: The Radial Tully-Fisher relation for the PS95 sample.

It is possible to compare the RTFs in different bands; in the case of absence of DM, true in the inner regions of spirals (except in the very luminous galaxies and LSB almost absent in our sample), for the reasonable values $s_r = 0.1$ and $s_I = 0$ the power law coefficient of the L_I vs velocity relationship is larger by a factor $(0.5+s_r)/(0.5+s_I)$ than that of the L_r vs velocity relationship, in details by a factor 1.2. This correction allows us to compare the a_n slopes as a function of R_n for our samples (see Figure 3.4). Remarkably, we find that the values of the slopes vary with R_n according to a specific pattern:

$$b_n = -2.3 - 9.9(R_n/R_{opt}) + 3.9(R_n/R_{opt})^2 \,. \tag{9}$$

It is worth to look at the scatter of the Radial TF relation (see Fig.3.5). We find that, near the galactic center the scatter is large $0.3 - 0.4$ dex, possibly due to a

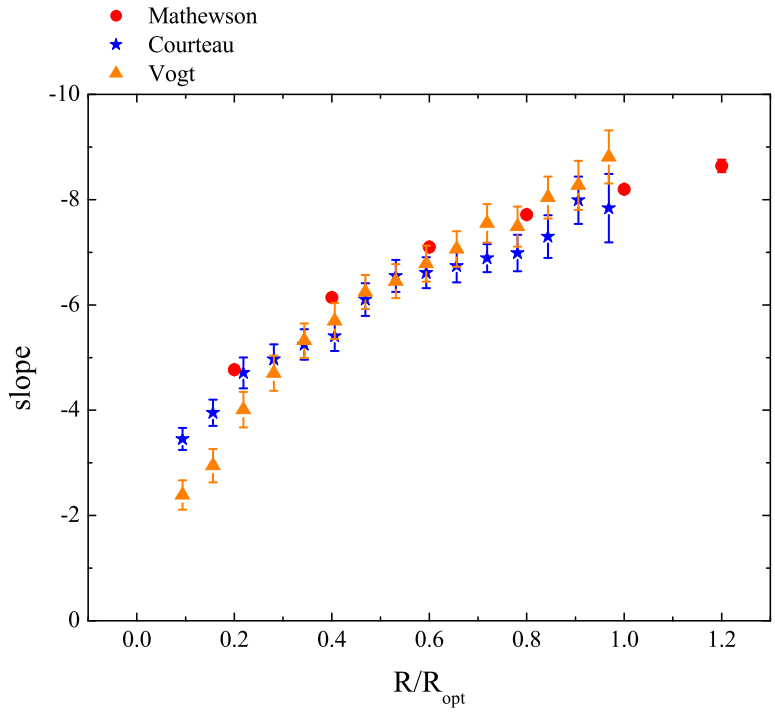

Figure 3.4: The slope of the Radial Tully-Fisher relation at different radii for the 3 samples. The slope for the standard TF is about to -7.5.

"random" bulge component governing the local kinematics in this region being almost independent of the total galaxy magnitude. The scatter starts to *decrease* with R_n, to reach a minimum of $0.15 - 0.3$ dex at R_n corresponding to two disk length scales, the radius where the contribution of the disk to the circular velocity $V(R)$ reaches the maximum. From $2R_D$ onward, the scatter increases outward reaching 0.3 dex, at the farthest distances with available data, i.e. at 3-4 disk length-scales.

Let us notice that these scatters are remarkably small. Most of the relations in the RTF family are statistically at least as significant as the standard TF relation, while the most correlated ones show a scatter of only 0.2 - 0.3 magnitudes (i.e. significantly smaller than that of the standard TF (see Figure 3.7)). Since they include also the effects of various observational errors, their small values could indicate that there is very small intrinsic scatter in the RTF relation.

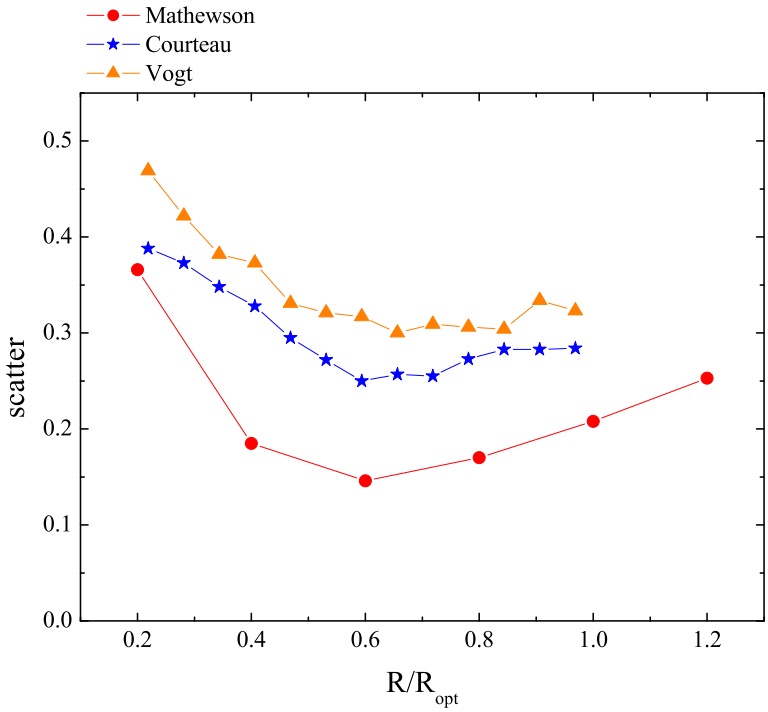

Figure 3.5: The scatter of the Radial Tully-Fisher relation at different radii for the 3 samples.

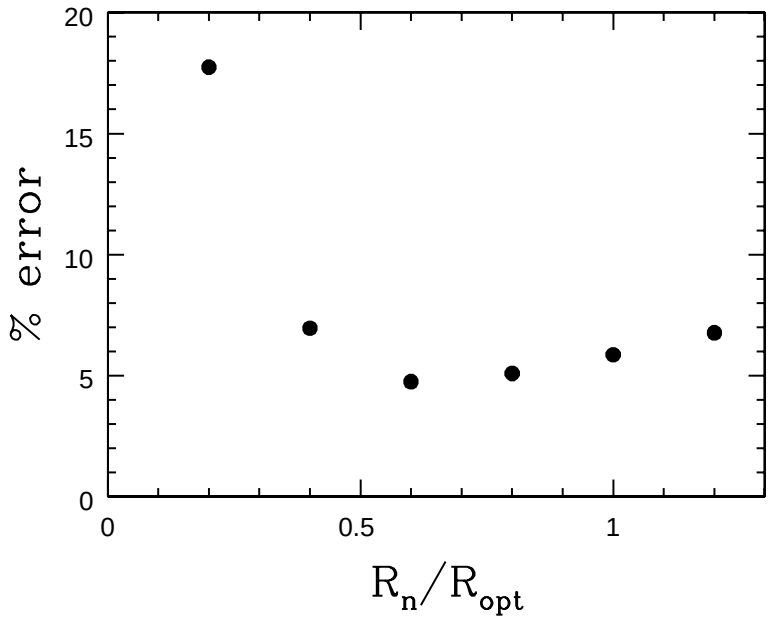

Figure 3.6: The % errors of the rotational velocity for different radii

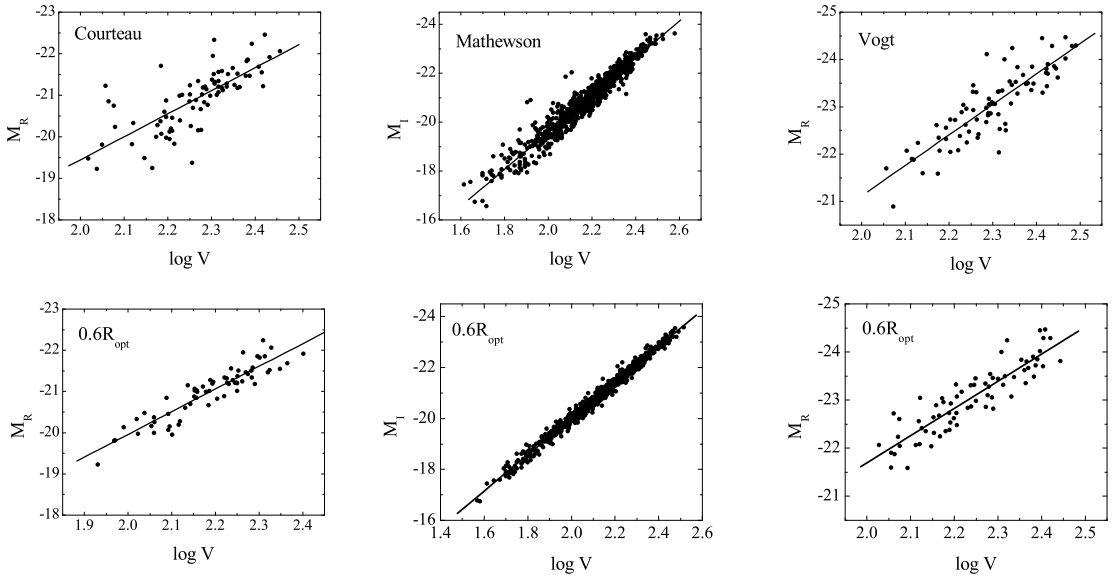

Figure 3.7: The standard TF relation for all 3 samples compared with the RTF relation at $R = 0.6R_{opt}$.

An important consequence of the smallness of the scatter of TF-like relationships is that it allows us to claim that, at *any radius* x, the luminosity empirically *predicts* the rotation velocity of spirals within the very small error of

$$\delta V_n/V_n = \ln(10) s_n/a_n \,. \tag{10}$$

that, using the data from the Tables 3.1, 3.2, 3.3, is found to range between 5%-7% for the PS95 sample and between 10%-12% for the other two samples. Even in the very inner bulge-dominated regions (not studied here and in PSS) it does not not exceed 20%. The smallness of $\delta V_n/V_n$ is remarkable also because this quantity includes distance and inclination errors so as a contribution from non circular motions, that in principle should be removed from the estimate of the "prediction error", intrinsic to the RTF. The fact that the latter relationship is able to reproduce the rotation velocities of spirals within few percent, it is a proof for the URC paradigm, additional

and perhaps more impressive than the small r.m.s. of the set of synthetic RC's in PSS.

Incidentally, the existence of a radius ($x = 0.6$) at which the TF-like relations show a minimum in the internal scatter (much less pronounced in the prediction error $\delta V_n/V_n$) is not related to the overall capability of the luminosity to "measure" the rotation velocities. In fact, at very small x the (random) presence of a bulge increases the scatter of the TF-like relation, in that, at these radii, the actual kinematical-photometric fundamental plane includes (as in ellipticals) a third quantity (the central brightness). At large x, the modest increas of the scatter is likely due to an increase of observational errors.

The scatter of the RTF in the R band for the corresponding samples is somewhat larger than that in the I band for the PS95 sample. This can be easily explained by the following: i) the former samples include also a (small) fraction of Sa objects and their RCs are of higher spatial resolution (lower bin size) and therefore less efficient in smoothing the non-circular motion caused by bars and spiral arms ii) the R band is more affected than the I Band by random recent episodes of star formation. A conservative estimate of these effects is $\sigma_{obs} \geq 0.2$, thus the intrinsic scatter of the RTF in the R band $(s_n^2 - \sigma_{obs}^2)^{0.5}$ results similar to that found in the I band.

3.4 Radial TF: implications

The marked systematic increase of the slopes of the RTF relationship, as their reference radius R_n increases from the galaxy center to the stellar disk edge, bears very important consequences. First, it excludes, as viable mass models, those in which:

i) The gravitating mass follows the light distribution, due to a total absence of non baryonic dark matter or to DM being distributed similarly to the stellar matter. In both cases, in fact, we do not expect to find any variation of the slopes a_n and

very trivial variations of the zero points b_n with the reference radius R_n, contrary to the evidence in Tables 3.1, 3.2, 3.3 and Fig. 3.4.

ii) The DM is present but with a *luminosity independent* fractional amount inside the optical radius. In this case, in fact, the value of the circular velocity at any reference radius R_n will be a *luminosity independent* fraction of the value at any other reference radius (i.e. $\log V(R_n) = k_{nm} + \log V(R_m)$, k_{nm} independent of luminosity). As a consequence the slopes a_n in the RTF will be independent of R_n, while the zero-points b_n will change in a characteristic way. It is clear that the evidence in Table 3.1, 3.2, 3.3 and Figure 3.4 contradicts this possibility.

The RTF contains crucial information on the mass distribution in spirals. In future works we will fully recover and test it with theoretical scenarios. Here, instead, we will use a simple mass model (SMM), that includes a bulge, a disk and a halo mass component and it is tunable by means of 4 free parameters. By matching this model with the slopes of the RTF relation vs reference radii relationship (hereafter SRTF) we derive the *gross* features of the mass distribution in spirals. Let us point out, that this method has a clear advantage with respect to the mass modelling based on RCs. In this latter procedure, since the circular velocities have a quite limited variation with radius, physically different mass distributions may reproduce the observations equally well. Here instead, on one side, we will use an observational quantity, the slope of the RTF relation, that shows large variation with reference radius; on the other side, physically different mass distributions predict very different slope vs reference radius relationships.

First, without any loss of generality affecting our results, we assume the well known relationships among the crucial structural properties of spirals: *i)*

$$R_D = R_1 l^{0.5}\,, \tag{11a}$$

see PSS, with $l \equiv 10^{(M_I - M_I^{max})/2.5}$ and $M_I^{max} = -23.5$ the maximum magnitude of

our sample, and *ii)*

$$M_D = M_1 l^{1.3}\,, \tag{11b}$$

(e.g. Shankar et al. 2006 and references therein). Notice that the constants R_1 and M_1 will play no role in the following. We will best fit the a_n data, i.e. the SRTF relation shown in Fig 3.4 with the slopes $a_{SMM}(x)$ we derive from the SMM. In this way we will fix the free structural mass parameters.

We describe in detail the adopted SMM, the circular velocity is a sum of three contributions generated by the bulge component, taken as a point mass situated in the center, a Freeman disk, and a dark halo, so

$$V^2_{SMM}(x) = GM_D/R_D[f_d(x) + \frac{M_b}{M_D}\frac{1}{(3.2x)} + \frac{M_{halo}}{M_D}\frac{1}{3.2}f_h(x,\alpha)],$$

where M_{halo} is the halo mass inside R_{opt}. It is useful to measure V^2_{SMM} in units of GM_1/R_1, and to set it to be equal 1. The disk component from Eqs. (5) and (11a), (11b) takes the form:

$$V^2_d(x,l) = l^{0.8} f_d(x)\,, \tag{12}$$

with $V^2_d(1,1) = 0.347$.

We set M_b the bulge mass to be equal to a fraction $(c_b/(3.2 \cdot 0.347)l^{0.5}$ of the disk mass, with c_b a free parameter of the SMM; the exponent 0.5 in the luminosity dependence is suggested from the bulge-to disk vs total luminosity trend found for spirals (de Jong 1996). Then, we get

$$V^2_b(x) = c_b V^2_d(1,l) l^{0.5} x^{-1}\,. \tag{13}$$

The halo velocity contribution follows the profile of Eq. 6 and at R_{opt} it is set to be equal to $c_h/(3.2 \cdot 0.347)l^{(k_h-0.5)}$ times the disk contribution c_b/c_h. Moreover, k_h and α are the free parameters of the SMM.

Then, we can write:

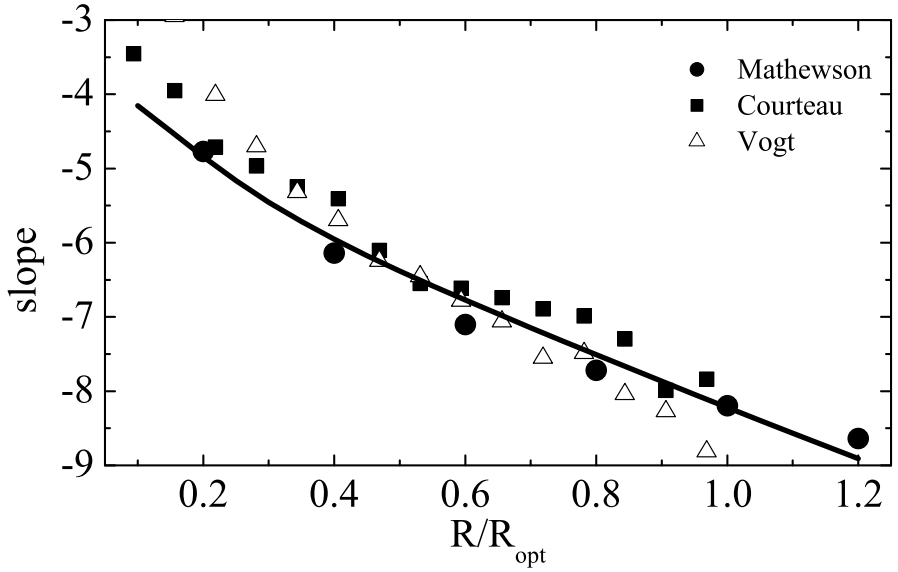

Figure 3.8: Slopes a_n of the RTF for the 3 samples as a function of the reference radius in units of R_{opt}. The solid line is the best fit relation for Eq. 14

$$V^2_{SMM}(x,\alpha,l) = (c_b l^{1.3}/x + l^{0.8} f_d(x) + c_h l^{(k_h-0.5)} f_h(x,\alpha))\,, \tag{14}$$

where f_d is given by Eq. (5), f_h by Eq. (6). Notice that the simple form of V_{SMM} allows us to get the predicted slope function $a_{SMM}(x)$.

The core radius α is a DM free parameter, however let us anticipate that, provided that this quantity lies between 0.5 and 2 (see Donato et al. 2004) it does not affect in a relevant way the SMM predictions. Instead the $a_{SMM}(x)$ relationship strongly depends on the values of c_h, k_h, c_b, and therefore they can be estimated with a good precision. We can reproduce the observational $a_n = a(R_n)$ relationship, by means of the SMM (see Fig. 3.8) with the following best fit parameters values: i) $k_h = 0.8 \pm 0.04$, that means that less luminous galaxies have larger fraction of dark matter, ii) $c_b = 0.13 \pm 0.03$, and iii) $c_h = 0.13 \pm 0.06$ that indicates that at $(l, x) = (1, 1)$ (i.e. inside R_{opt}), 20% of the mass is in the bulge component, 20% in the halo, while 60% is in the stellar disk. The quoted uncertainties are the formal χ^2 fitting uncertainties.

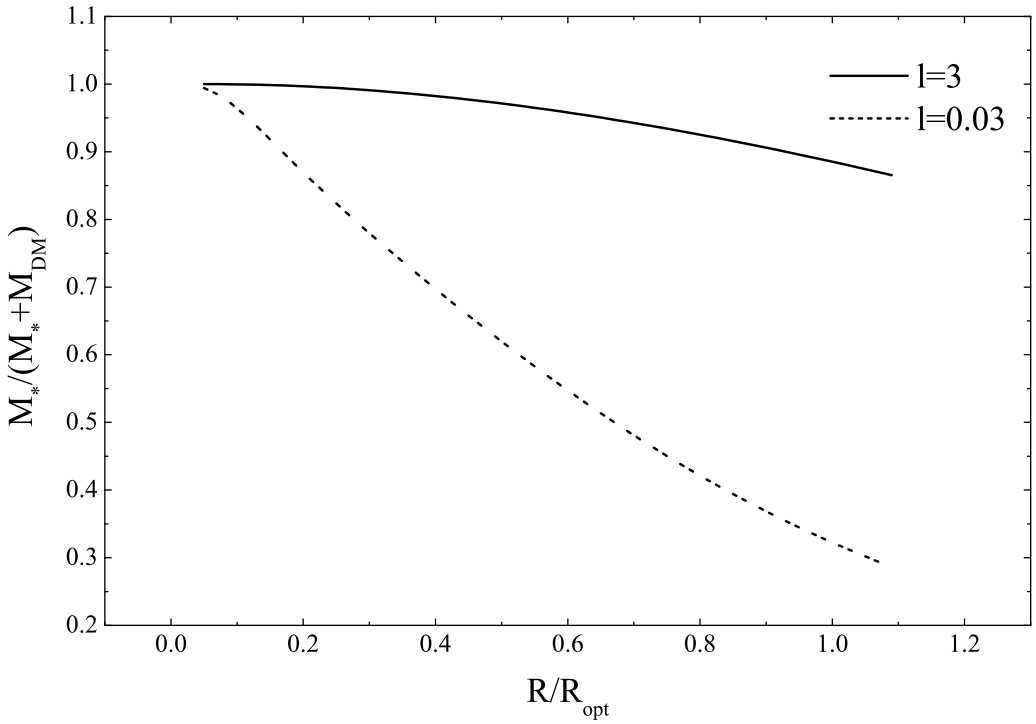

Figure 3.9: Baryonic mass fraction as a function of normalized radius for high and low luminosity objects.

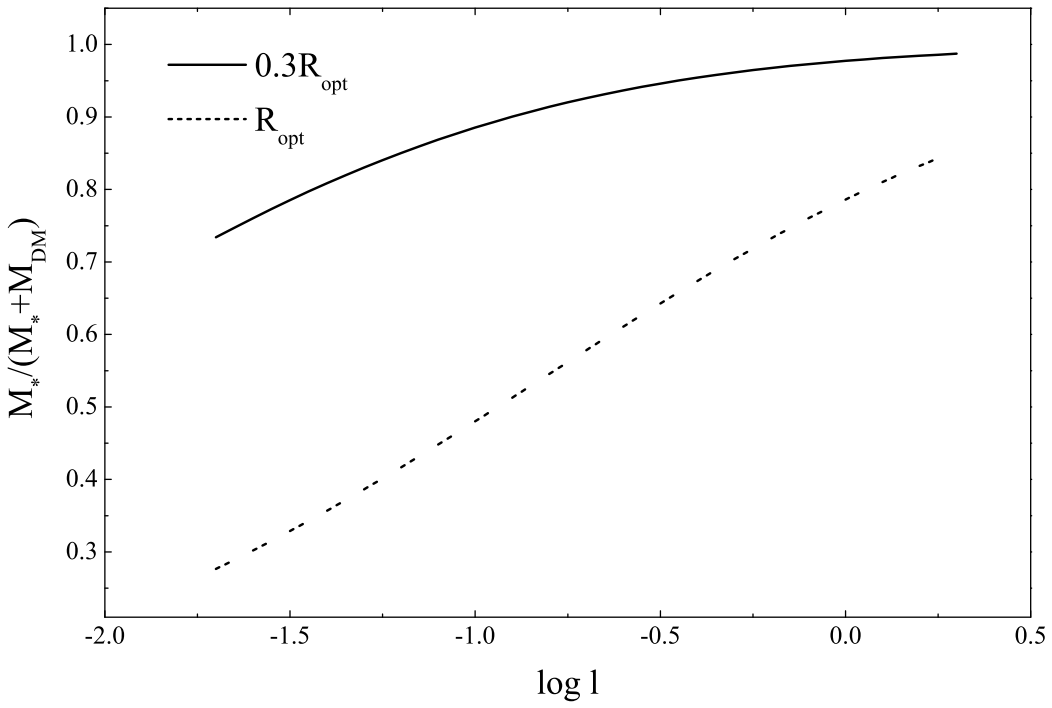

Figure 3.10: Baryonic mass fraction at two different radii as a function of luminosity.

3.5 Discussion of the obtained results

In spirals, at different galactocentric distances measured in units of disk length-scales jR_D ($j = 0.2, ..., 4$), there exists a family of independent Tully-Fisher-like relationships, $M_{band} = b_j + a_j \log V(R_j)$, that we call the Radial Tully-Fisher relation, it contains crucial information on the mass distribution in these objects. In fact:

1) The RTF relationships show large systematic variations in their slopes a_j (between -4 and -8) and a r.m.s. scatter generally smaller than that of the standard TF. This rules out the case in which the light follows the gravitating mass, and, in particular, all mass models that imply: a) an absence of dark matter, b) a single mass component, c) the same dark-to-luminous-mass fraction within jR_D in all galaxies.

2) The slopes a_j decrease monotonically with R_j, which implies the presence of a non luminous mass component whose dynamical importance, with respect to the

stellar disk, increases with radius.

3) The existence of the RTF and the features of the slope vs R_j can be well reproduced by means of a three components mass model that includes: a dark halo, with $1.6R_D < R_c < 6.4R_D$, and mass $M_{halo}(R_{opt}) \propto l^{0.8}$, a central bulge with $M_{bulge} \propto l^{1.8}$, an exponential thin disk of mass $M_d \propto l^{1.3}$ with, at $10^{11}L_{B,\odot}$, 80% of the mass inside R_{opt} in stellar form.

Let us also notice that we have produced a qualitatively new evidence for the presence of a luminosity dependent mass discrepancy in spirals, different from that obtained from the non Keplerian shapes of the RC's. While, the latter originates from a failure: we *do not* observe the Keplerian fall-off of the circular velocities at the disk edge, and therefore we must postulate a new component, here, we provide a *positive* evidence for the existence of such dark component: we *detect* radial change of the slope and the scatter of existing relations between observables that positively indicates the presence of a more diffuse dark component.

The small scatter of the RTF implies that, in spirals, at any radius, the luminosity is an extremely efficient statistical estimator of the *rotation* velocity. This, since otherwise the strong correlation between luminosity and rotation velocities would be an unacceptably fortiousus coincidence, strongly supports in contrast with a different claim (Hayashi) that in spirals this velocity coincides with the *circular* velocity, i.e. with the centrifugal equilibrium velocities V_c associated with the central galaxy gravitational potential Φ, $V_c = (-Rd\Phi/dR)^{1/2})$.

Finally, let us stress that any model of formation of spiral galaxies must be able to produce (e.g. in the I band) a M_I vs $\log V(2R_D)$ relationship with a slope of 7 ± 0.1 and an intrinsic scatter of ≤ 0.15 magnitudes.

3.6 Additional tables and figures

In this appendix we present tables and figures related to our result and the galaxies of Samples 2 and 3.

Table 3.1: Parameters of the Radial Tully-Fisher relation at different radii for the Mathewson sample

R/R_{opt}	zero point	error	slope	error	SD	N
0.2	-11.78	0.103	-4.77	0.054	0.366	739
0.4	-8.241	0.068	-6.141	0,033	0.185	786
0.6	-5.787	0.063	-7.102	0.029	0.146	794
0.8	-4.22	0.09	-7.718	0.042	0.17	657
1.0	-3.034	0.146	-8.197	0.067	0.208	447
1.2	-1.979	0.261	-8.639	0.118	0.253	226

column 1 - the isophotal radius,

column 2 - intercept value b_n,

column 3 - the standard error of b_n,

column 4 - the slope a_n,

column 5 - the standard error of a_n,

column 6 - the scatter,

columns 7 - the number of observational points

Table 3.2: Parameters of the Radial TF relation at different radii for the Courteau sample

R/R_{opt}	zero point	error	slope	error	SD	N
0.03	-18.217	0.287	-1.8	0.189	0.516	75
0.09	-15.615	0.39	-2.878	0.209	0.381	74
0.16	-14.355	0.495	-3.336	0.249	0.388	75
0.22	-13.379	0.55	-3.707	0.27	0.397	76
0.28	-12.155	0.741	-4.194	0.355	0.465	79
0.34	-11.7	0.613	-4.374	0.291	0.361	74
0.41	-11.11	0.617	-4.586	0.289	0.338	72
0.47	-9.962	0.674	-5.086	0.31	0.295	68
0.53	-9.114	0.699	-5.445	0.321	0.296	71
0.59	-8.919	0.733	-5.519	0.334	0.293	68
0.66	-8.623	0.752	-5.61	0.341	0.279	65
0.72	-8.351	0.625	-5.737	0.284	0.255	63
0.78	-8.172	0.763	-5.799	0.345	0.274	61
0.84	-7.329	1.0	-6.152	0.456	0.32	53
0.91	-6.372	1.0	-6.58	0.449	0.286	44
0.97	-7.573	1.54	-6.042	0.688	0.31	37
1.03	-7.728	1.993	-5.984	0.888	0.311	25
1.09	-9.265	2.254	-5.307	1.0	0.212	14
1.16	-6.853	1.767	-6.35	0.789	0.281	15

Table 3.3: Parameters of the Radial Tully-Fisher relation at different radii for the Vogt sample

R/R_{opt}	zero point	error	slope	error	SD	N
0.09	-19.351	0.526	-1.992	0.278	0.55	78
0.16	-18.118	0.64	-2.456	0.316	0.528	78
0.22	-16.142	0.714	-3.309	0.339	0.472	76
0.28	-14.787	0.728	-3.869	0.338	0.43	77
0.34	-13.583	0.73	-4.365	0.334	0.394	77
0.41	-12.646	0.78	-4.747	0.354	0.386	77
0.47	-11.746	0.784	-5.112	0.353	0.365	77
0.53	-11.342	0.805	-5.264	0.361	0.361	75
0.59	-10.698	0.778	-5.51	0.347	0.327	72
0.66	-9.804	0.77	-5.885	0.341	0.309	71
0.72	-9.244	0.83	-6.125	0.368	0.318	70
0.78	-9.227	0.936	-6.104	0.414	0.341	68
0.84	-7.873	0.906	-6.7	0.4	0.304	60
0.91	-7.435	1.057	-6.893	0.466	0.334	58
0.97	-6.377	1.153	-7.343	0.505	0.323	50
1.03	-8.398	1.414	-6.435	0.62	0.345	41
1.09	-7.953	1.377	-6.628	0.599	0.301	35
1.16	-8.683	1.38	-6.947	0.622	0.228	24
1.22	-9.616	1.444	-6.842	0.714	0.275	23
1.28	-7.394	2.467	-6.834	1.072	0.347	16

Table 3.4: Parameters of the standard Tully-Fisher relation for 3 samples.

Data	zero point	error	slope	error	SD	N
Mathewson	-4.455	0.15	-7.57	0.069	0.327	841
Courteau	-8.398	1.26	-5.526	0.556	0.495	81
Vogt et al.	-8.277	0.997	-6.423	0.433	0.389	79

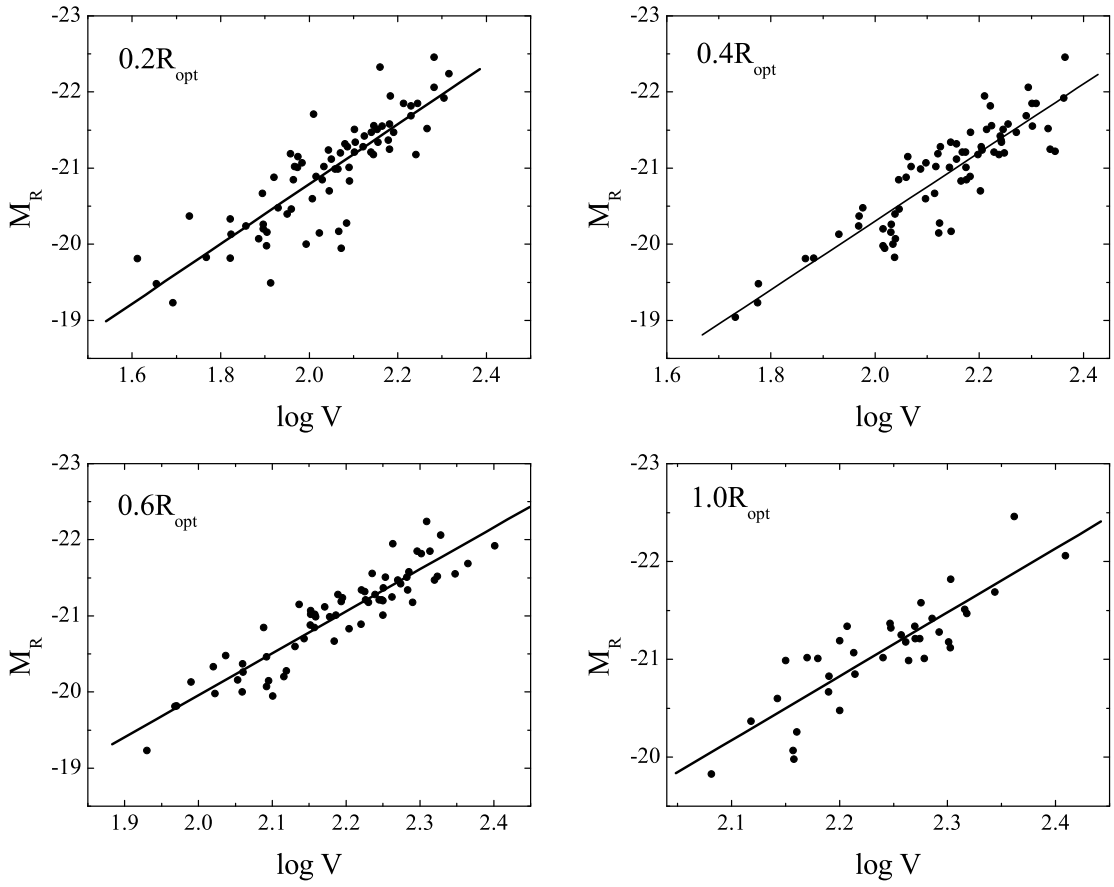

Figure 3.11: The Radial Tully-Fisher relation for the Courteau sample.

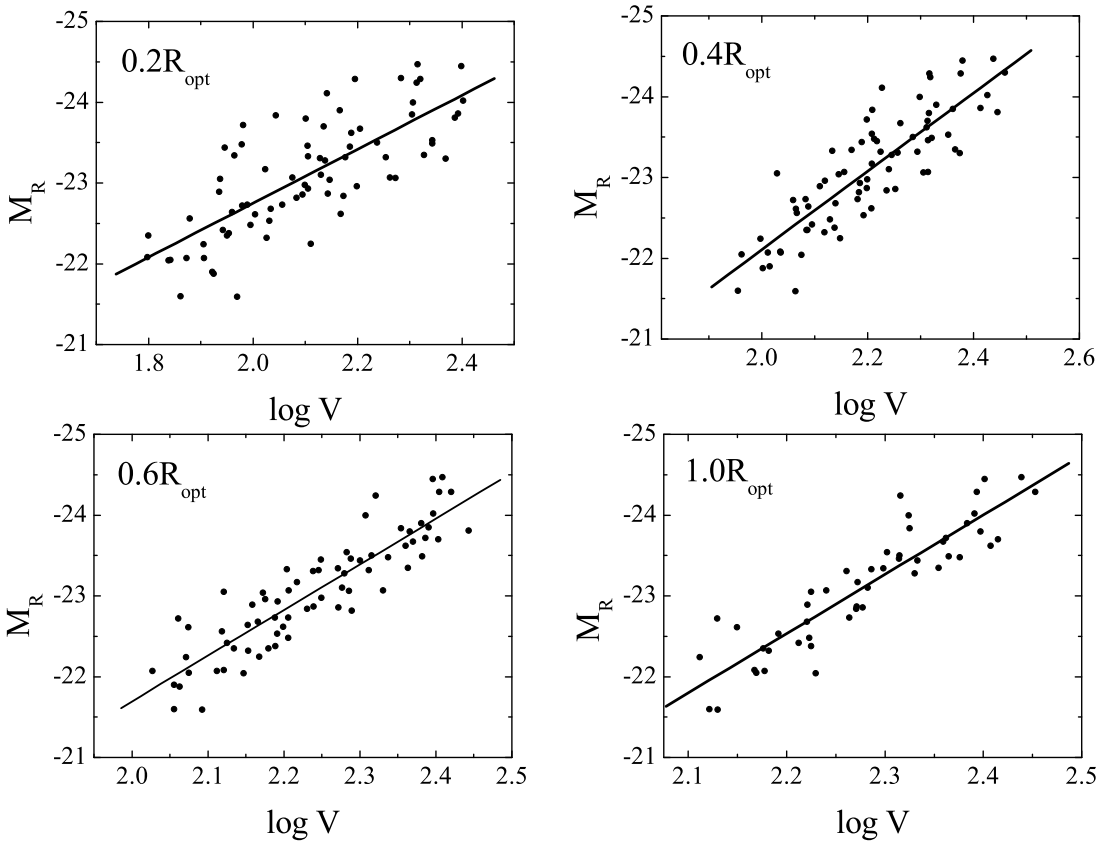

Figure 3.12: The Radial Tully-Fisher relation for the Vogt sample.

Chapter 4

The disk mass of spiral galaxies

In this Chapter I present our study of the disk mass of spiral galaxies. We are using two methods. One is kinematical and another one is spectro-photometrical. The data sample contains galaxies of different luminosity and Hubble Type.

4.1 Introduction to the problem

The disk mass M_D, together with disk length-scale R_D, is the main physical property of the baryonic component of normal spiral galaxies. In the current framework of galaxy formation theory, in an halo of mass M_{vir}, the present day value of M_D indicates the efficiency with which the stellar formation process acted in proto-spirals on the large primordial reservoir of $\sim \frac{1}{6}M_{vir}$ HI material and bears the imprint of the physical processes (supernovae feedback, cooling, previrialization) that have prevented the latter in entirely transforming in a stellar disk (see Shankar et al. 2006). The quantity $(M_D R_D)^{1/2}$ is proportional to the angular momentum unit mass for disk matter, very likely the same value of that of dark particles (e.g. Tonini et al, 2006) and linked to the tidal torques that the galaxies experience from neighbors at their turnarounds. Finally, let us remind that $M_D R_D^{-2}$ is a measure of the central stellar surface density.

The mass modelling of the rotation curves is a robust and reliable method (that we call the kinematical method, hereafter *kin*) to derive the disk mass (Tonini & Salucci, 2004). However, as it is well known, RC's do not match the distribution of the stellar component, so that an additional invisible mass component must be properly taken into account (e.g. Persic, Salucci, Stel, 1996). This can be done in a simple way since spiral disks form from infalling baryons in a DM potential well that, unlike the DM, radiate, lose kinetic energy and contract in a disk saturating the gravitational field of the central regions, where dominate the local mass distribution and therefore the kinematics (Salucci & Persic, 1999). Then is relatively easy to derive the disk mass, caveat a small correction that takes into account the residual presence of DM, in turn, estimated from the kinematics of the outer region where it dominates the potential (Persic, Salucci, Stel, 1996).

A second independent way to measure the disk mass (that we call the spectro-photometric method, hereafter *pho*) is by fitting their broadband SED with stellar population models as pioneered by Tinsley, 1978. We use combined SDSS and 2MASS photometry covering the *ugrizJHK* bands to fit each galaxy's SED to a broad range of stellar population models of varying star formation history, age, dust content, and burst fraction.

Advantages and disadvantages are present in both methods, though, remarkably, they are almost orthogonal. The photometric method relies on the not trivial caveat that, given a SED there is an unique stellar mass that explain it, moreover, it takes a number of assumptions on the stellar populations of spirals, it depends on the estimate of the galaxy distance as D^2 (uncertain to some level for local objects). Moreover, it carries theoretical uncertainties (in $\log M_D$) as high as 0.3 dex. The kinematical method could suffer from the uncertainty on the actual distribution of DM in galaxies, depends on the disk inclination angle as $(1/\sin i)^2$, uncertain for low inclination galaxies, and it depends on the estimate of the galaxy distance as D. The main advantage of the photometric method is that it takes no assumption on the

mass distribution, the main of the kinematical method is that the disk mass can be obtained straightforwardly from observables and within an uncertainty of $0.15dex$: set as $M_D \sim fG^{-1}V^2(2R_D)2R_D$, with f estimated from the slope of the RC inside $2R_D$, within the above uncertainty (Persic and Salucci, 1990a,b).

To compare, for a fair sample of galaxies, the disk mass estimates obtained with the two different methods is worth for two reasons. First, the average of the two estimates will give a very reliable measure of the stellar disk mass for objects of different luminosities, providing so a unprecedented accurate stellar mass vs light relationship. Second, it allows to investigate the assumptions taken by each of the two methods, providing so additional information on the structure and evolution of galaxies.

The sample of 18 galaxies we use in this thesis (see Fig. 4.1 for their images) includes all the SDSS local spirals with 8 band measurements necessary for a precise estimate of the "photometric" mass and with a smooth, regular, high resolution ($>$ 10 independent data inside two disk length-scales) rotation curve. Disk masses have been obtained in literature for a much larger number of objects, however, the specific aim of this work requires very stringent selection criteria the greatly limit the latter.

4.2 The kinematical method

In spirals the stellar component is represented by a Freeman disk (Freeman 1970) of surface density

$$\Sigma_D(r) = \frac{M_D}{2\pi\ R_D^2}\, e^{-r/R_D} \tag{1}$$

that contributes to the circular velocity V as:

$$V_d^2(x) = \frac{1}{2}\frac{GM_D}{R_D}x^2(I_0K_0 - I_1K_1) \tag{2}$$

where $x = r/R_D$ and I_n and K_n are the modified Bessel functions computed at $x/2$. A bulge of mass ($M_b = \epsilon\ M_D$, $\epsilon = (1/20 - 1/5)$ concentrated inside $R_b < 1/3R_D$ is

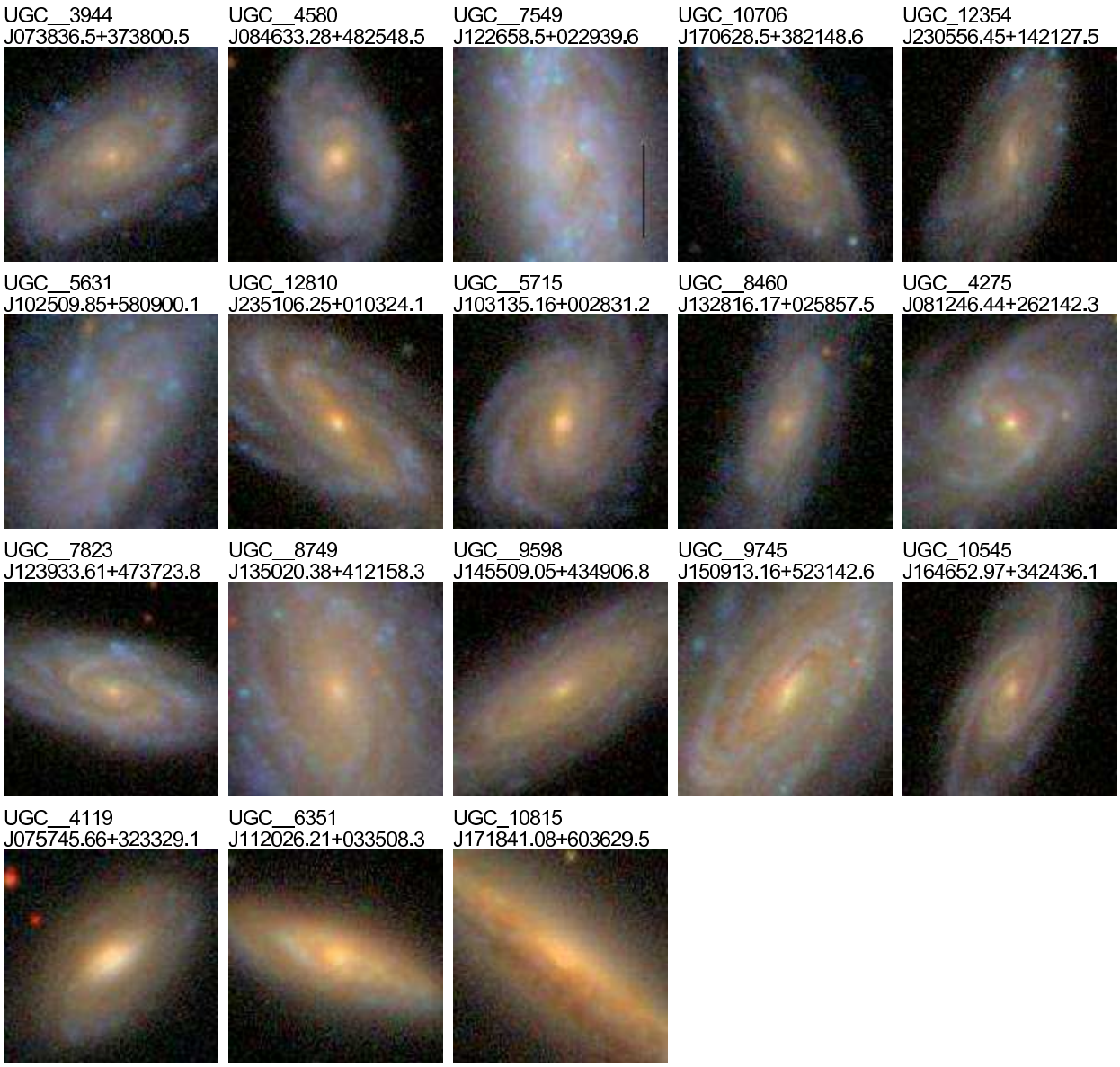

Figure 4.1: SDSS *gri* composite color images of the galaxies in our sample

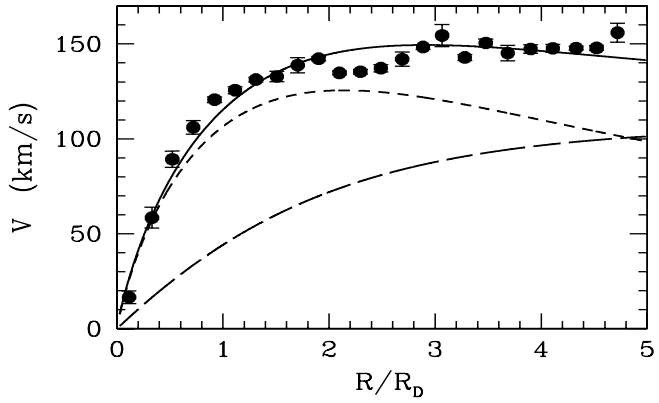

Figure 4.2: UGC 8460. Filled circles with errorbars - the observed RC, short dashed line - the contribution of the stellar disc, long dashed line - the contribution of the dark halo, solid line - the model circular velocity

often present. The amplitude and the profile of the RCs for $R > R_b$ is influenced by the central bulge in a negligible way for $\epsilon < 1/5$. Furthermore, in the RC mass modelling, even if neglect a quite significant stellar bulge component ($\epsilon = 0.2$), we obtain a disk mass value higher than the actual one but matching that of the total stellar mass ($M_D + M_b$). (Persic, Salucci, Ashman, 1993), therefore, a mass proper to be compared with the total galaxy luminosity and with the spectro-photometric mass estimate. Given the aim of this work, it is worth to describe the dark matter component with the simplest halo velocity profile $V_h^2(r)$ (linked to the mass profile by ($V_h^2(r) = \frac{GM_h(<r)}{r}$):

$$V_h^2(x) = V_h^2(1)(1 + a^2)x^2/(a^2 + x^2) \qquad (2b)$$

with $V_h^2(1) \equiv V_h^2(R_D)$ and a free parameters. The above velocity profile implies a density profile with an inner flat velocity core of size $\sim aR_D$, a constant central density and an outer r^{-2} decline, which, however is never reached in our RCs, generally extended not beyond $R_{last} \sim 3R_D$. Let us notice that in the region in which most of the baryons lie and where we will measure the disk mass eq(2b) can approximate,

with proper values of the free parameters, a number of different halo distributions, including the NFW, the Burkert and the pseudo-isothermal ones. Obviously, for $R > R_{last}$, V_h needs not to be represented by eq(2b).

The kinematical estimate of the disk mass M_{kin} is obtained by fitting the observed rotation velocities V to the model velocity curve V_{mod}:

$$V^2(x) = V^2_{mod} \equiv V^2_d(x, M_D) + V^2_h(x; V_h(1), a) \tag{3}$$

the model parameters, including the disk mass, are obtained by minimizing the usual quantity (data-model)^2.

We have also computed the disk masses by means of a different approach: a) by means of the equation: $|d\log\ V_d(x)/d\log\ x \simeq d\log V(x)/d\log\ x| < 0.05$, we have determined the inner baryon dominance region (Salucci and Persic 1999), i.e. the region inside which the slope of the disk contribution to the circular velocity coincides, within the observational errors, with the slope of the latter; b) we have fit the RC's of this region with only the disk contribution. The two ways yields very similar results for the value of the disk mass which is not surprising: in fact, with the exception of the smallest objects, DM-dominated also at inner radii, the quantity $G^{-1}V^2(1)(I_0K_0 - I_1K_1)|_{0.5}R_D$ is certainly an upper limit to the disk mass and very likely a good estimate.

The RC fits are excellent (see a typical case in Fig. 4.2) on the line of the results in Ratnam & Salucci (2000) and Salucci et at (2000) showing, for large samples that in the inner parts of spirals light traces the dynamical mass. Thus the inner RC of spirals are reproduced by just considering a stellar disk with a suitable choice for its mass to light ratio. We get the value M_{kin} for the disk mass and the formal uncertainty σ_k of $\log\ M_{kin}$ that it is found to range between 0.10 and 0.20 dex

The resulting values for the disk masses in our Sample are given in Table 1.4 alongside with their luminosities.

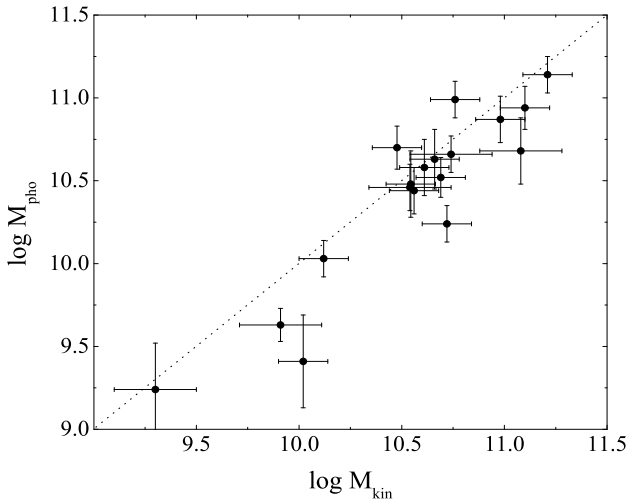

Figure 4.3: The $log\ M_{kin}$ vs $log\ M_{pho}$ relationship.

4.3 The Spectro-Photometric method

We infer stellar masses from multi-color photometry following Drory, Bender, & Hopp (2004). We compare multi-color photometry to a grid of stellar population synthesis models covering a wide range in star formation histories (SFHs), ages, burst fractions, and dust extinctions.

We use photometric data in the ugriz bands from the Sloan Digital Sky Survey (SDSS) Data Release 4, augmented by JHK data from the 2 Micron All Sky Survey. We perform matched-aperture photometry with apertures defined in the SDSS r-band image to obtain integrated galaxy colors to the Petrosian radius. Photometric errors are 0.03-0.08 in J, H, and K, respectively, $\sim$ 0.1 mag in the u band, and $\sim$ 0.01 mag in the g, r, i, and z bands.

Our stellar population model grid is based on the Bruzual & Charlot (2003) stellarpopulation synthesis package. We also use an updated version of these models. We parameterize the possible SFHs by a two-component model: a main component with a smooth analytically described SFH, and, superimposed, a short recent burst of star formation.

The main component has a star formation rate of the form $\psi(t) \propto \exp(-t/\tau)$, with $\tau \in [0.1, \infty]$ Gyr and a metallicity of $-0.6 <$ [Fe/H] < 0.3. The age, t, is allowed to vary between 0.5 Gyr and the age of the universe (14 Gyr). We superimpose a burst of star formation, modelled as a constant star formation rate episode of solar metallicity and of 100 Myr duration. We restrict the burst fraction, β, to the range $0 < \beta < 0.15$ in mass (higher values of β are degenerate and unnecessary since this case is covered by models with a young main component). We adopt a Chabrier (2003) initial mass function for both components. The main component and the burst are allowed to independently exhibit a variable amount of extinction by dust. This takes into account the fact that young stars are found in dusty environments and that the starlight from the galaxy as a whole may be reddened by a (geometry dependent) different amount.

We compute the full likelihood distribution on a grid in this 6-dimensional parameter space $(\tau, [\mathrm{Fe/H}], t, A_V^1, \beta, A_V^2)$, the likelihood of each model being $\propto \exp(-\chi^2/2)$. In each object, we compute the likelihood distribution of the stellar mass-to-light ratios that will give the best estimated value M_{pho}/L, by weighting the mass-to-light ratio relative to a spectro-photometric model and marginalize it over all stellar population parameters. The uncertainty in the derived M_{pho}/L , and hence in stellar mass, is obtained from the width of this distribution. While estimates of stellar population parameters such as the mean age, the star formation history, the burst fraction, and the dust content are subject to degeneracies and often are poorly constrained by the models, the value of the stellar disk mass obtained by marginalizing over the stellar population parameters is a lot more robust. On average σ_{pho}, the width of the distribution of the likelihood of M_{pho}/L, at 68% confidence level is between 0.1 and 0.2 dex.

The uncertainty in the stellar mass has a weak dependence on the stellar mass itself (in that it increases with lower S/N photometry) and much of the variation of the erorrs is in spectral type: early-type galaxies have more tightly constrained

masses than late types because their star formation histories are tightly constrained while the ones of late-type galaxies are less well constrained due to degeneracies with age and recent burst fractions. This dependence of the uncertainties on spectral type is the dominant source of uncertainty in the photometric mass of our sample. The contribution to the uncertainty due to photometric errors is negligible in our relatively high S/N photometry, however about 20% of the uncertaity is due to errors in the determination of the extrapolated total magnitudes and colors.

Note that masses computed with the BC07 models are lower by 0.1 to 0.15 dex compared to the ones using the BC03 models. This is due to the higher red and infrared luminosities of intermediate age ($\sim$ 0.8-2 Gyr) stellar populations in the newer models which owing to a larger contribution of post-AGB stars in the newer models. This particularly affects our sample of mostly relatively late type spiral galaxies with extended star formation histories and significant recent star formation.

4.4 Results from two methods

The two different estimates of the disk masses are shown in Figure 4.3. A correlation yields:

$$\log\ M_{pho} = (-0.4 \pm 1.27) + (1.02 \pm 0.12) \log\ M_{kin} \qquad (2)$$

with a r.m.s of 0.23 dex. By considering the errors on the separate determination of M_{kin} and on M_{pho} the slope and zero-point of the relation are not too far of 1 and 0. From Fig. 3.3 and eq(2) it is evident that the two estimates are statistically equivalent, i.e. $M_{pho} = M_{kin}$ within a very small scatter and both mass estimates are suitable measures of the true disk (stellar) mass.

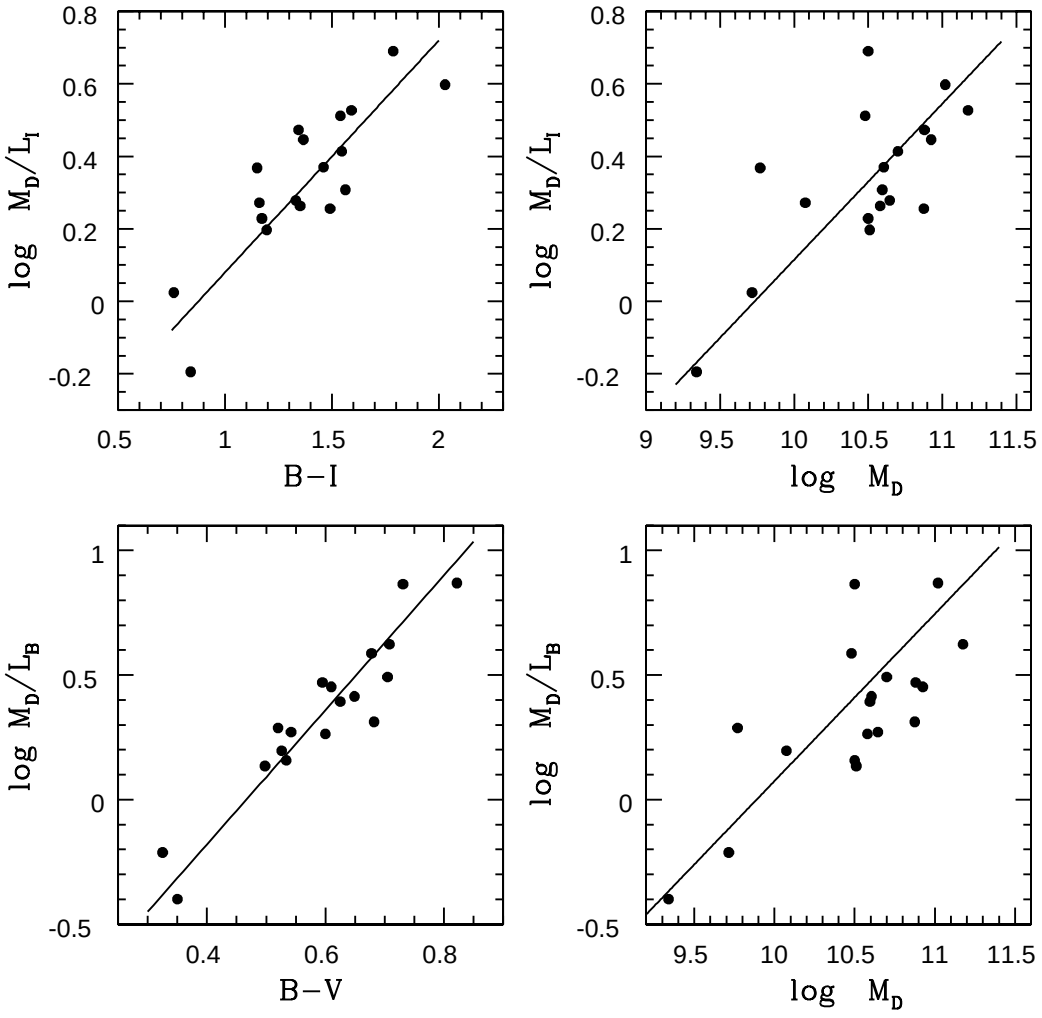

Figure 4.4: Mass-to-light ratios vs color and luminosity

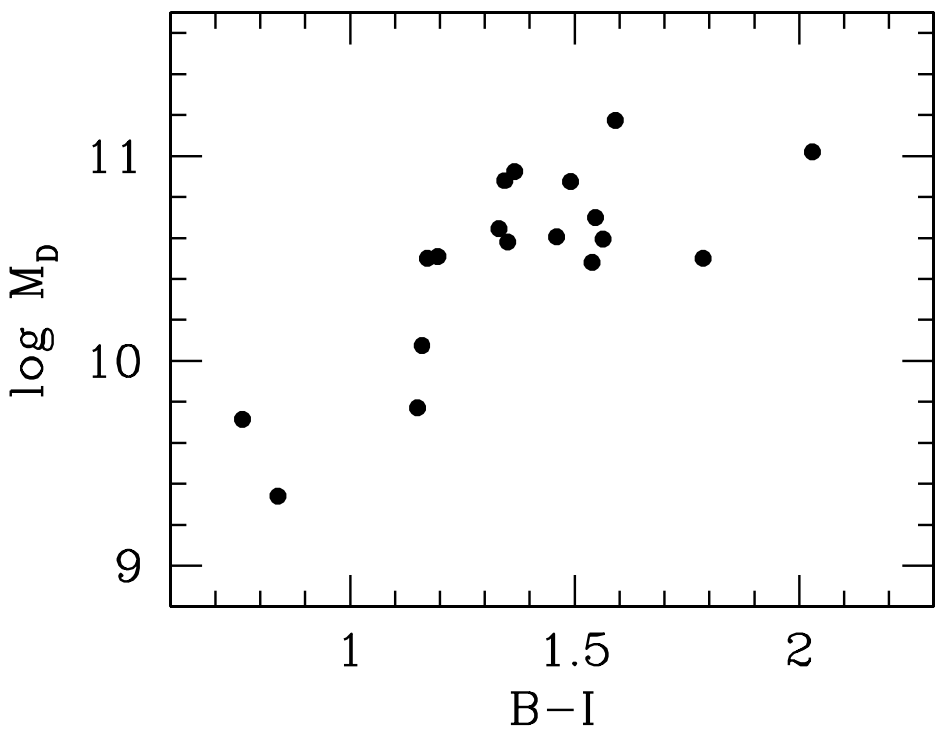

Figure 4.5: Colour vs total mass

4.5 The mass-to-light ratios in spirals

Biases, observational errors and systematics of the two determinations are independent, therefore we can define as an accurate measure of the disk mass M_D the log average of the two different estimates:

$$\log M_D \simeq \frac{1}{2}(\log M_{pho} + \log M_{kin}) \tag{3}$$

From this we compute the spiral mass-to-light ratio. We find that this quantity ranges over 0.8 dex in spirals and, not unexpectedly depend on the broad-band galaxy color. In fact, we get (see Fig. 4.4)

$$M_D/L_B = (1 \pm 0.25) \times 10^{(0.68\pm0.05)(B-K)-1} \tag{4}$$

reflecting that the older stellar populations are redder and have higher mass-to-light ratios. This allow to establish from K luminosity and B-K broad band color a solid estimate the stellar mass of spirals (i.e. within an uncertainty of 0.15 dex, that it reduces to 0.1 dex when the whole SED is involved), useful and especially unbiased in tackling a number of issues of galaxy structure and evolution such as the mass modelling of RC's and the consistency between present day disk masses and their SFR history.

The mass to light ratio depend on stellar mass (and on galaxy luminosity) in a weak way, (see Fig 4.4),

$$M_D/L_K = (5 \pm 2) \times (M_D/10^{11} M_\odot)^{0.2\pm0.08} \tag{5}$$

within a r.m.s. of 0.2 dex in the B band and in the K. This relation derives from the above, via the well known color magnitude relation (in our sample we find $logL_K = (B-K) + 8.45$ within a r.m.s of 0.3 dex).

In Fig 4.5 I show colour vs mass.

Conclusions

In this work we find that the two main methods to measure the disk masses in spirals, namely the SED and the RC fitting are both robust, solid and consistent. In an illustrative way, in bulge-less systems, the quantities $L_B 10^{0.68(B-K)-1}$ and $G^{-1}V^2(1)/(I_0K_0 - I_1K_1)^{0.5}R_D$ that we obtain from simplified implementations of the two methods are already excellent measures of the disk mass, that further can be improved with the full implementation.

The agreement between the two methods implies a further support for a) the existence of a Inner Baryon Dominated region, inside which the stellar disk saturates the gravitational potential overwhelming the DM halo b) the assumed IMF and SFR histories: significantly different choices would lead to $M_{pho} \neq M_{kin}$. If they are different from galaxy to galaxy we would not have such a good fit.

The reliable values of the disk masses allow to realize that spiral galaxies, unlike ellipticals, show a quite wide range in the mass-to-light ratios, i.e. almost a dex, reflecting an intrinsic spread of ages of their average stellar population.

In this study it is evident that spiral disks are significantly less massive than the elliptical spheroids of the same luminosity. In the following we use the B band and the mass-to-light vs luminosity relation for simplicity, the same result is obtained using K band and the mass-to-light vs color relationship, of stronger physical significance. For ellipticals we have: $M_{sph}/L_B \sim 4\ \lambda^{0.2}$, $\lambda = L_B/(2\ 10^{10} L_{B\odot})$ (e.g. Borriello et al 2000), with $0.5 \leq \lambda \leq 10$, while for spirals we have found: $M_D/L_B \sim 2\ \lambda^{0.4}$ with $0.01 \leq \lambda \leq 5$. In the luminosity range where ellipticals and spiral coexist, spheroids are therefore more massive by an amount $1.3 - 2.5$ than disks with the same luminosity.

Finally, let us stress that the luminosity, also in an infrared band, is only a approximate indicator of the disk mass, if the average age of its stellar population is not known. Therefore, it is not justified, in accurate cosmological investigations, to assume that the spiral luminosity reliably measures the disk mass.

Name	V_d	M_{kin}	M_{pho}	ref
(1)	(2)	(3)	(4)	(5)
UGC3944	100	1.3×10^{10}	1.1×10^{10}	1
UGC4580	135	2.4×10^{10}	5.0×10^{10}	1
UGC7549	62	2.4×10^{9}	1.7×10^{9}	1
UGC10706	208	1.2×10^{11}	4.8×10^{10}	1
UGC12354	100	1.0×10^{10}	2.6×10^{9}	1
UGC5631	90	8.2×10^{9}	4.3×10^{9}	1
UCG12810	220	1.6×10^{11}	1.4×10^{11}	1
UGC5715	190	5.7×10^{10}	9.8×10^{10}	1
UGC8460	145	3.6×10^{10}	2.7×10^{10}	2
UGC4275	190	7.6×10^{10}	3.0×10^{10}	2
UGC7823	165	4.5×10^{10}	4.3×10^{10}	1
UGC8749	170	5.2×10^{10}	1.7×10^{10}	1
UGC9598	160	4.9×10^{10}	3.3×10^{10}	1
UGC9745	155	4.0×10^{10}	3.8×10^{10}	1
UGC10545	155	9.5×10^{10}	7.4×10^{10}	1
UGC4119	290	7.4×10^{10}	4.6×10^{10}	3
UGC6351	220	3.5×10^{10}	2.9×10^{10}	3
UGC10815	229	1.3×10^{11}	8.7×10^{10}	1

Chapter 5

Rotation curves of luminous spiral galaxies

In this chapter I will present studies of high luminosity (M < -22.5) spiral galaxies. Analysing their rotational velocities we want to derive the average rotational curve. That can shed new light to the amount of dark and luminous matter in these galaxies.

5.1 Luminous spirals

As I already described in Chapter 2 the most detailed information on the distribution of matter in spiral galaxies comes from their rotation curves (RCs). The detailed studies of the shapes RCs gives us crucial information about the distribution of matter in spiral galaxies what could lead to a better understanding of the properties and the nature of dark matter. To this respect, it is illustrative to remind that, after we define ∇ ∇_h ∇_d the log slopes of the observed RC and of the two different mass components, and $\beta \equiv V_d^2/V^2$ the fractional contribution to the circular velocity of the luminous disk, these quantities are related, at any radius, by:

$$\nabla = (1 - \beta)\nabla_h + \beta\nabla_d$$

where ∇_d is known from the photometry. The observed slope of the circular velocity ∇ therefore indicates, not necessarily in a straighforward way, two crucial properties of the mass distribution in spirals: through β the disk mass and through ∇_h the halo density slope.

Let us point out to the work on this subject already done. Using a large sample of galaxies (616 galaxies) Persic, Salucci & Stel (1996, hereafter PSS96) derived the universal rotation curve (URC) out to 3 disk lengthscales and extended it out to 6 disk lengthscales with HI data.

Recently Catinella, Giovanelli and Haynes (2006) have analyzed a sample of about 2200 low redshift disk galaxies. They constructed the template RC's for objects of different luminosities. The result for the low luminosity galaxies are in agreement with the URC. For high luminosity galaxies there is a disagreement for $R > 3R_d$. While the URC shows a clear decline, the template Catinella et al RC's have a rising-flat shape.

Let us notice that, proven the existence of an Universal Curve, that built in PSS, that uses the luminosity as the galaxy identifier and the disk lenght-scale as unit of measure of the radial coordinate, must be considered just as its (already efficient) proto-type, that however can be still improved to better reproduce any individual RC.

Therefore, the issue of the outer shape of the RC's for high luminosity systems is an open question after Catinella et al that confirm the zeroth order of the URC paradigma but claimed a difference Universal function.

In both studies Persic, Salucci & Stel (1996) and then Catinella et al. (2006) the systematics was "collected" into a number of coadded RC's, large at low luminosity but small at high luminosity due to the cut-off in the Luminosity function of Spirals. Given the disagreement and the limitness of the URC at the highest end of the luminosity function it is necessary to study "individually" the kinematics of such objects. Here we will present the detailed RC's of 33 high luminosity spiral galaxies

-24.5 < M < -22.5 and study the systematics of their outer profiles.

5.2 Data selection

We selected the high-quality RC's of high luminosity massive galaxies. We have imposed the following selection criteria for RC's:

1. B < 0.5 R_D, where B is the resolution of the observations;
2. at least 4 independent measures in the region of interest;
3. no warps;
4. small errors in velocity < $\triangle$ V/ V < 0.04 >;
5. V(3 R_D) > 200 km/s;
6. luminosities in the range -24.5 < M < -22.5

We restricted our sample to late-type spirals (Sb or later) and of course we did not considered those in PSS.

We found 33 objects, where optical data is 4 galaxies from the Courteau sample (Courteau 1997), 10 galaxies from the Vogt sample (Vogt 2004) and 11 galaxies from SFI++. And radio data is 4 galaxies from SFI++, 4 galaxies from KvdK04 (Kregel& van der Kruit 2004).

5.3 Analysis of the data

We decided to analyze separetely optical (Hα) and radio (HI) data. In the region under study each of the two channels has its own well known observational advantages and disadvantage and a comparison its well worth. For each galaxy we measure the distance from the center in units of R_D - the exponential disc length-scale. Then we

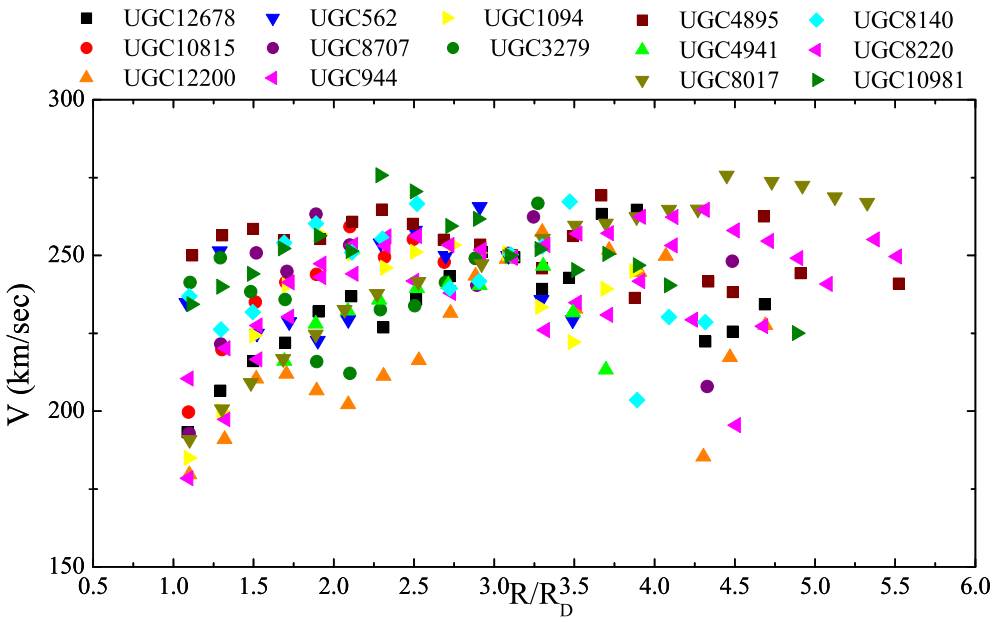

Figure 5.1: RCs of the 14 galaxies from Courteau and Vogt samples. $H\alpha$ data

consider a number of radial bins. For the Hα RC's we take the bin size $\delta = 0.2R/R_D$. And for the HI) RC's we take the bin size $\delta = 0.6R/R_D$ (for the details see Chapter 3).

Since in the range in question the luminosity dependence of the slope is certainly less than the discrepancy we are to solve we normalize the RC's by setting their values at $3R/R_D$ to the reference value of 250 km/s. The resulting *normalized* RC's are shown on Fig.5.1, Fig.5.2, Fig.5.3.

We then average the velocity in each radius bin and obtain the final average rotation curve that is shown on Fig.5.4 and Fig.5.5. It is apparent that the rotational velocity in high luminosity spiral galaxies, between $3R_D$ and $6R_D$ is declining with distance (for $R > 3R_D$), as R, though slightly slower than that found for the URC.

We used rotational curves of 33 high luminosity (M < -22.5) spiral galaxies to derive the average rotational curve. We have analyzed separetely $H\alpha$ and HI data. We find that this average rotational curves remaining constant or is decreasing with

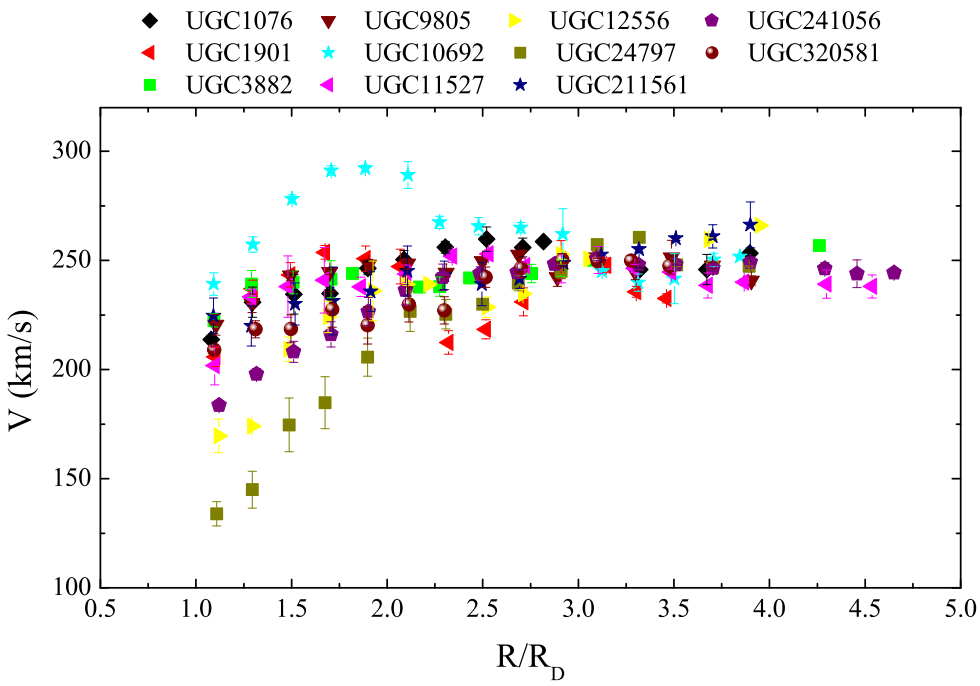

Figure 5.2: RCs of the 11 galaxies from SFI++ sample. $H\alpha$ data

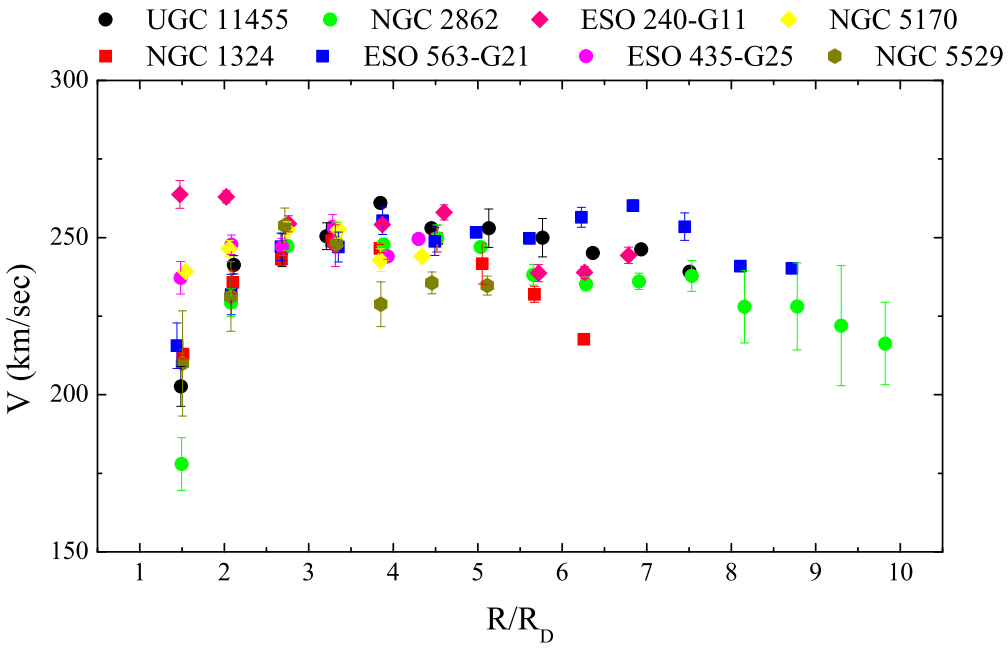

Figure 5.3: RCs of the 8 galaxies from SFI++ and KK samples. *HI* data

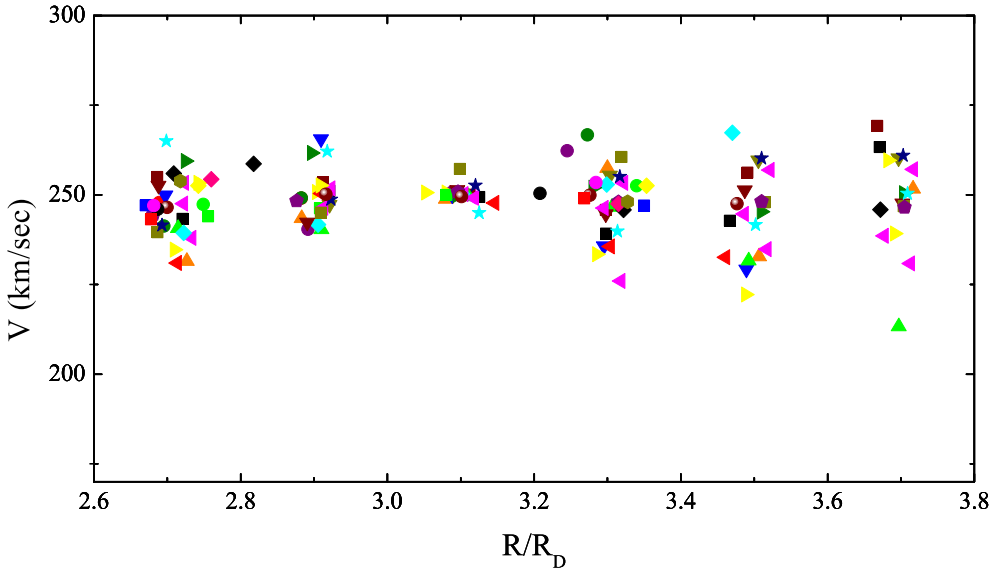

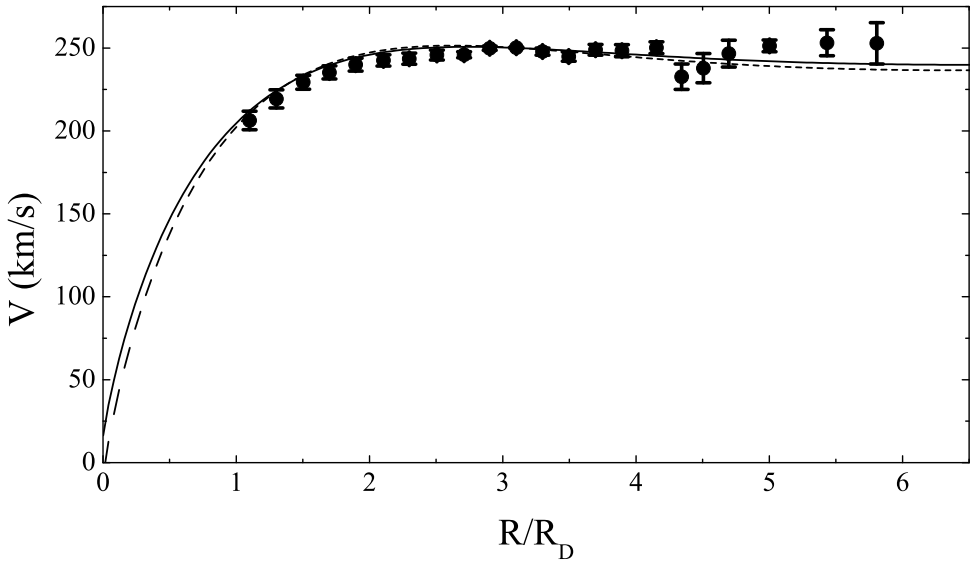

Figure 5.5: The average RC of the 25 spiral galaxies of Courteau, Vogt and SFI++ samples. $H\alpha$ data

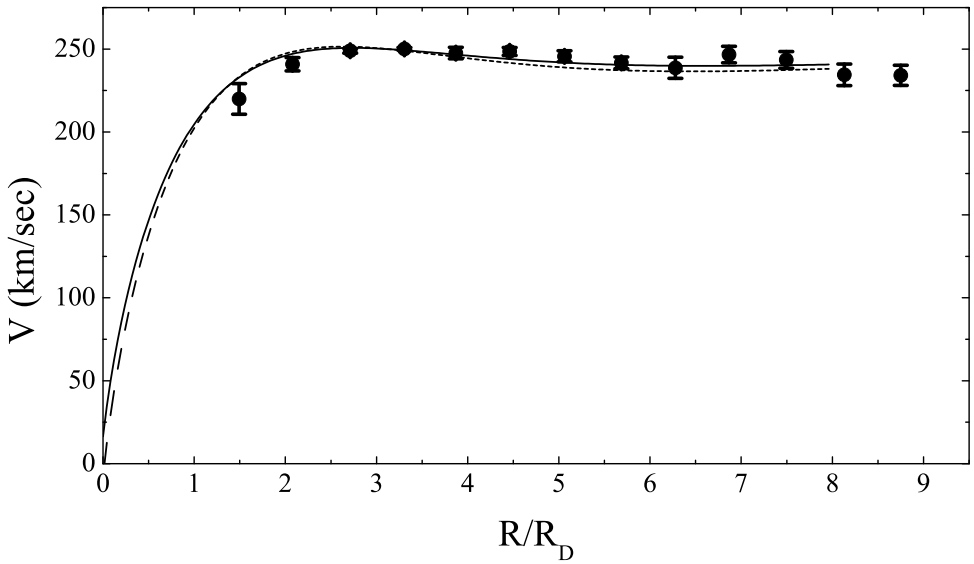

Figure 5.6: The average RC of the 8 spiral galaxies of SFI++ and KvdK04 samples. HI data

Table 5.1: Information on the galaxies of the sample. Name, absolute magnitude in I and R bands, inclination, reference

Name	M_I	M_R	inc	reference
(1)	(2)	(3)	(4)	(5)
UGC562		-22.46	68	2
UGC944	-23.70		81	1
UGC1076	-23.47		72	3
UGC1094	-23.67		80	1
UGC1901	-23.00		66	3
UGC3279	-24.47		82	1
UGC3882	-23.36		62	3
UGC4895	-23.35		70	1
UGC4941	-23.48		83	1
UGC8017	-23.62		73	1
UGC8140	-23.49		78	1
UGC8220	-23.9		86	1
UGC8707		-21.69	56.8	2
UGC9805	-23.15		68	3
UGC10692	-23.12		77	3
UGC10815		-21.55	77.6	2
UGC10981	-24.29		66	1
UGC11455	-23.3		84	3
UGC11527	-22.81		78	3
UGC12200		-22.06	56.8	2
UGC12556	-23.40		68	3
UGC12678	-23.80		90	1
UGC24797	-23.29		72	3
UGC211561	-23.36		60	3
UGC241056	-23.59		80	3
UGC320581	-23.19		65	3
NGC1324	-23.6		78	3
NGC2862	-23.2		86	3
NGC5170	...		90	4
NGC5529	...		90	4
ESO240-G11	-22.8		90	4
ESO435-G25	-22.75		90	4
ESO563-G21	-23.6		83	3

column 1 - galaxy name,

column 2 - the absolute I magnitude,

column 3 - the absolute R magnitude (Courteau 1996)

column 4 - inclination of the galaxy,

column 5 - RC reference: Vogt - 1, Courteau - 2, SFI++ - 3, KvdK04 - 4.

radius in the range $3R_D - 6R_D$. This indicates that in the more luminous spiral galaxies the fraction of luminous matter is larger than in galaxies of lower luminosity showing a rising RC.

Chapter 6

Probing dark matter halos of spiral galaxies at unexplored distances through satellites kinematics

In this Chapter I present our new approach in studying the dark matter halos of spiral galaxies. We want to probe the halos at large distances and that is why we propose to use the satellites of spirals in order to probe the dark matter halo of primaries. The project is still in progress. Here I will present the preliminary results.

6.1 Satellites as a tracer of dark matter

It has been firmly established that the dark matter halos extend far beyond the optical boundaries of galaxies. However the real extent and the distribution of the dark matter in the part of the halos well outside the galactic disks is still unknown. Dark matter plays a crucial role in the process of galaxy formation. The gravitational potential wells created by dark matter perturbations provide the necessary environment for condensation of the baryonic component leading to formation of proto galaxies. The initial stage of this process can be studied analytically but the later nonlinear

phase can be only modeled numerically. In analytical approximations the dark matter halos are treated as isothermal spheres. Numerical studies show that independently on the halo mass, the spectrum of initial density perturbations and the values of cosmological parameters, the density profiles of virialized systems can be well fitted by a simple universal profile proposed by Navarro, Frenk and White (1997). But there is a disagreement between the universal profile and observed rotational velocity curves. Analysis of observed gravitational lensing by galaxies indicates that dark matter halos extend more than five times further than the visible disk of galaxies. Observed rotational velocity curves provide so far the best information on the distribution of dark matter in central parts of galactic halos. The real distribution of dark matter in the halos far from the galactic centers is not known. The main problem here is to find an appropriate, visible tracer at a sufficiently large radius in the halo.

We decided to use satellites that surround host galaxies as tracers of dark matter around galaxies. Satellite galaxies are one of the best available probes of outer galactic halos. They are sufficiently bright and sufficiently smaller than their associated primary and can be treated as test particles in a dynamical analysis. Several works using this technique has been done already Zaritsky (1997), Sales & Lambas (2004), Brainerd (2004). Very interesting results have been obtained, extending our understanding of the nature of dark matter. But in most cases studied so far the primary galaxy possessed not more than 3 satellites. Our approach is different we decided to select a small number of galaxies (comparing with the previous studies), but to use more powerful telescope. In order to be able to find more satellites around the primary galaxy.

6.2 Sample selection

The important step is the sample selection. We wanted to choose primary galaxies that have similar characteristics. And this is one of the advantages of proposed

method. The previous studies (Zaritsky 1997, Brainerd 2004) were using galaxies of different Hubble types and luminosities. On the base of information from the Sloan Digital Sky Survey we choose 8 galaxies. The list of the galaxies is in the Table 7.1. The galaxies that we have selected are:

- all galaxies are the late type spiral galaxies;
- isolated: all objects within a radius of 500kpc and 1000km/s in velocity have a magnitude at least 2.5 below the primary galaxy;
- all galaxies are the late type spiral galaxies;
- have an inclination between 40° and 70°;
- have a redshift $0.029 < z < 0.085$ (in order to have in VIMOS field of view region of 500 x 500 kpc that we want to observe);
- have at least 4 known satellites (from the Sloan Digital Sky Survey SDSS).

Table 6.1: Selected primary galaxies

Name	z	Mag
J003828+000720	0.042	14.60
J221957-073958	0.038	13.57
J145211+044053	0.046	14.62
J152621+035002	0.083	14.94
J134215+015126	0.029	13.60
J153221-002549	0.085	15.18
J154904-004023	0.077	15.73
J154040.5-000933.5	0.076	15.7

Target	Exp.Time (s)	date
J003825+001316	2×2200	Aug 18 2007
J134215+015126	2×2000	Apr 20 2007
J145211+044055	3×2000	Apr 20 2007
J152621+035002	2×2000	Apr 20 2007
J153221-002549	2×2200	Apr 20 2007
J154040-000933	$4 \times 2700 + 1800$	Apr 7 2005, May 27 2005
J154904-004023	2×2200	Apr 20 2007
J221957-073958	1800	Aug 31 2007

Table 6.2: Log of the scientific exposures executed with EMMI+NTT

6.3 Observations

The observations have been conducted with 2 instruments: the kinematics of primary galaxies has been measured with EMMI (mounted at the NTT) in visiting mode while the hunt for satellites and the measurement of their radial velocity with VIMOS at VLT-Melipal in service mode.

6.3.1 Kinematics of primary galaxies

The major axis ionized gas rotation curve of the primary galaxies has been obtained by means of long-slit spectroscopy using the EMMI instrument mounted on NTT (la Silla, ESO). EMMI was equipped with grating 6 and a 1.0" slit in the Red Arm and the wavelength was chosen in order to detect the Hα, the [NII]658nm and [SII]671,673nm emission lines and measure the galaxy rotation curve. Typical exposure time was $2 \times 2000s$ or more depending on the observability of the target galaxies. In tab.6.2 we report the observing log of the scientific exposures obtained with EMMI+NTT.

Data reduction has been done with MIDAS and IRAF standard routines. Wavelength calibration has been curried out using the Helium-Argon calibration lamp. All frames have been bias subtracted, flat field corrected, cosmic ray cleaned (by means of the IRAF routine "*lacosspec*" by P. van Dokkum, 2001) and wavelength calibrated.

After wavelength calibration repeated exposures on the same target have been aligned and summed. At this stage, we used the night-sky emission lines to assess the quality of the wavelength calibration. In fact, we will use this data not only to derive the rotation curve of the galaxies but also to define their recession velocity. This velocity will be compared with the one measured for the satellites using VIMOS. The instrumental FWHM is typically 1.3 ± 0.1 $\AA$ that corresponds to an instrumental velocity dispersion $\sigma = 25 \pm 2$km/s. In Fig.6.2 we show an example of FWHM measurements for the primary galaxy J145211+044053. To identify sky-lins we used the spectroscopic atlas by (Osterbrock et al.1997). Small offsets in the wavelength calibration has been found, ranging from 0km/s to 5km/s and the data have been corrected accordingly. In Fig.6.3 we show the case of J145211+044053 where the sky emission lines indicates a residual velocity offset of less than 0.6km/s after the wavelength calibration curried out using the Helium-Argon calibration lines.

The sky emission has been then subtracted by means of the IRAF task *background*. Finally, a self written IDL routine has been used to derive the galaxy rotation curve. The routine run in a quasi-automatic way, allowing to check the visually the result. The velocity is measured by simultaneously fitting the Hα, the [NII]658nm and [SII]671,673nm emission lines with Gaussian line profiles, adopting the same velocity and line-width for all the lines. In the external region it is possible to sum the spectrum in a radial ranges in order to increase the signal-to-noise of the emission lines. The routine take into account the instrumental line-width and remove the continuum by fitting a first order polynomial.

The rotation curves derived for the sample galaxies are plotted in fig.6.14-6.19. Once the kinematics has been derived, we fold it around the center and derive the rotation curve. In doing this we allow a small change in the center that has been previously taken as the photometric center of the spectrum. The folded rotation curves are plotted in fig.6.20-6.24.

Target	Exp.Time (s)	date
J003825+001316	2×120	Jul 4 2006
J134215+015126	2×120	Mar 2 2006
J145211+044055	2×120	Mar 2 2006
J152621+035002	2×120	Mar 2 2006
J153221-002549	2×120	Mar 2 2006
J154040-000933	8×120	Mar 18 2005
J154904-004023	2×120	Mar 2 2006
J221957-073958	2×120	May 29 2006

Table 6.3: VIMOS. Log of the preimaging exposures. All images have been taken with a seeing better than $1.2''$

6.3.2 Satellites radial velocity

We used the VIsual MultiObject Spectrograph VIMOS to identify satellites orbiting our primary galaxies and measure their radial velocity. The instrument consists of four independent spectrographs each observing a quadrant of about $7' \times 8'$. In the high spectroscopic resolution mode, we can accomodate about 50 slits on each quadrant. The product of each exposure is therefore four FITS images, one for each quadrant observed. A complete description of the instrument can be found at the URL http://www.eso.org/instruments/vimos/ on the ESO web pages. Taking MOS spectra with VIMOS is done in two phases, the preimaging and the spectroscopy. The preimaging consists in the acquisition of an image of the field we are going to observe spectroscopically. This image is used to draw the mask containing the slits we want to use. In tab.6.3 we list the observing log of preimaging.

The images obtained have then been used to draw the mask (one for each quadrant) that will be used to obtain the spectra of the cantitade satellites. In principle, it is possible to define several set of masks for the same pointing. However, because of the complexity of the data reduction we decided to define only one set and to repeat the same pointing several times in order to increase the signal-to-noise.

We used the VIMOS Mask Preparation Software (VMMPS) to prepare the set of masks. VMMPS interactivelly allows to physically draw each single slit on the

Target	Exp.Time (s)	date
J003825+001316	2×2180	Aug 14 2006
J134215+015126	5×2180	Apr 20 2006
J145211+044055	6×2180	Apr 7,21,23,26 2006
J152621+035002	5×2180	May 22,24,28 2006
J153221-002549	8×2180	Apr 26,27,28 2006
J154040-000933	6×1000	May 2, Jun 6,9, Jul 9 2005
J154904-004023	5×2180	May 2,27,29 2006
J221957-073958	5×2180	Jul 17,18 2006

Table 6.4: VIMOS. Log of the Multi Object Spectroscopy exposures. All images have been taken with a seeing better than $1.2''$

preimage frame, visually inspecting the candidate satellites. The constrains that limited the choise of target candidate satellites was only the superposition of slits. We therefore have drawn a slit over each extragalactic-like object present in the field of view, prefering the brightest ones when they were on the same column and the resulting spectra would overlap. Slits were drawn longer than the objects in order to allow a proper sky subtraction. We know the redshift of few object in the field we know observed spectroscopically in the SDSS. Priority has been given to known satellites, while known not-satellites have been excluded.

As set-up of the instrument we adopted the grism HR_orange on the four arms of the instrument. The grism is used in combination with the ording sorter filter GG435. The grism is characterized by a dispersion of 0.6Å/pix that correspond to a spectral resolution of 2150 for a 1" slit. The spectra that are produced cover the whole CCD and therefore is not possible do observe two targets alligned on the same column. Since we are keeping the default orientation of the instrument without changing the position angle on the sky, we can not observe targets with identical RA. In average, we could accomodate about 50 slits in each quadrant tat is about 200 slits for each primary galaxy. In table 6.4 we give the observing log of the observations. The phase two of the proposal, containing finding charts and Observing Blocks has been submitted in March 2006. We organized the observations by repeating the same pointing with

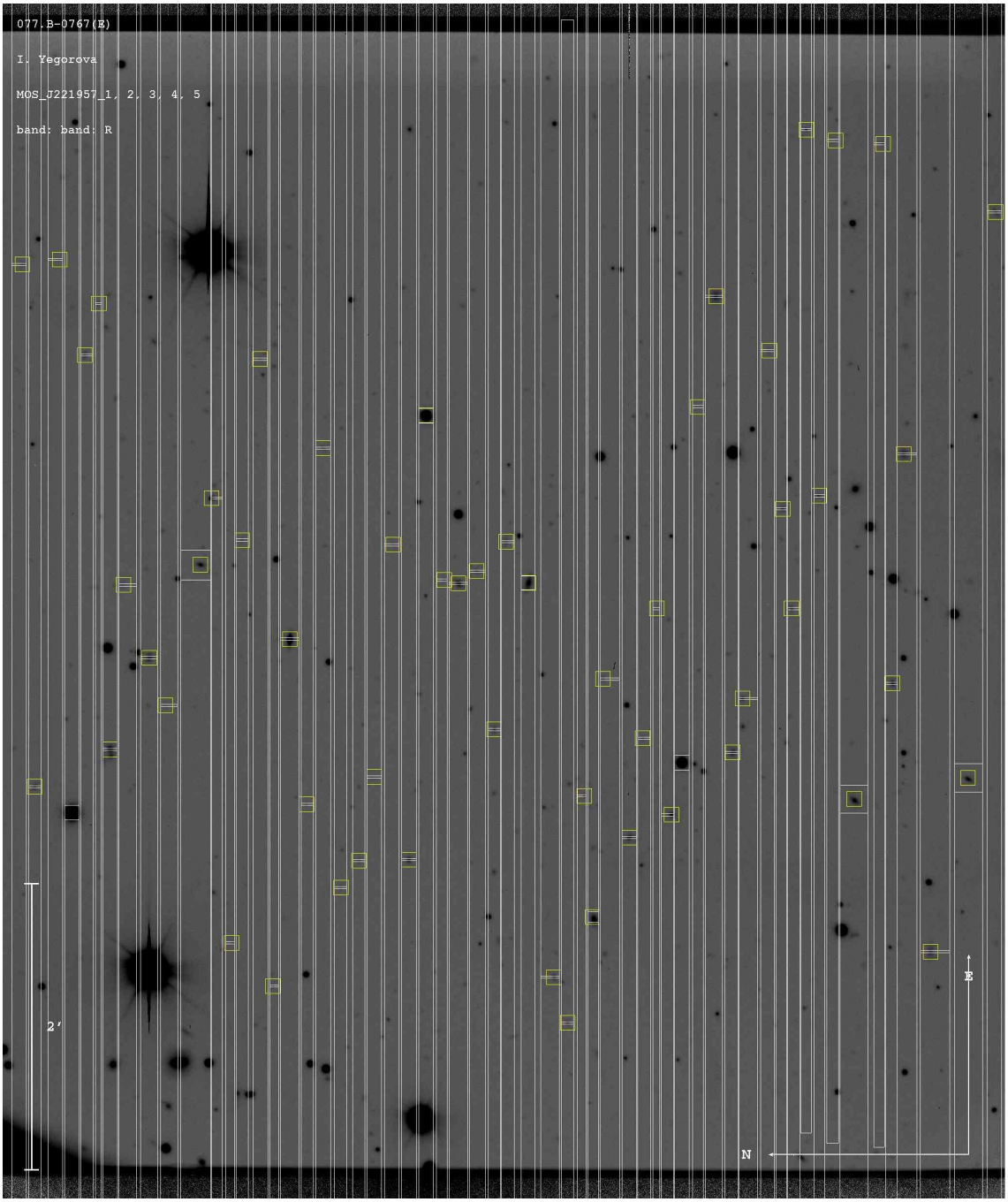

Figure 6.1:

the same mask 5 times. Each exposure is 2180 seconds long. Considering overheads, our observing block were of one hour of telescope time as requested by ESO rules for service observing. We also requested a dark/grey sky, not photometric but clear sky and a seeing better than 1.2". Some exposures that did not fulfill our requirement have been repeated. For this reason we obtained more exposures than requestes. Extra exposures, executed under weather conditions not complaning what requested, have been used only if the data quality was good. The exposures reported in table 6.4 are the one actually used in our final data reduction.

The data delivered by ESO are the original raw data and the data automatically reduced by the pipeline GASGANO. Because of the large data volume we have to reduce, which consists of eight fields, each producing about 200 spectra, fora total of about 1600 spectra, we decided to use the reduced data without running the pipeline. In fact, we will refine the calibration only of the objects that are found to be satellites, considerably reducing the ammount of spectra to be reduced. We therefore started our data reduction from the frames bias subtracred, flat field corrected and wavelength calibrated by the ESO data reduction pipeline. Data furter reduction of the spectroscopic data has been done with MIDAS. The first step was to assess the quality of each integration. We focused our attention on few spectra (typically of a bright and a faint object) and visually checked if the quality was the same in all exposures. Once the selection have been done and the low quality spectra (because of bad seeing or absorbtion by thin cluds) discarted, we computed the average spectrum for all frames. The second step was to approximativelly derive, in the sky subtracted spectra, the redshift of all targets. To this aim we used the following emission and absorbtion lines listed in teb 6.5

This second step allowed us to select possible satellites and reject all other background or foreground objects characterized by a radial velocity more than 2000km/s different than the primary galaxy. In the drawing of the masks containing the slits, we did not consider any constrain concerning the wavelength range. Indeed, slit po-

Line	wavelentgh Å
Lyα	1215.67
OII	3726.03
OII	3728.82
CaII K	3933.66
CaII H	3968.47
Hδ	4101.73
Hγ	4340.36
Hβ	4861.31
OIII	4958.92
OIII	5006.84
Mg	5183.6
Hα	6562.80
NII	6583.41
SII	6716.47
SII	6730.85

Table 6.5: Emission and absorbtion lines used in the preliminary redshift determination.

sitioned on the north side of each quadrant produced spectra in the red range, with wavelength larger than 5500Å. Slit positioned on the south side of each quadrant produced spectra in the blue range, with wavelength shorter than 6500Å. Our strategy is to derive the redshift of satellites either from the Hα,[NII] emission lines or from the Hβ,[OIII] emission lines that always fall in the observed spectral range. We could typically identify about 150 redshift for each primary galaxy. In Fig.6.4 we plot the redshift distribution obtained for J145211+044053. The redshift of the galaxy is 0.046 and we found 4 satellites. As a second example we plot in Fig.6.5 the same kind of histogram for J152621+035002 (z=0.083) where we found 17 satellites. After the satellites of a primary galaxies have been identified, we proceed with the measure of their radial velocity. Again, we used all emission lines available (typically Hα, [NII] or Hβ, [OIII]) and used the sky emission lines to refine the wavelength calibration. We first spatially average the spectrum of each satellite and derive its one-dimensional spectrum. We then measure the wavelength of a number of night-sky emissions and

SDSS identification	RA degrees	DEC degrees
(1)	(2)	(3)
J145211.01+044053.6	223.045901717	4.681570877
J145225.31+043801.0	223.10549813	4.63363286
J145215.25+043503.7	223.06356797	4.58438508
J145156.61+043255.5	222.985905	4.54875991
J145150.67+043844.4	222.96115163	4.64567645
J145156.01+045122.2	222.9834140	4.8562112
J145204.71+044653.9	223.0196530	4.7816439
J145207.46+044118.5	223.0310970	4.6885052

Table 6.6: J145211+044053: list of satellites detected. Entries (1)-(3) are taken from SDSS. Columns are: (1) name; (2)-(3) RA and DEC

the one of the emission lines of our satellite. We then compute the difference between the expected night-sky wavelength values and the measured ones, we fit a one-degree polynomial, discard outliers and re do fit fit. In Fig.6.6 we show the typical result of this procedure. We then use this regression to correct the wavelength measured for the satellite emission lines.

This procedure has been aaplied to all satellites found in our survey. As last step, we used a table, produced by the pipeline, that allows us to identify the spectra of the satellites to their position on the pre-images. Finally, we identified the satellites on the SDSS database in order to know their position on the sky. In Tab.6.6-6.8 I show the satellites found for one field, showing the difference in velocity with respect to the primary galaxies and the projected distances.

6.4 Data analysis

We have found for 7 primaries in total 77 satellites. In Table 6.2 I show the number of satellites found for each primary galaxy (for J003828+000720 the quality of the data was not sufficient for the analysis).

Then we derived precise radial velocity measurements for each satellite. To this

SDSS identification	u	g	r	i	z
(1)	(2)	(3)	(4)	(5)	(6)
J145211.01+044053.6	26.89	22.29	14.62	21.44	14.54
J145225.31+043801.0	18.91	17.50	16.77	16.39	16.11
J145215.25+043503.7	22.31	21.29	20.86	20.76	20.63
J145156.61+043255.5	19.73	18.42	18.06	17.88	18.04
J145150.67+043844.4	21.64	20.64	20.04	19.96	19.60
J145156.01+045122.2	19.00	17.65	17.13	16.79	16.50
J145204.71+044653.9	18.99	17.18	16.35	15.97	15.67
J145207.46+044118.5	19.15	17.85	17.25	16.89	16.71

Table 6.7: J145211+044053: list of satellites detected. Entries (1)-(6) are taken from SDSS. Columns are: (1) name; (2)-(6) magnidutes.

SDSS identification	redshift	Dist (kpc)	Δ V (km/s)
(1)	(2)	(3)	(4)
J145211.01+044053.6	0.046±0.00010		
J145225.31+043801.0	0.047±0.00009	246.6	93.3
J145215.25+043503.7		319.1	20.7
J145156.61+043255.5		470.5	22.0
J145150.67+043844.4		296.5	-71.6
J145156.01+045122.2	0.047±0.00018	599.0	165.2
J145204.71+044653.9	0.046±0.00015	334.2	-134.5
J145207.46+044118.5	0.046±0.00008	52.7	-134.5

Table 6.8: J145211+044053: list of satellites detected. Entries (1)-(4) are taken from SDSS. Columns are: (1) name; (2) redshift (if available); (3) projected distance of the satellites to the primary galaxy; (4) velocity of the satellites with respect to the primary galaxy. For the last three objects column (4) has been computed from the SDSS redshift.

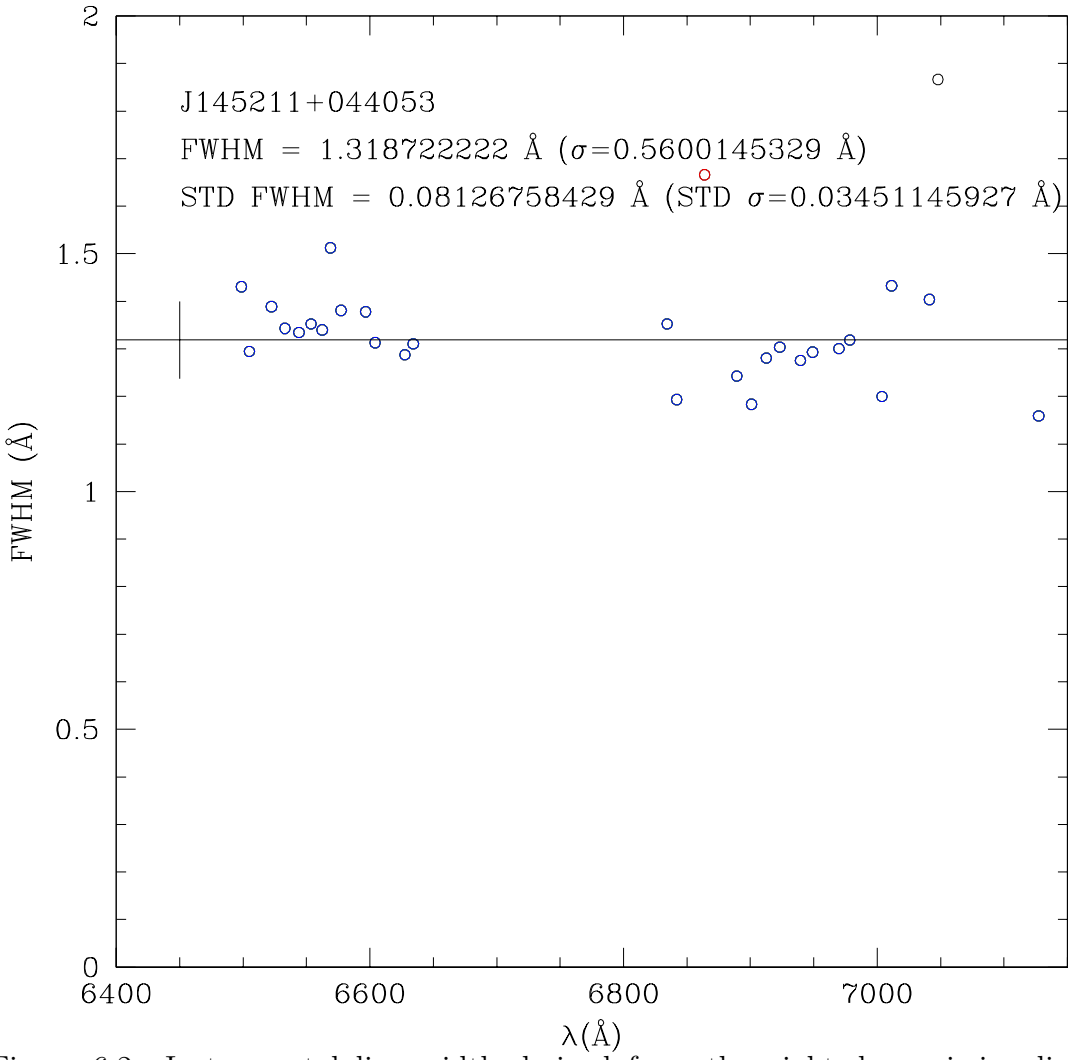

Figure 6.2: Instrumental line width derived from the night-sky emission lines as a function of wavelength. *Circles* are the FWHM measurements for several lines, the *orizontal line* indicates the mean FHWM and the *vertical segment* the STD of single FHWM measurements. The mean value of FWHM (and the corresponding $\sigma = FWHM/2.3548$) and its STD are also indicated numerically. For this example we used the measurements done on the combined spectrum of J145211+044053.

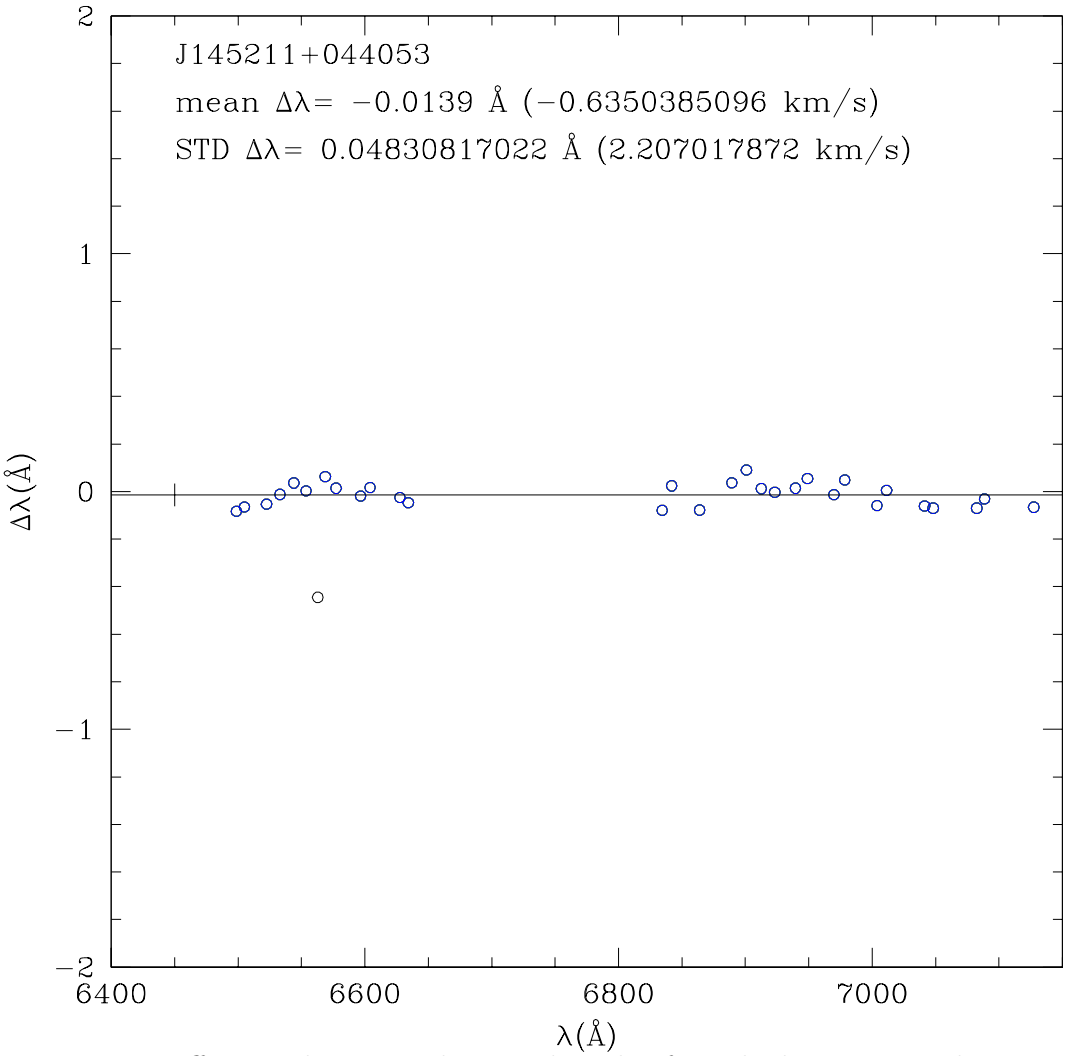

Figure 6.3: Difference between the wavelength of nigth-sky emission lines and the measured one at differend wavelengths. *Circles* are the datapoints, the *orizontal line* indicates the mean differencee and the *vertical segment* the STD. The mean value of $\Delta\lambda$ (and the corresponding velocity at Hα) and its STD are also indicated numerically. For this example we used the measurements done on the combined spectrum of J145211+044053.

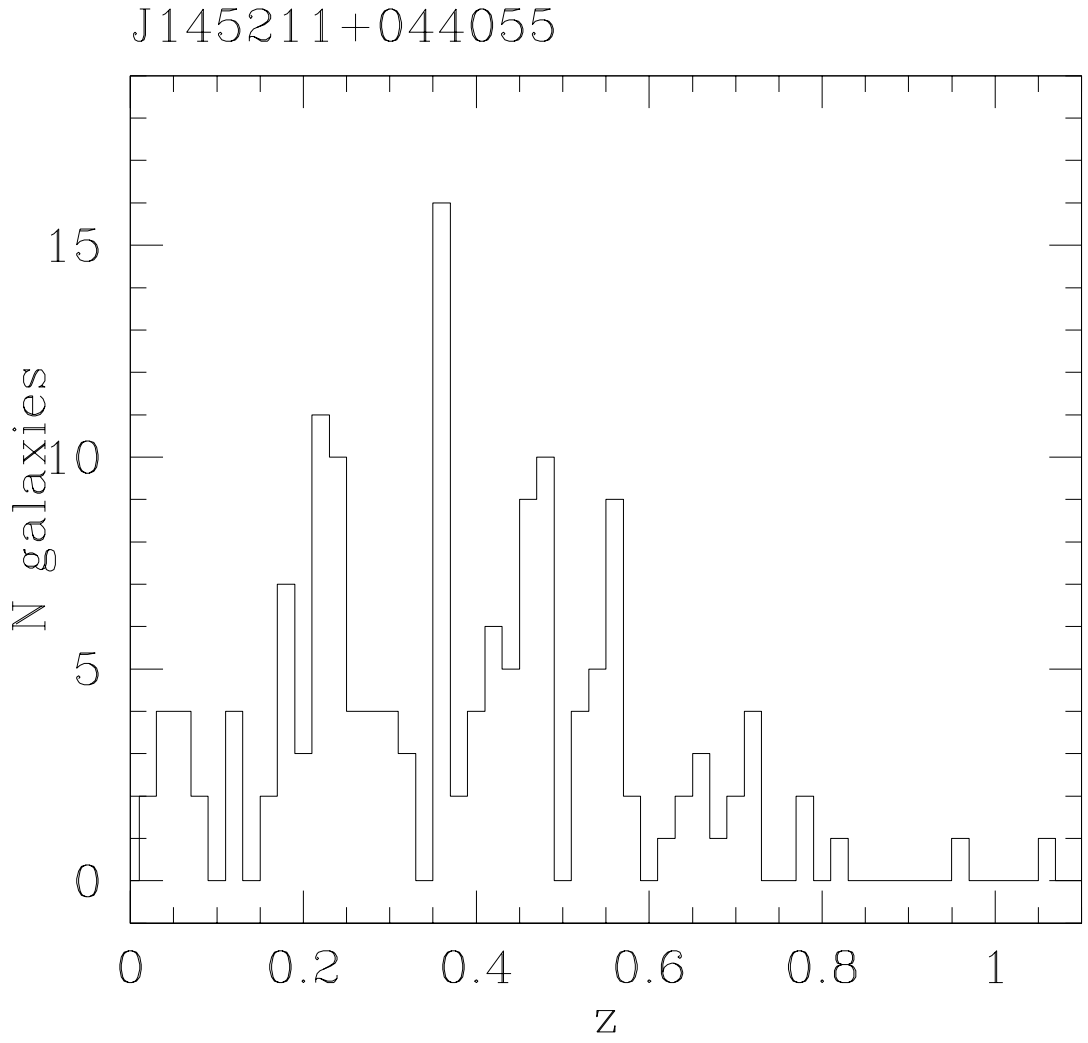

Figure 6.4: Redshift distributions measured for 153 objects in the field of J145211+044055.

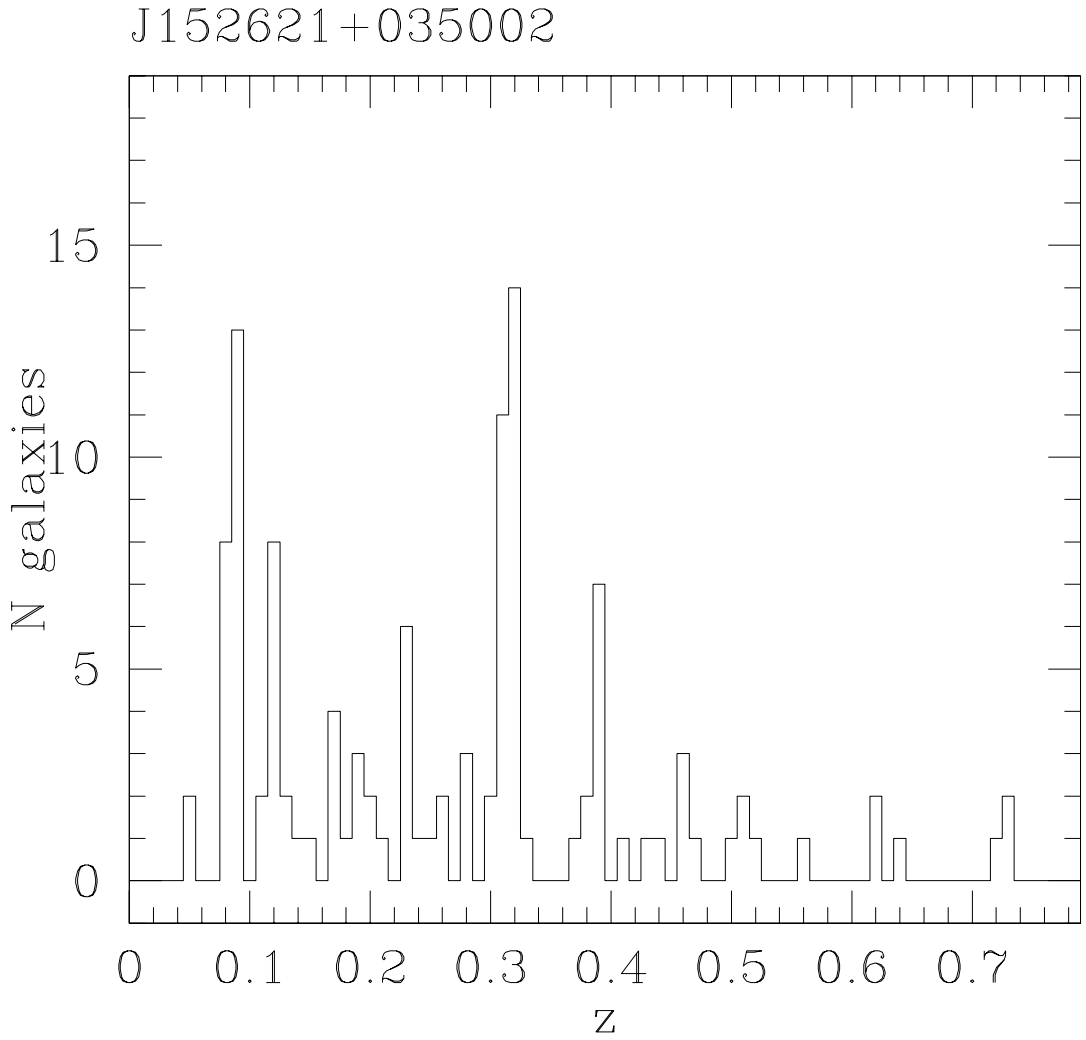

Figure 6.5: Redshift distributions measured for 117 objects in the field of J152621+035002.

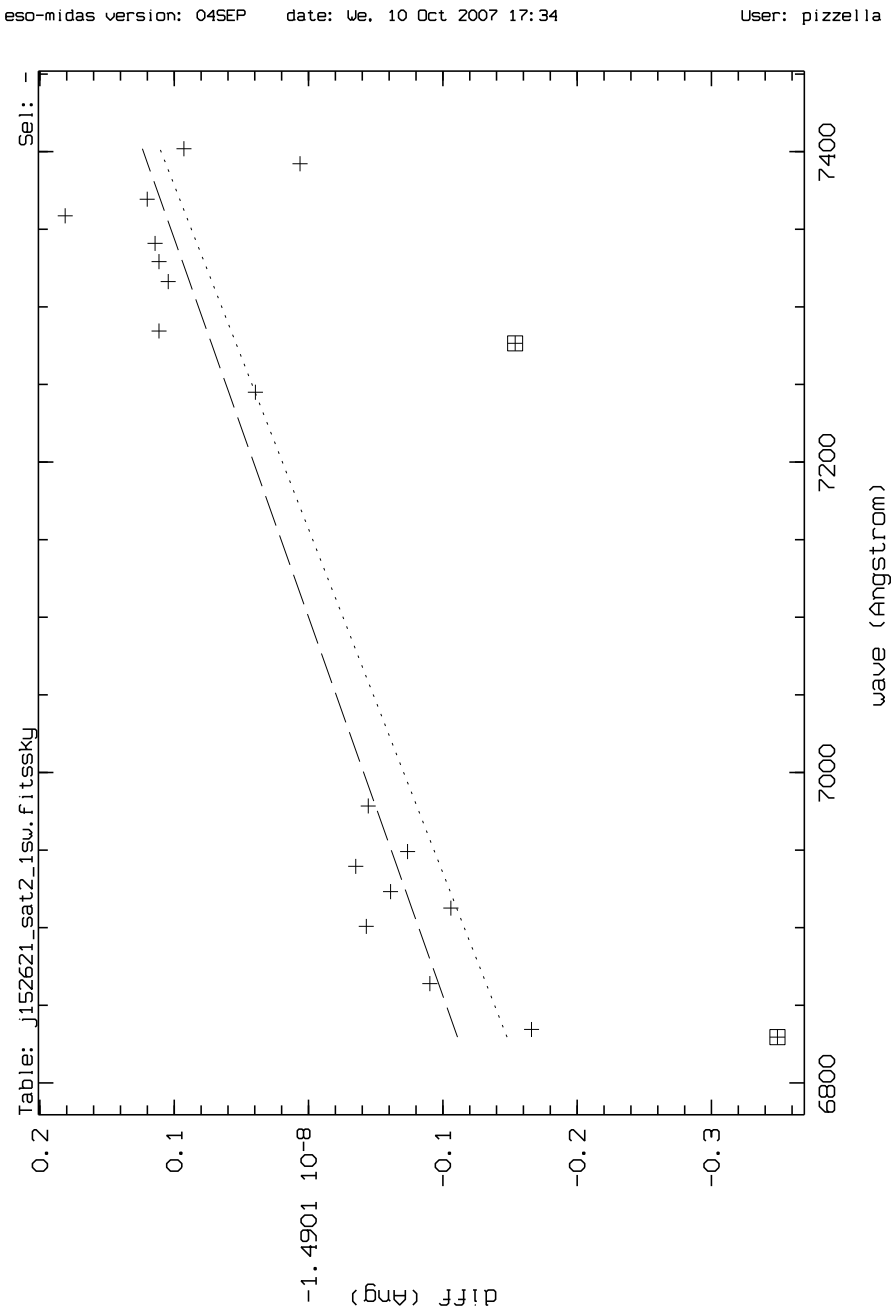

Figure 6.6: Wavelength calibration fine tuning for one satellite of J152621+035002. The plot shows the difference of measured and real wavelength for different lines (*crosses*) and a linear fit to the redisuals before (*dotted line*) and after *dashed line*) the rejection of two outlying points (*squared crosses*).

Table 6.9: Number of satellites found for each galaxy

Name	N of satellites
J003828+000720	-
J221957-073958	7
J145211+044053	7
J152621+035002	17
J134215+015126	8
J153221-002549	19
J154904-004023	8
J154040.5-000933.5	7

aim we measured the wavelength of all emission lines visible in the spectrum, using skylines to refine the wavelength calibration. The radial velocities are measured with a typical uncertainty of 10km/s. We identified the satellites on the SDSS catalog, obtaining their position and deriving their distance to the primary galaxy.

Since the work is still in progress for now I present some results. In Fig. 6.7-6.12 for three galaxies of the sample I show RC, velocity of the satellites, and the position of the satellites respect to the primary.

For three galaxies J134215, J145211, J153221 we made the binning for the velocity of their satellites (15 satellites) and the result is in Fig. 6.13. We fit it with the universal rotation curve from Salucci et al. 2007. The last point probably is not trustable, because the satellites situated far enough from the primaries. Otherwise the universal rotation curve fits very well the data point. Although the work is still in progress we can say that our approach works very well. First, because we have found a double amount of the satellites (that it was known before from the SDSS). And second, since we use primary galaxies of the same type it gives the advantage of reliable studies.

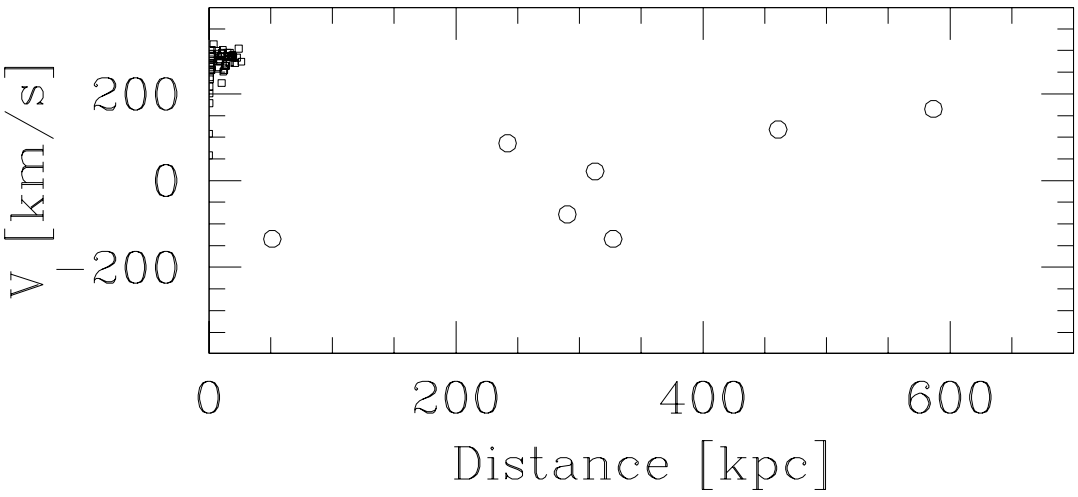

Figure 6.7: RC and velocity of the satellites for J145211

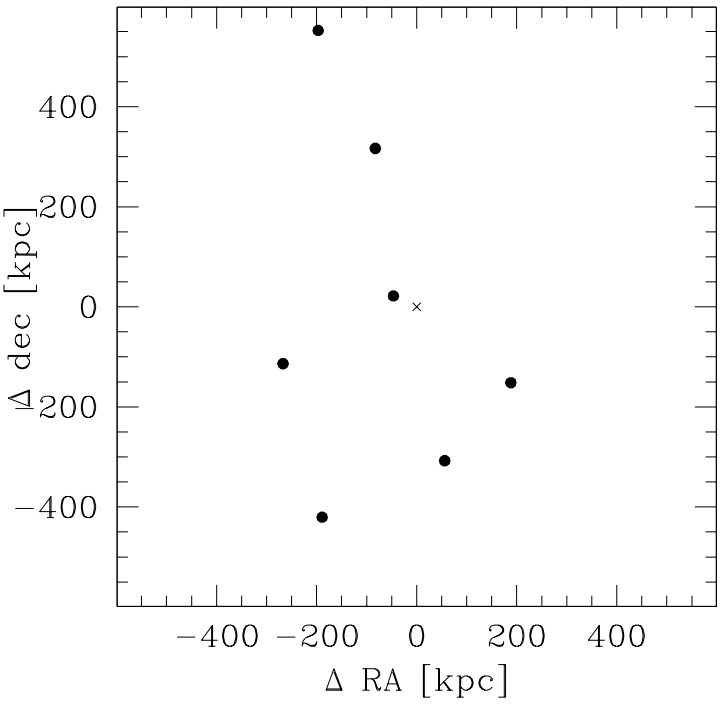

Figure 6.8: Position of the satellites for J145211

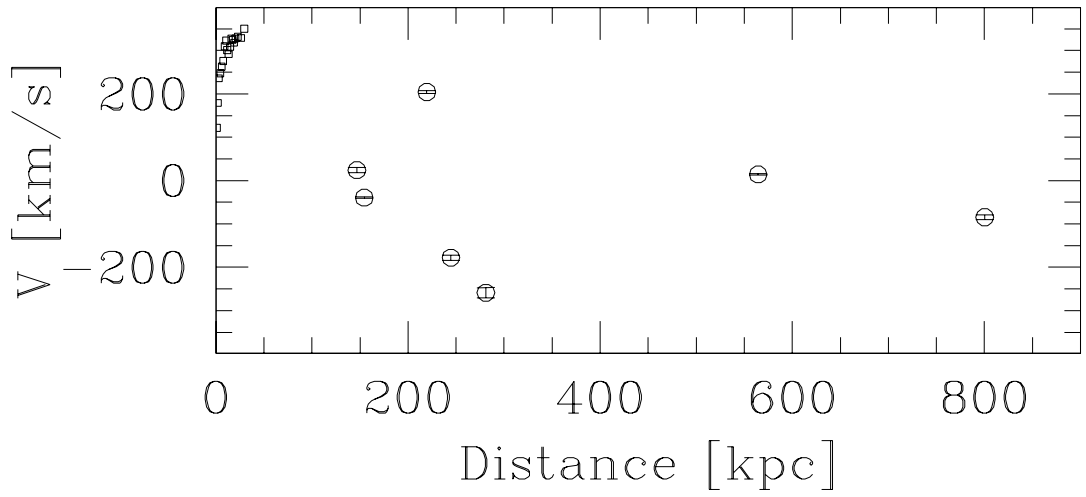

Figure 6.9: RC and velocity of the satellites for J154040

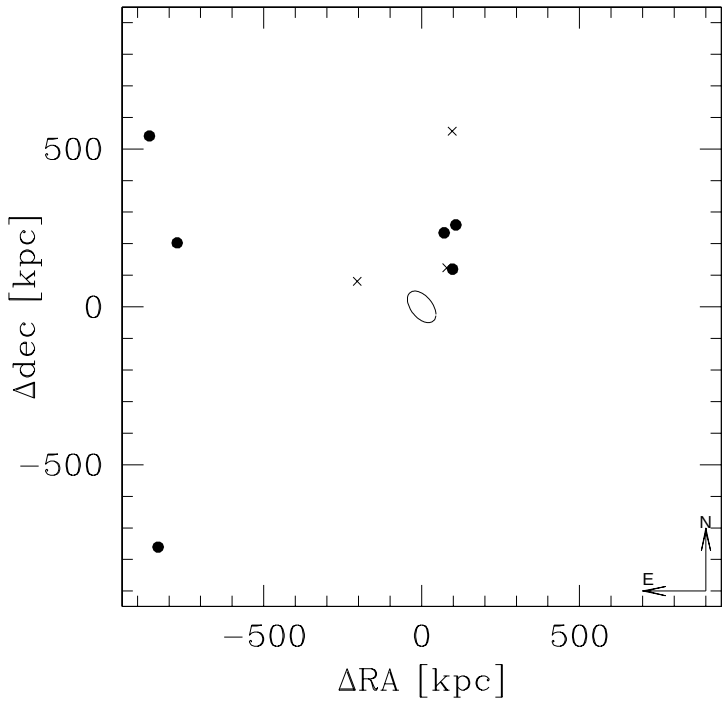

Figure 6.10: Position of the satellites for J154040

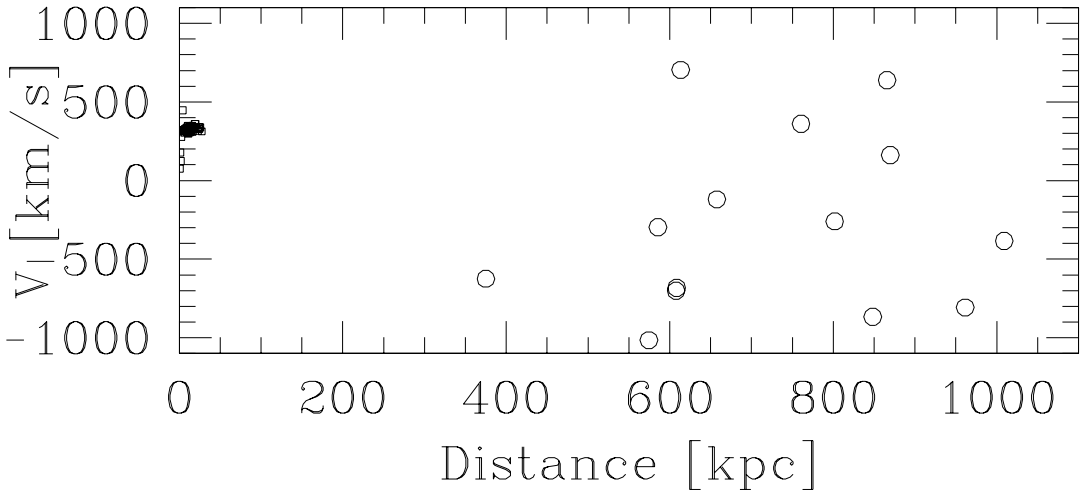

Figure 6.11: RC and velocity of the satellites for J153221

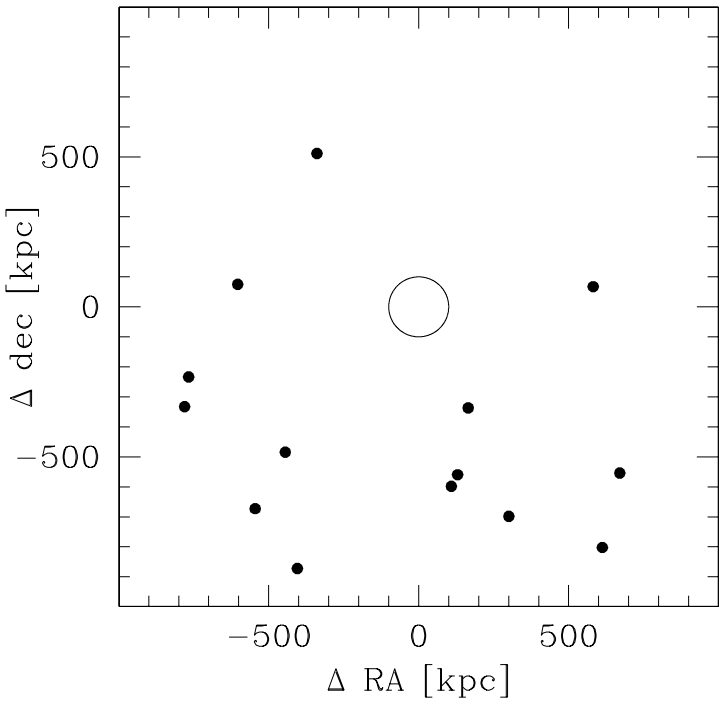

Figure 6.12: Position of the satellites for J153221

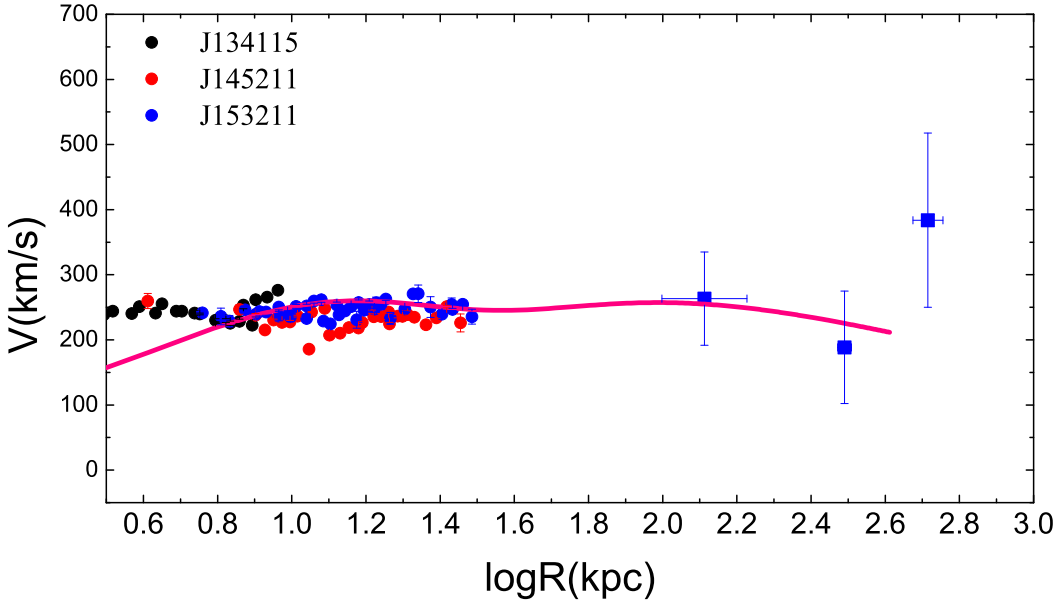

Figure 6.13: RC, binning satellites velocities and URCII

6.5 Figures related to this chapter

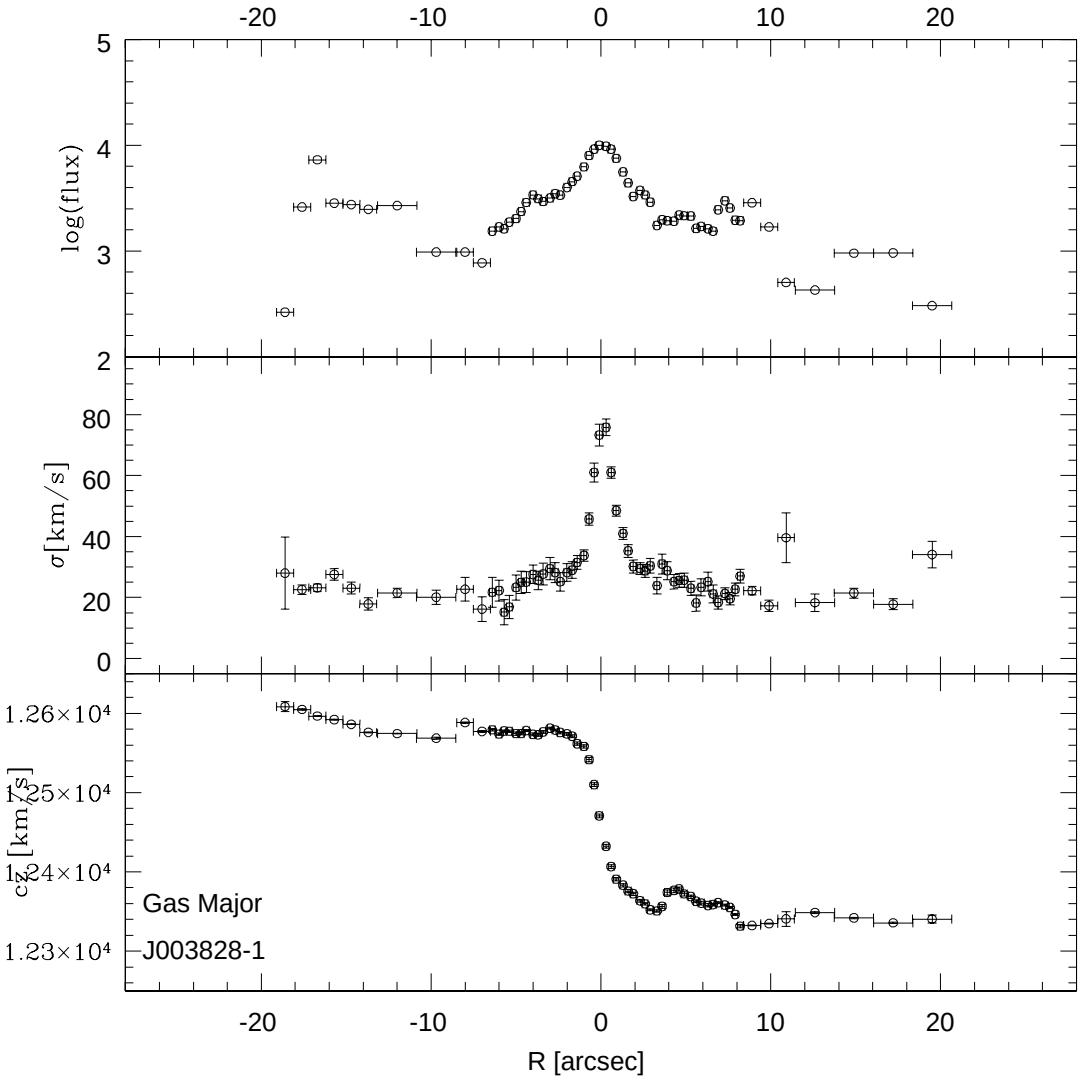

Figure 6.14: Emission line fitting result for J003828. *Lower panel*: radial velocity; *middle panel*: line veloocity dispersion; *upper panel*: Hα intensity (in arbitrary units). The radius at which the emission of the continuum is maximum has been adopted as center.

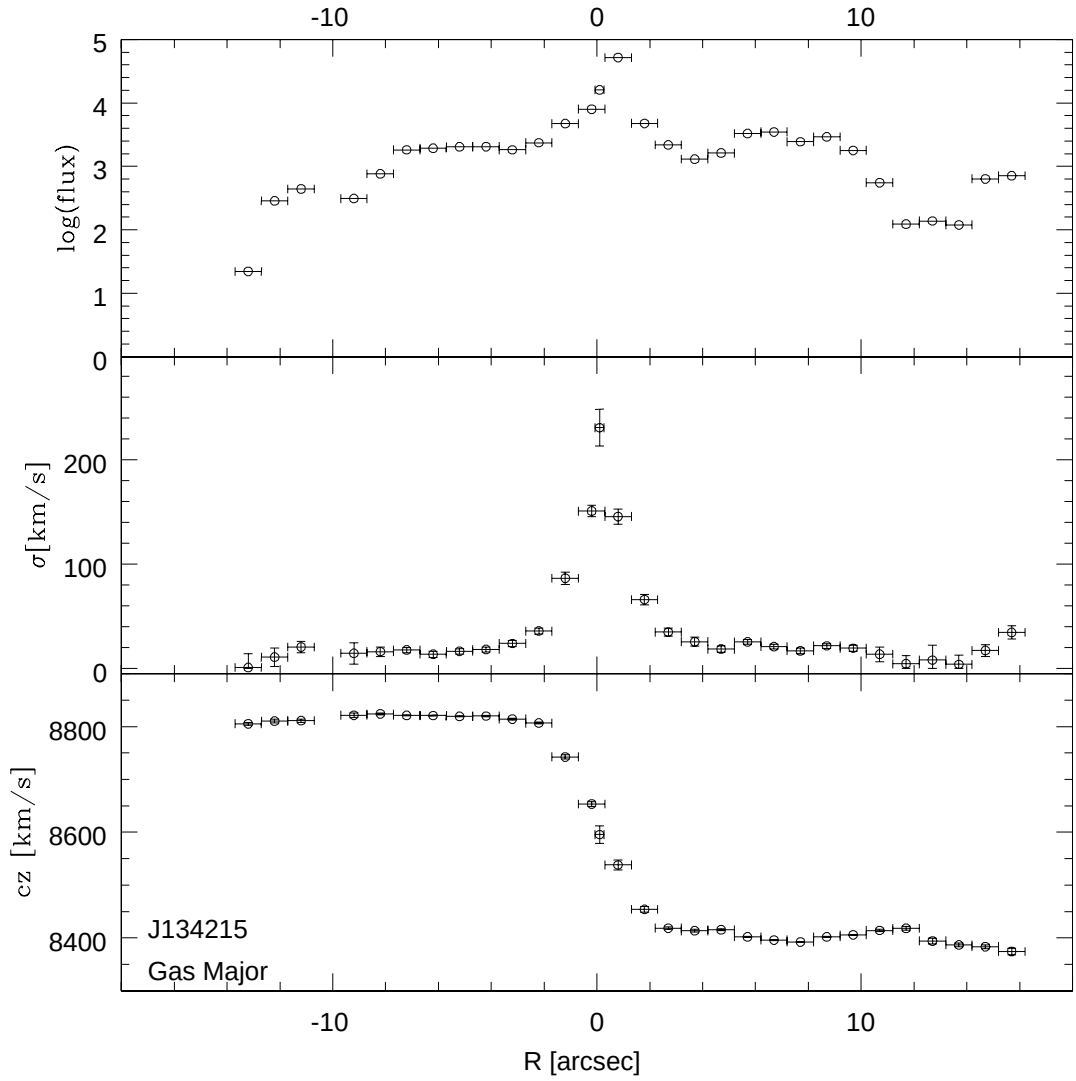

Figure 6.15: Emission line fitting result for J134215. *Lower panel*: radial velocity; *middle panel*: line veloocity dispersion; *upper panel*: Hα intensity (in arbritrary units). The radius at which the emission of the continuum is maximum has been adopted as center.

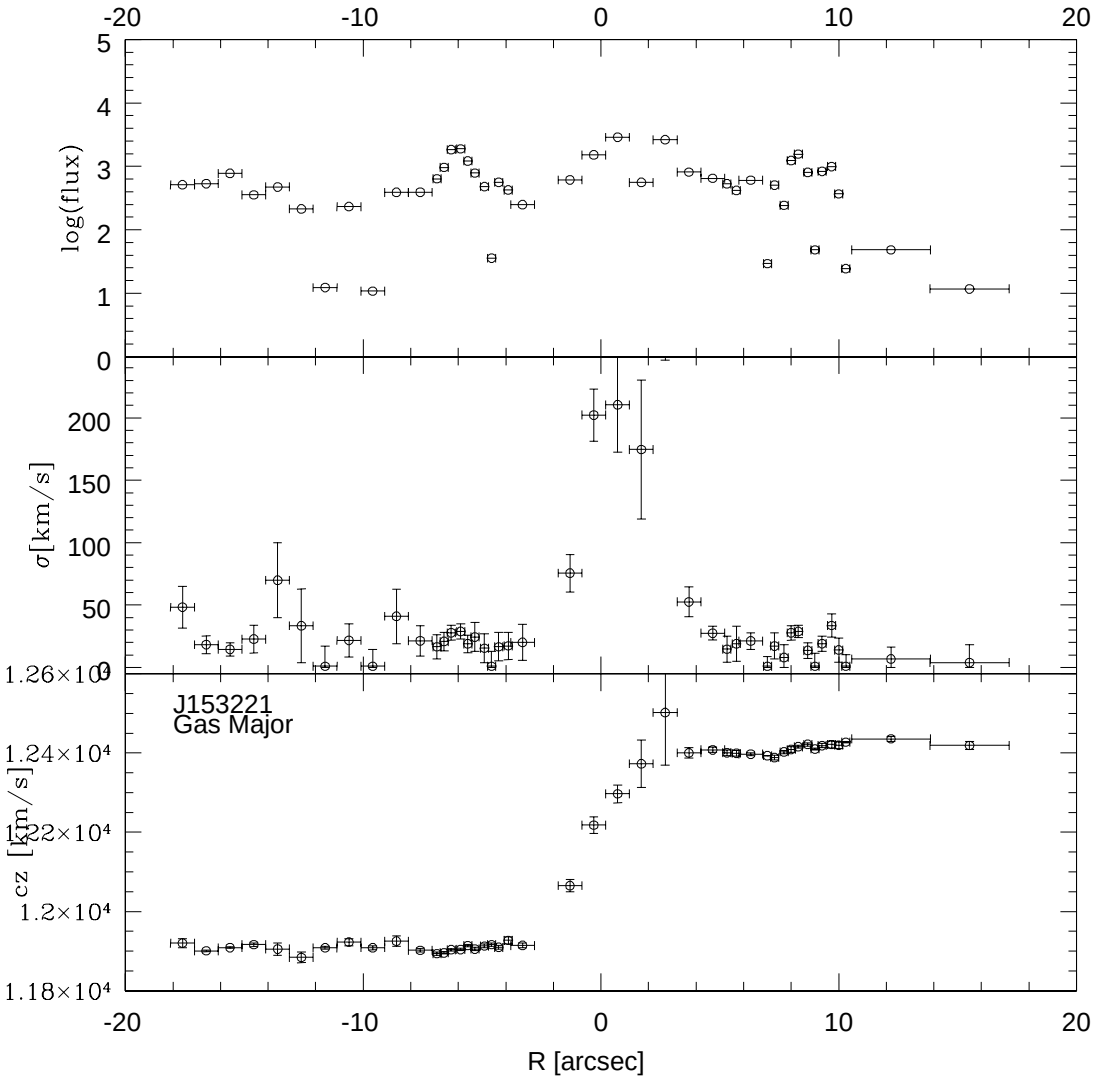

Figure 6.16: Emission line fitting result for J153221. *Lower panel*: radial velocity; *middle panel*: line veloocity dispersion; *upper panel*: Hα intensity (in arbitrary units). The radius at which the emission of the continuum is maximum has been adopted as center.

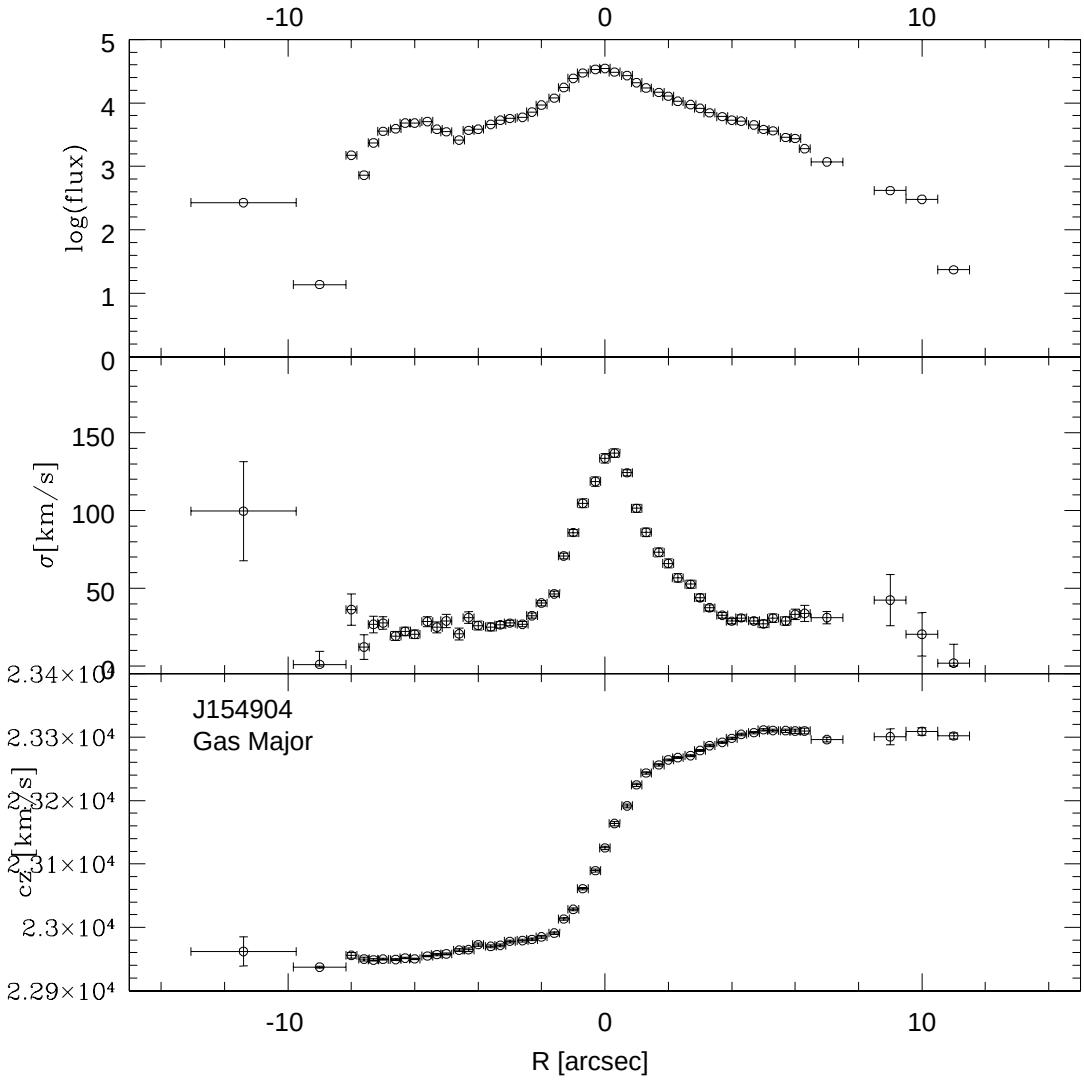

Figure 6.17: Emission line fitting result for J154904. *Lower panel*: radial velocity; *middle panel*: line veloocity dispersion; *upper panel*: Hα intensity (in arbritrary units). The radius at which the emission of the continuum is maximum has been adopted as center.

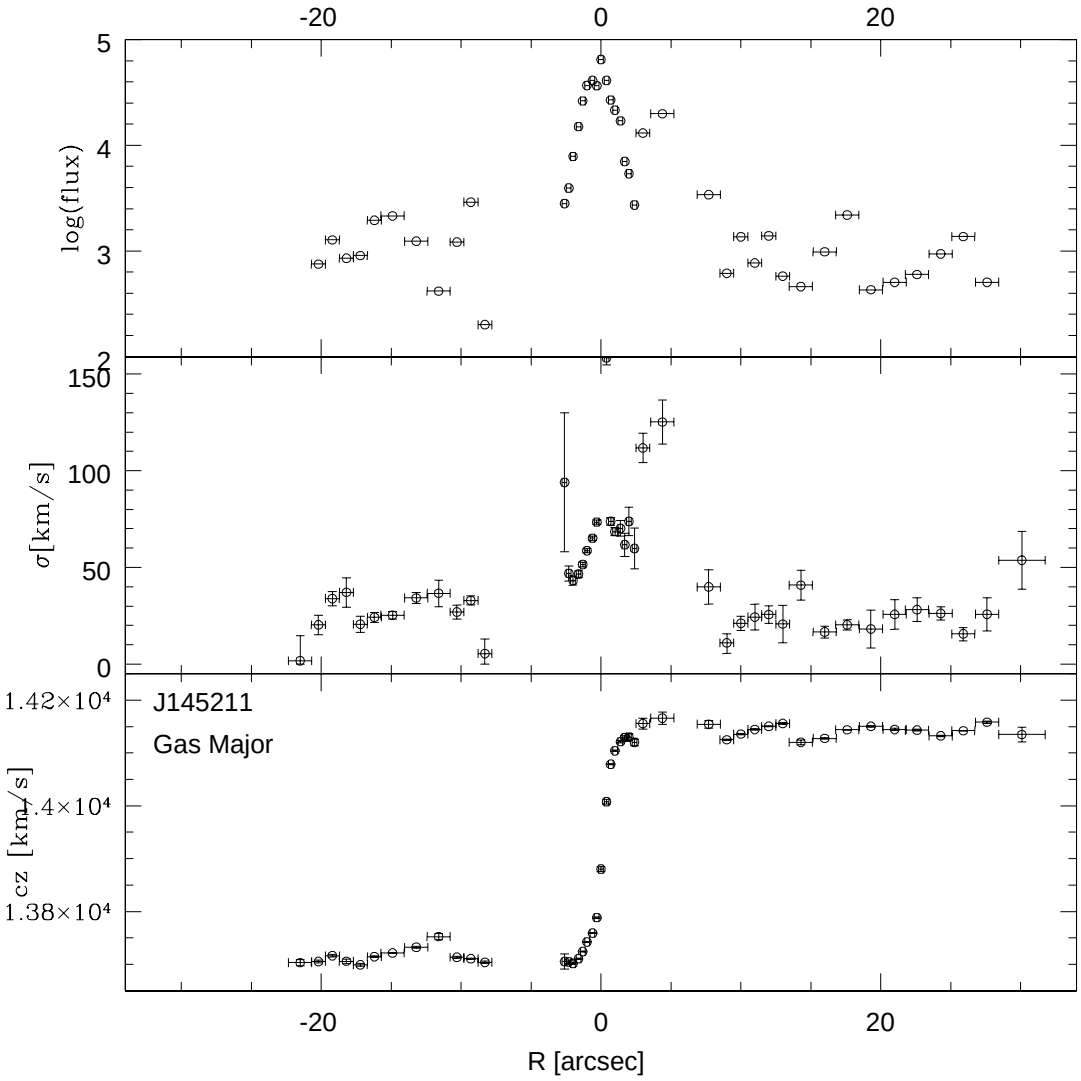

Figure 6.18: Emission line fitting result for J145211. *Lower panel*: radial velocity; *middle panel*: line veloocity dispersion; *upper panel*: Hα intensity (in arbritrary units). The radius at which the emission of the continuum is maximum has been adopted as center.

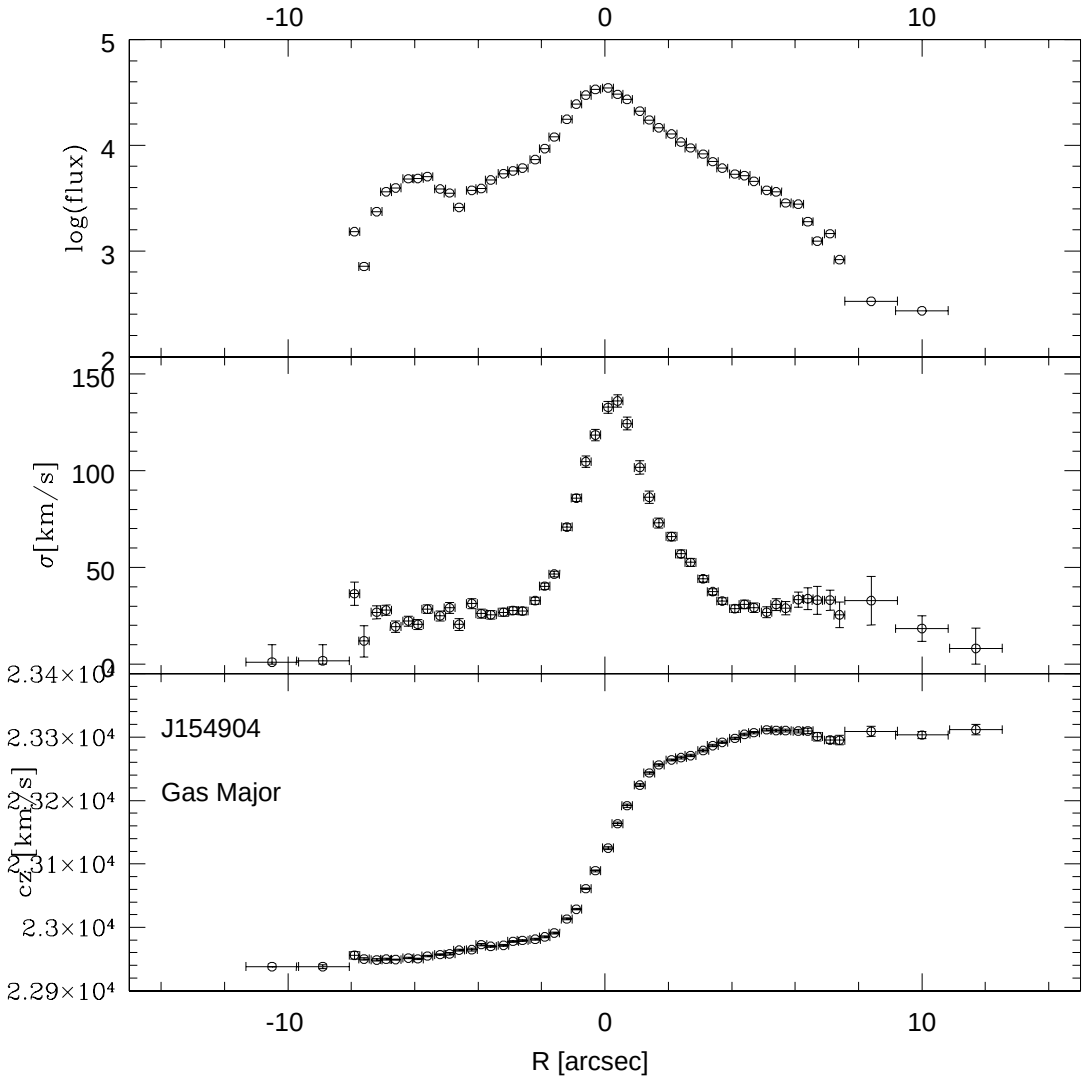

Figure 6.19: Emission line fitting result for J154904. *Lower panel*: radial velocity; *middle panel*: line veloocity dispersion; *upper panel*: Hα intensity (in arbritrary units). The radius at which the emission of the continuum is maximum has been adopted as center.

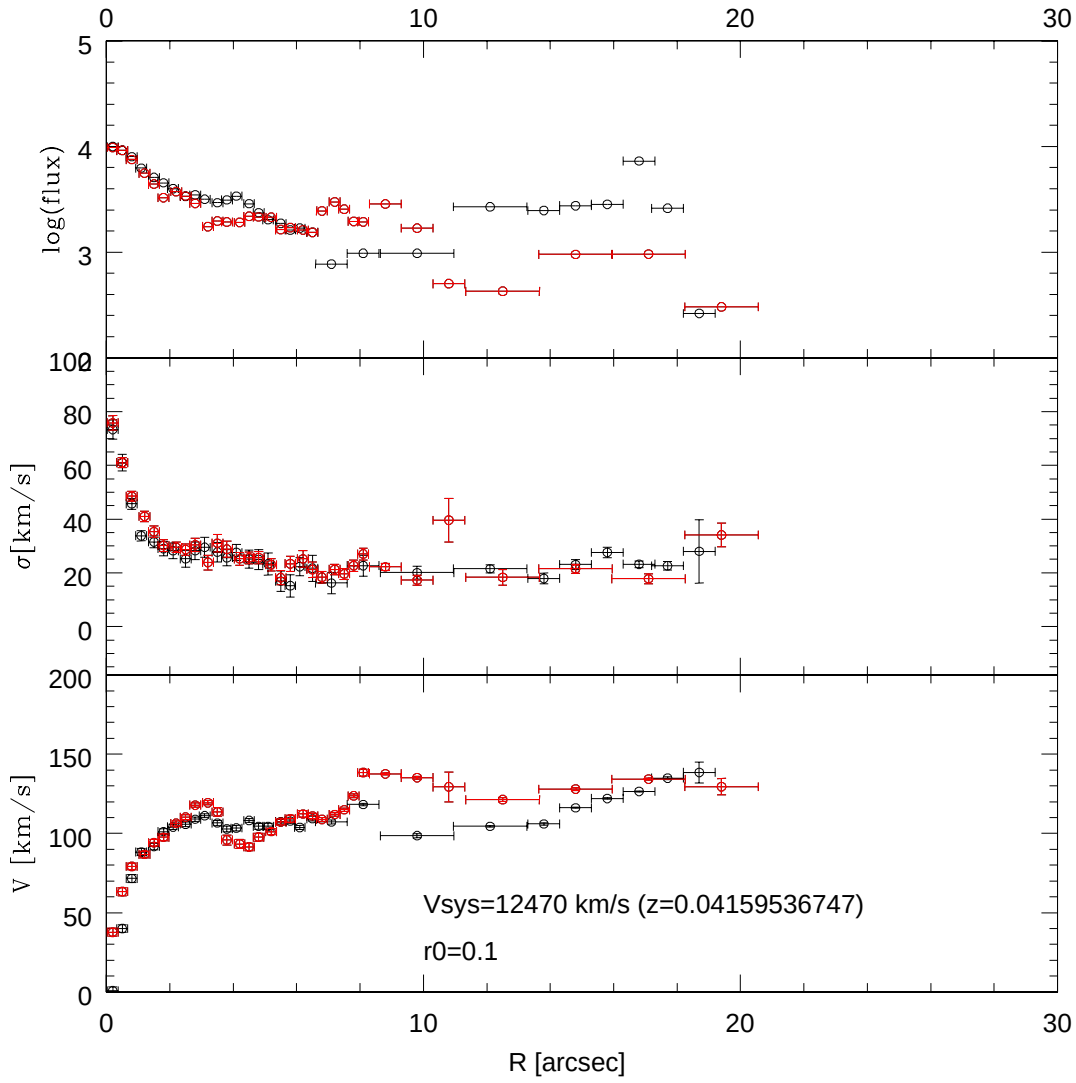

Figure 6.20: Galaxy J003828. After the folding of the curves around the center. The label on the lower panel indicates the adopted system velocity and adopted offset from the photometrical center.

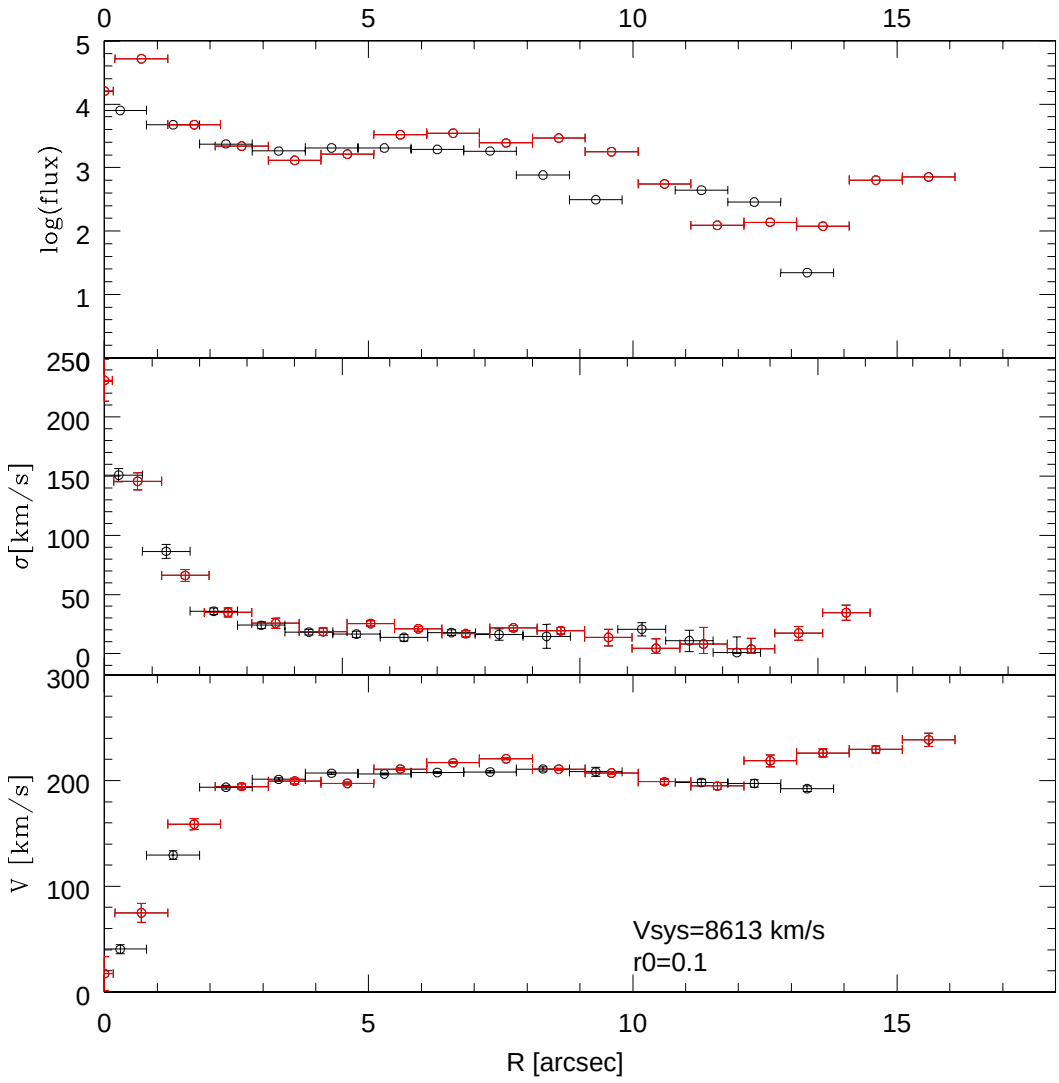

Figure 6.21: Galaxy J134215. After the folding of the curves around the center. The label on the lower panel indicates the adopted system velocity and adopted offset from the photometrical center.

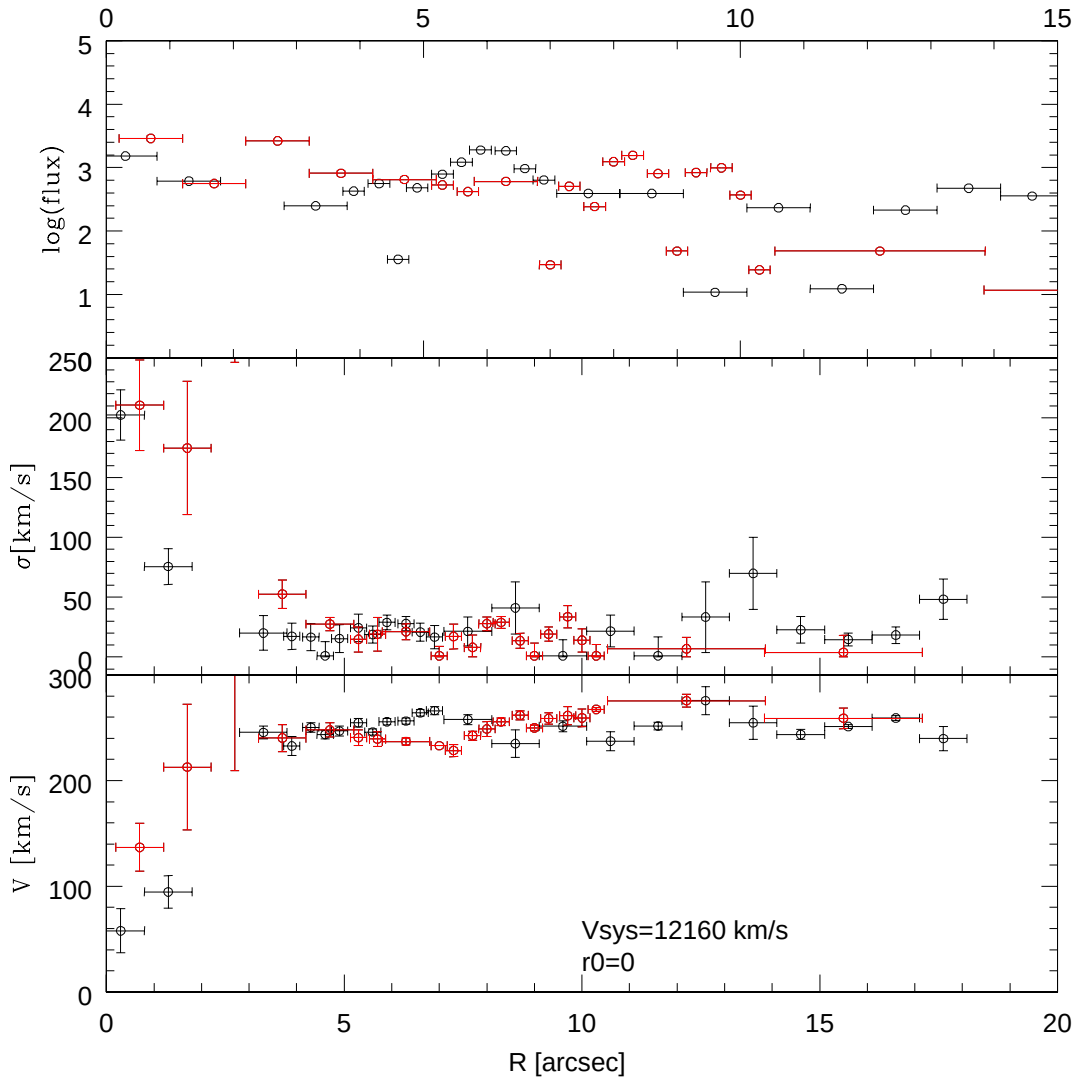

Figure 6.22: Galaxy J15322. After the folding of the curves around the center. The label on the lower panel indicates the adopted system velocity and adopted offset from the photometrical center.

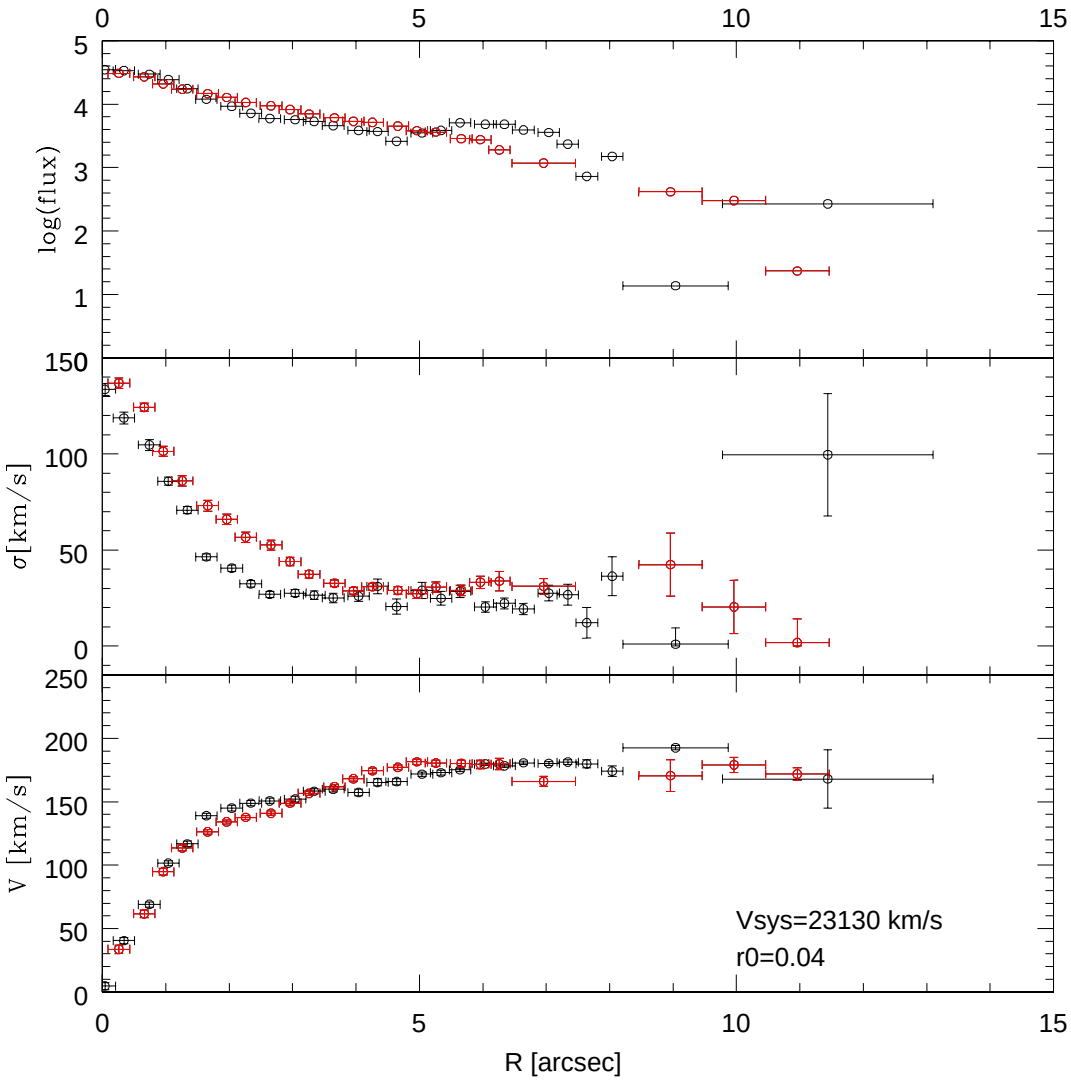

Figure 6.23: Galaxy J154904. After the folding of the curves around the center. The label on the lower panel indicates the adopted system velocity and adopted offset from the photometrical center.

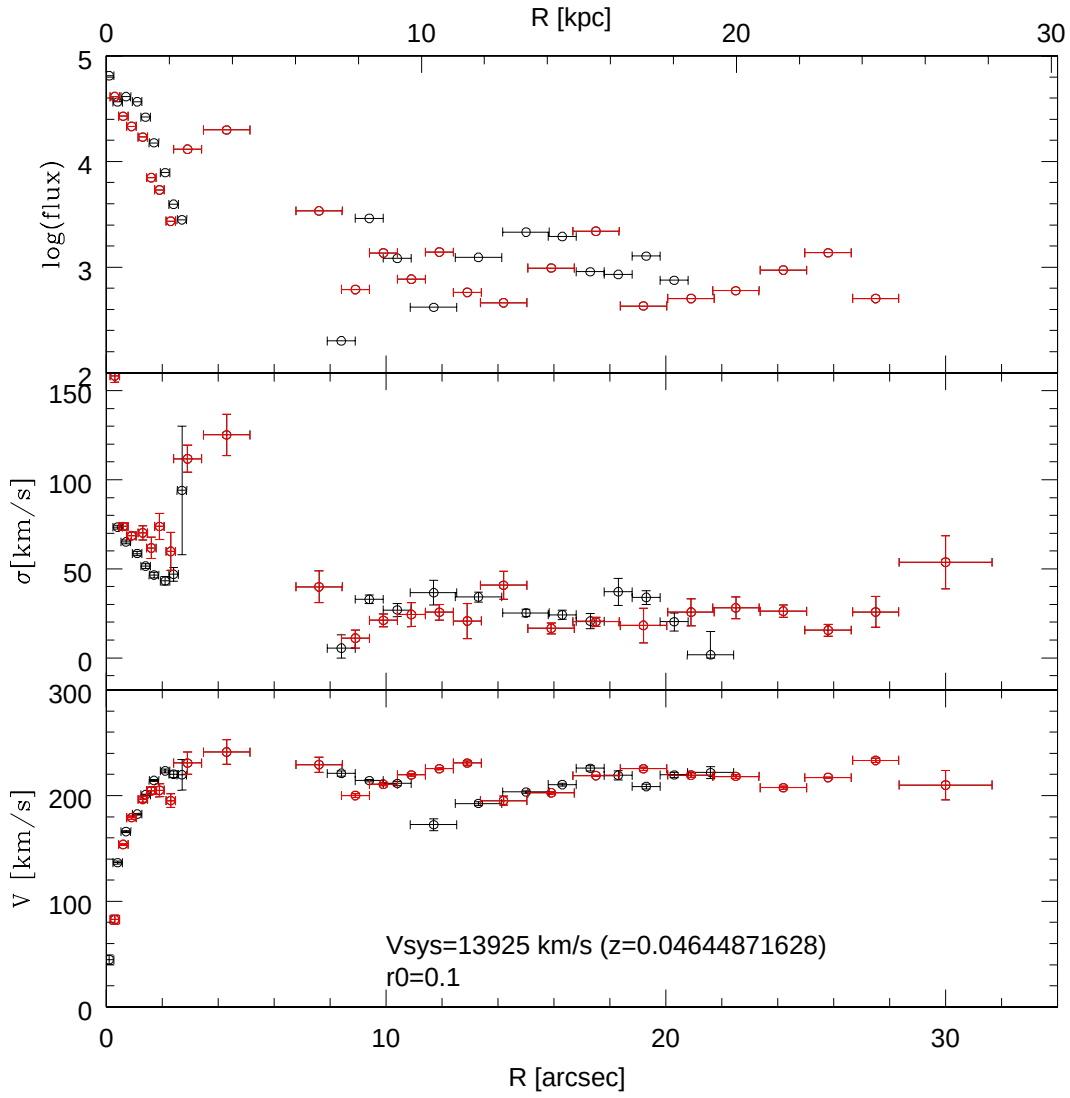

Figure 6.24: Galaxy J145211. After the folding of the curves around the center. The label on the lower panel indicates the adopted system velocity and adopted offset from the photometrical center.

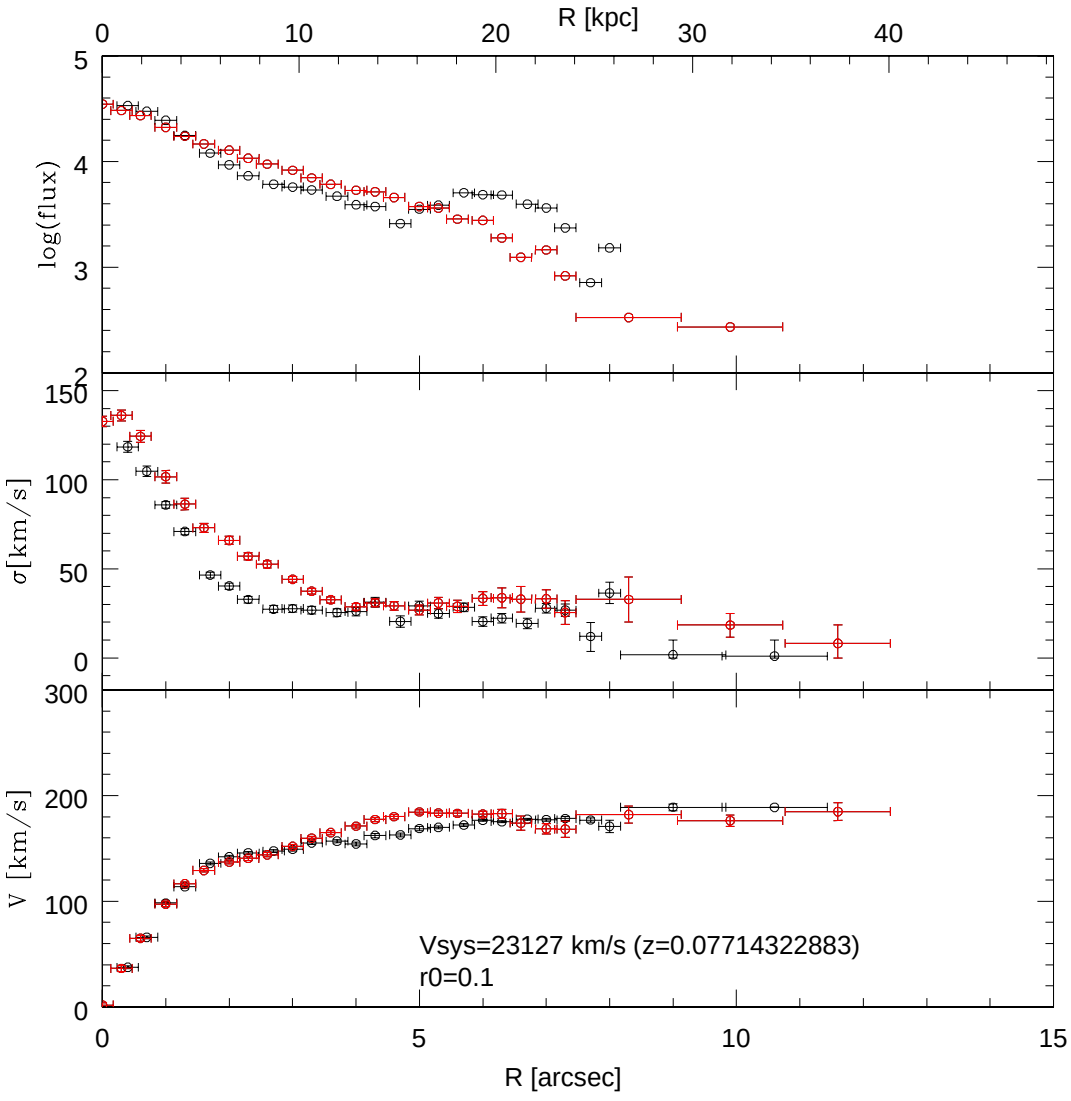

Figure 6.25: Galaxy J154904. After the folding of the curves around the center. The label on the lower panel indicates the adopted system velocity and adopted offset from the photometrical center.

Conclusions and future prospects

Undoubtedly, the dark matter problem in galaxies is one of the interesting and important problems of modern astrophysics. The distribution of luminous and dark matter in galaxies shows amazing properties and a remarkable systematics that make it one of the hottest cosmological issues. Below I describe the main results that we have obtained from our studies of spiral galaxies of different Hubble type, mass and luminosities. These results clearly show that the mass distribution in spiral galaxies shows systematical properties.

We discovered the existence of the new Tully-Fisher-like relationships. At different galactocentric distances measured in units of disk length-scales R_D, we found the existence of independent relationships, $M_{band} = b_j + a_j \log V(R_j)$, (where $j = 0.2, ..., 4$). We have called this relationships, the Radial Tully-Fisher relation (RTF). It contains crucial information on the mass distribution in spiral galaxies. We applied the Radial Tully-Fisher relation to three different samples of rotation curves of spiral galaxies and found that the RTF relationships show large systematic variations in their slopes a_j (between -4 and -8) and a r.m.s. scatter generally smaller than that of the standard TF. This rules out the case in which the light follows the gravitating mass. The slopes decrease monotonically with radius, which implies the presence of a non luminous mass component whose dynamical importance, with respect to the stellar disk, increases with radius.

We performed a measurements of stellar disk of spiral galaxies using two different methods. One is kinematical method, using the rotational velocities of the galaxies.

And another one is spectro-photometric method. The agreement between two methods is quite good. It implies that: the existence of a Inner Baryon Dominated region, inside which the stellar disk saturates the gravitational potential overwhelming the DM halo. The reliable values of the disk masses allow to realize that spiral galaxies, unlike ellipticals, show a quite wide range in the mass-to-light ratios, reflecting an intrinsic spread of ages of their average stellar population. In this study it is evident that spiral disks are significantly less massive than the elliptical spheroids of the same luminosity.

Analyzing a sample of high luminosity (M < -22.5) spiral galaxies we found that that the average rotational curve of these galaxies remaining constant or is decreasing with radius in the range $3R_D - 6R_D$. This indicates that in the more luminous spiral galaxies the fraction of luminous matter is larger than in galaxies of lower luminosity showing a rising rotational curves.

We proposed to use a new method to study the dark matter halos of spiral galaxies at large distances. To use the satellites of large spirals in order to probe dark matter distribution in their halos. The approach is new because we were using smaller number of primaries, but searching for satellites with the help of powerful Very Large Telescope (VLT). Also the novelty of the approach is that we have choose galaxies with the similar properties. Although the work is still in progress we can make some conclusions. For each galaxy we have found already at least double number of satellites that was known before (for example from the SDSS database). This result gives an unique opportunity to perform a detailed study of dark matter halos of spirals.

So the main conclusion that can be done that the spiral galaxies show a clear systematics in the distribution of dark and luminous matter. However the new approaches and new astronomical data will give a precious information to understand better the galaxies formation and evolution.

Already more than for 50 years we are studying the dark matter in spirals using

their rotation curves. Although with the help of the rotation curves we already got an important information about the structure and formation of spirals, still a lot can be done:

- Rotational velocities of the high-redshift galaxies. With the help of a new generation telescopes we may be able to observe protogalactic rotation and dynamical evolution of primeval galaxies.

- Using the $Br\gamma$ and H_2 molecular lines in K-band the extinction-free measurements can be obtained.

- Sophisticated methods of analysis, perhaps involving line shapes and velocity dispersions, will produce more accurate rotation curves for large samples of spirals. These will lead to more tightly constrained mass deconvolution. Distribution of dark and luminous matters within the halo, disk, bulge, and core will be mapped in detail from more sophisticated M/L ratio analyses.

The new generation ground-base telescopes (such as ELT) and space telescopes (Hubble, FUSE, GALEX and Spitzer) will give a great possibility to improve already known techniques, such as: strong and weak lensing, X-ray observations, observations of intergalactic medium (IGM), optical and radio observations of individual galaxies and clusters. This will help obtain new results on properties of dark and luminous matter in galaxies. And finely can give an opportunity to reveal the nature of mysterious matter that we call dark matter.

Bibliography

[1] Argyle E. 1965, Ap. J. 141, 750

[2] Babcock HW. 1939, Lick Obs. Bull. 19, 41

[3] Baldry, I.K., Glazebrook, K., Brinkmann, J., Ivezic, Z., Lupton, R.H., Nichol, R.C., & Szalay, A.S. 2004, ApJ, 600, 681

[4] Bell, E.F., McIntosh, D.H., Katz, N., & Weinberg, M.D. 2003, ApJS, 149, 289

[5] Bender R. 1990, Astron. Astrophys. 229, 441

[6] Bertola, F., Pizella, A., Persic, M. & Salucci, P. (1993), Astrophys. J. 416, 248

[7] Bertin G., Saglia R.P. and Stiavelli M., 1992, Astrophys. J. 384, 427

[8] Borriello A., Salucci P., Danese L., 2003, MNRAS, 341, 1109

[9] Breimer T.G. & Sanders, R.H., 1993, Astron. Astrophys. 274, 96 bibitem[10] Bruzual, G. & Charlot, S. 2003, MNRAS, 344, 1000

[11] Burbidge EM, Burbidge GR. 1960, Ap. J. 132, 30

[12] Burkert, A. 1995, ApJ, 447L, 25

[13] Catinella, B., Giaovanelli, R., Haynes, M. P., 2006, ApJ, 640, 751C

[14] Catinella, B., Giaovanelli, R. 2006, astro-ph/0605542

[15] Carollo, C.M., de Zeeuw, P.T., van der Marel, R.P., Danzinger, I.J. & Qian, E.E., 1995, Astrophys. J. 441, L25

[16] Cole & Lacey, 1996, MNRAS 281, 716 1996

[17] Courteau, S., 1996, ApJS, 103, 363

[18] Courteau, S., 1997, AJ, 114, 2402

[19] Clowe et al., 2006, ApJ, 648L,109

[20] Czoske, O., Moore, B., Kneib, J.-P., & Soucail, G. 2002, A&A, 386, 31

[21] Dalcanton, Sperge, Summers, 1997, ApJ, 482, 659

[22] e Jong, R.S. 1996, A&A, 313, 45

[23] de Paolis, F., Ingrosso, G. & Strafella, F., 1995, Astrophys. J. 438, 83

[24] Donato, F., Gentile, G., Salucci, P., 2004, MNRAS, 353L, 17

[25] Drory, N., Bender, R., & Hopp, U. 2004, ApJ,616, L103

[26] Federspiel, M., Sandage, A., Tammann, G. A., 1994, ApJ, 430, 29

[27] Fischer, P. 1999, AJ, 117, 2024

[28] Freeman, K.C., 1970, ApJ, 160, 811

[29] Fukushige & Makino, 2001, ApJ 557, 533

[30] Gray, M.E., Taylor, A.N., Meisenheimer, K., Dye, S., Wolf, C. & Thommes, E. 2002, ApJ 568, 141

[31] Gentile, G.; Salucci, P.; Klein, U.; Granato, G. L., 2007, MNRAS, 375, 199

[32] Gentile, G., Salucci, P., Klein, U., Vergani, D., Kalberla, P., 2004, MNRAS, 351, 903

[33] Hayashi E. et at. 2004, MNRAS, 355, 794

[34] Hayashi, E., Navarro, J.F., Springel, V., astro-ph/0612327

[35] Jee at al., 2007, ApJ, 661, 728J

[36] Kaiser, N., Wilson, G, Luppino, G. et al. 1998, astro-ph/9809268

[37] Kochanek C., 1995, Astrophys. J. 445, 559

[38] Kregel, M.; van der Kruit, P. C., 2004, MNRAS, 352, 787

[39] Kregel, M.; van der Kruit, P. C.; Freeman, K. C. 2005, MNRAS, 358, 503

[40] Mateo, M. et al. 1992, in B. Barbury and A. Renzini (Eds.), The stellar population of galaxies, IAU 149, Kluwer

[41] Mathewson DS, Ford VL, Buchhorn M. 1992, Ap. J. Suppl, 81, 413

[42] Mathewson, D. S., Ford, V. L., Buchhorn, M., 1992, ApJS, 81, 413

[43] Mathewson, D. S., Ford, V. L., Buchhorn, M., 1992, ApJ, 389L, 5

[44] Mathewson, D. S., Ford, V. L., 1996, ApJS, 107, 97

[45] Mayall NU. 1951, In The Structure of the Galaxy. Ann Arbor: Univ. Mich. Press, p. 19

[46] Milgrom M. 1983a, Ap.J., 270, 36570

[47] Milgrom M. 1983b, Ap.J., 270, 37183

[48] Milgrom M. 1983c, Ap.J., 270, 38489

[49] Moore et al., 1999, MNRAS 310, 1147

[50] Mould J.R., Oke J.B., de Zeeuw P.T. & Nemec, J.M., 1990, Astron. J. 99, 1823

[51] Navarro, Julio F.; Frenk, Carlos S.; White, Simon D. M., 1996, ApJ 462, 563

[52] Navarro, Julio F.; Frenk, Carlos S.; White, Simon D. M., 1997, ApJ 490, 493

[53] Navarro, J. F., 1998 ASPC, 136, 409

[54] Nishiyama K, Nakai N. 1998, In IAUSymp. No. 184: The Central Regions of the Galaxy and Galaxies, ed. Y. Sofue, p. 245. Dordrecht: Kluwer Academic

[55] Oort JH. 1940, Ap. J. 91, 273

[56] O'Sullivan E. & Ponman T. J., 2004, MNRAS, 354, 935

[57] Osterbrock, D.E., Fulbright, J.P., & Bida, T.A. 1997, PASP, 109, 614

[58] Page T. 1952, Ap. J. 116, 63

[59] Pease FG. 1918,. Proc. Natl. Acad. Sci. USA, 4, 21

[60] Persic M., Salucci P., 1988, MNRAS, 234, 131

[61] Persic, M., Salucci, P., 1995, ApJS, 99, 501, PS95

[62] Persic, M., Salucci, P., Stel, F., 1996, MNRAS, 281, 1, 27-47, PSS

[63] Pierce, M., Tully, R. B., 1988, ApJ, 330, 579

[64] Pierce, M., Tully, R. B., 1992, Apj 387,47

[65] Piatek S., Pryor C., 1995, AJ, 109, 1071

[66] Power et al., 2003, MNRAS 338, 14

[67] Ratnam C., Salucci P., 2000, NewA, 5, 427

[68] Rhee, M., H., 1996, Phd Thesis, Groningen

[69] Romanowsky A. J. et al., 2003, Sci, 301, 1696

[70] Rubin V.C., Ford WK Jr, Thonnard N. 1980, Ap. J., 238, 471

[71] Rubin VC, Ford WK Jr, Thonnard N. 1982a, Ap. J. 261, 439

[72] Rubin VC, Waterman AH, Kenney JDP. 1999, Astron. J. 118, 236

[73] Salucci P., Lapi A., Tonini C., Gentile G., Yegorova I., Klein U. 2007, MNRAS, 378, 41

[74] Salucci P., Walter F., Borriello A., 2003, A&A, 409, 53

[75] Salucci, P., Gentile, G., astro-ph/0510716, in press in Phys.Rew.Lett.D 2006

[76] Salucci, P., Frenk, C. S., Persic, M., 1993, MNRAS, 262, 392

[77] Sandage A. 2000 PASP 112, 504

[78] Sanders R.H., McGaugh S.S. 2002, ARA&A, 40, 263

[79] Shankar, F., Lapi, A., Salucci, P., De Zotti, G., Danese, L., astro-ph/0601577

[80] Sargent WLW, Schechter PL, Boksenberg A, Shortridge K. 1977, Ap. J., 212, 326

[81] Simkin S.M. 1974, Astron. Astrophys. 31, 129

[82] Schneider P, 2003, astro.ph, 6465S

[83] Schweizer, F., van Gorkom, J.H. & Seitzer, P., 1989, Astrophys. J. 338, 770

[84] Slipher VM. 1914, Lowell Obs. Bull. 62, Vol.11, 12

[85] Swaters R., 1999, ASPC, 182, 369 Sofue Y. 1995, Publ. Astron. Soc. Jpn. 47, 527

[86] Sofue Y. 1996, Ap. J. 458:120

[87] Sofue Y. 1999, Publ. Astron. Soc. Jpn. 51,445

[88] SofueY, Tomita A, Honma M, TutuiY. 1999a. Publ. Astron. Soc. Jpn. 51:737

[89] Sofue Y, Tutui Y, Honma M, Tomita A, Takamiya T, et al. 1999b. Ap. J. 523:136

[90] Sofue, Y.; Rubin, V, 2001ARA&A, 39, 137

[91] Strauss, M. A., Willick, J. A., 1995, Physics Reports, 261, 271

[92] Tonini C., Salucci P., 2004, bdmh.conf

[93] Tully, R. B., Fisher, J. R., 1977, A&A, 54, 661

[94] van Dokkum, P.G. 2001, PASP, 113, 1420

[95] van de Hulst HC, Raimond E, van Woerden H. 1957, Bull. Astron. Inst. Neth. 14, 1

[96] Vogt, N. P., Haynes, M. P., Herter, T., Giovanelli, R., 2004, AJ, 127, 3273

[97] Vogt, N. P., Haynes, M. P., Herter, T., Giovanelli, R., 2004, AJ, 127, 3325

[98] Volders L. 1959, Bull. Astron. Inst. Neth. 1, 323

[99] Warner PJ, Wright MCH, Baldwin JE. 1973, Mon. Not. R. Astron. Soc. 163:163

[100] Wolf M. 1914, Vierteljahresschr Astron. Ges. 49, 162

[101] Yegorova I., Salucci P. 2007, MNRAS, 377, 507